Proceedings of the 20th International Conference on Biomedical Applications of

ELECTRICAL IMPEDANCE TOMOGRAPHY

Edited by Alistair Boyle, Kirill Aristovich,
Anna Witkowska-Wrobel and David Holder

July 1–3, 2019
UCL, London, UK

This document is the collection of papers accepted for presentation at the
20th International Conference on Biomedical Applications of Electrical Impedance Tomography (EIT2019), London, UK.

Cover design: Alistair Boyle
Photo credits: Ilya Tarotin

Printed in the United Kingdom

DOI: 10.5281/zenodo.2691705 (revision 0; conference)
Medical Physics and Biomedical Engineering
UCL
London,
United Kingdom
www.ucl.ac.uk/medphys

eit2019.co.uk

Table of Contents

Electrical Impedance Tomography with Radio Frequency Excited Gold Nanoparticles

Nazanin Neshatvar[12], Rui Damaso[1], Nima Seifnaraghi[1], Yevhen Ivanenko[3], Sven Nordebo[3], Andreas Demosthenous[2], and Richard Bayford[12]

[1]Dept. Natural Sciences, Middlesex University, UK, n.neshatvar@mdx.ac.uk, [2]Dept. Electronic and Electrical Engineering, University College London, UK, [3]Dept. Physics and Electrical Engineering, Linnaeus University, 35195 Växjö, Sweden.

Abstract: An approach for electrical impedance tomography (EIT) using radio frequency excited gold nanoparticles has been proposed for GHz. However there is advantages in using frequencies in the MHz range. Results are presented using citrate coated 5nm gold nanoparticles enhances impedance tomography at a frequency of 13.56 MHz.

1 Introduction

Gold nanoparticles (AuNPs) with unique optical properties may be used as agents in medical imaging, hyperthermia, drug delivery and many more applications [1]. Compared to other metal nanoparticles, they are non-cytotoxic and can easily conjugate to a variety of biomolecular ligands [1]. Due to surface plasmon resonance (SPR) frequency of gold nanoparticles, when placed in presence of a magnetic field at certain frequency they have the ability to efficiently convert absorbed light into localized heat [1]. This can be employed for therapy based on photothermal destruction of cancerous cells. The use of AuNPs in EIT has been presented earlier in [2] in presence of a radio frequency field at 2.6 GHz frequency. This paper illustrates the temperature variation of a medium including 5nm spherical gold nanoparticles that are excited at 13.56 MHz. Because of the relatively low penetration depth of radiation at infrared (IR) and visible frequencies, radio frequency (RF) energy the use of frequencies in the MHz range would allow imaging in deeper regions of the body, thus reaching important internal organs [3].

2 Methods

A 32 electrode EIT system from SenTec has been used for imaging the AuNPs where they are placed at the central ring of the electrodes. These commercial 5nm AuNPs were filtered with 10kDa centrifuge filter tubes. The pellet re-suspended in PBS solution and concentrated to approximately four times the original concentration to be used in the measurements. The excitation radio frequency of 13.56 MHz was provided by a high efficiency class E power amplifier where the load of the amplifier is a coil and the samples are placed in the middle of it. Measurement results after 30 minutes (3 minutes with no RF excitation as the reference and 27 minutes with RF excitation) represent 18.9% increase in conductivity of the medium as a result of change in the temperature gradient as shown in Fig.1a and b respectively. There is also an overall 30% increase with respect to the medium with no AuNP while excited by RF amplifier.

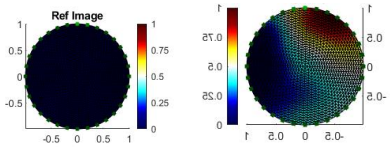

(a) (b)

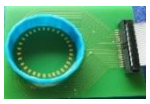

(c)

Fig.1: EIT images of commercial AuNP by using SenTec device with 32 electrodes, (a) The PA is off and (b) after 30 min with PA on. (c) PCB with 32 electrodes for EIT measurements without coil shown.

3 Conclusions

Gold nano particles excited at 13.56 MHz frequency can enhance EIT imaging via difference imaging methods. The change in temperature by just a few degrees would not kill cells and hence allow its use in humans.

4 Acknowledgements

This project has received funding from the Engineering and Physical Sciences Research Council (EPSRC) under the grant no. EP/R04192X/1.

References

[1] S. Nordebo, M. Dalarsson, Y. Ivanenko, D. Sjöberg, and R. Bayford, "On the physical limitations for radio frequency absorption in gold nanoparticle suspensions," *J. Phys. D. Appl. Phys.*, vol. 50, no. 15, 2017.

[2] R. Bayford *et al.*, "Nanoparticle Electrical Impedance Tomography," in *Proceedings of the 18th International Conference on Biomedical Applications of Electrical impedance tomography*, 2017, p. 56.

[3] G. W. Hanson, R. C. Monreal, and S. P. Apell, "Electromagnetic absorption mechanisms in metal nanospheres: Bulk and surface effects in radiofrequency-terahertz heating of nanoparticles," *J. Appl. Phys.*, vol. 109, no. 12, pp. 1–6, 2011.

Logarithmic amplifier in the signal processing circuit of an EIT system used for cell imaging applications

Mukta Verma[1] , D C Gharpure[1] and V G Wagh[2]

[1]Department of electronic Science, Savitribai Phule Pune University, Pune, Maharashtra, India muktavrm@gmail.com
[2]V N Naik college, Nasik, Maharashtra, India

Abstract: A novel signal processing circuit using Logarithmic amplifier is proposed to improve the spatial resolution of an EIT system consisting of a mini-sensor used for biological cell imaging applications. The property of logarithm to compress higher values and expand lower values enables to acquire data even with low resolution ADC.

1 Introduction

Recently the application of EIT for biological cell imaging has gained popularity because of the development of micro-technologies [1]. Since these applications are at cellular level, the boundary measurements have very small difference and hence require high resolution ADC cards. One of the solutions is to amplify the signal using Instrumentation amplifier [2], however it also amplifies the noise. According to the property of logarithm, it expands lower values and compresses higher values. This allows the use of low resolution ADC cards and hence must improve the spatial resolution of the system[3].

2 Methods

A mini EIT sensor is developed consisting of 16 electrodes fabricated on a single sided PCB. The exposed copper is electroplated with gold for biocompatibility. The well made of rubber with diameter 15mm is mounted on the PCB. The adjacent method is used where current is injected to a pair of electrodes and voltages are measured across remaining electrode pairs [4]. 1mA of current is injected at 15KHz frequency**.** Fig 1 shows the block diagram for the proposed design.

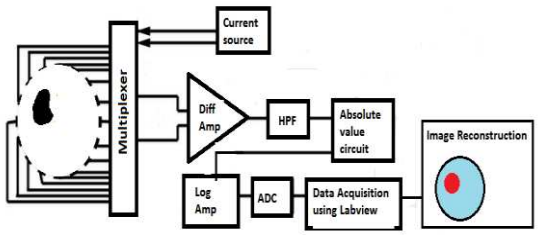

Figure 1: Data acquisition system with Log amplifier in the signal conditioning circuit

The differential signal from difference amplifier(Diff Amp) is first filtered using High pass filter(HPF) to remove any dc offset. Since we cannot obtain Logarithm of a negative value, therefore the filtered signal is fed to the absolute value circuit to have only positive values of the signal. The signal is input to the Log amplifier(Log Amp) designed with operational amplifier before it is fed to the ADC.

2 Results and Discussion

The circular well on the developed EIT mini sensor is filled with the PBS with conductivity 1.5 S/m for the reference. PBS is selected since it is used as the cell culture medium [4]. A small object made of plastic with 1mm thickness and lemon pulp are used as the inhomogenities in the PBS solution as shown in Fig 2. As the worst case scenario for adjacent method, inhomogenities are kept in the middle with the minimal applied current. Data is acquired with the proposed circuit as well as with the conventional circuit which uses instrumentation amplifier for amplification of the signal and the results are compared. Fig 2 shows the reconstructed images for the same along with the quantitative measures like Resolution(RES) and Contrast to noise ratio(CNR)[5,6]. Without amplification, the inhomogenity is not even detected. Reconstructed images

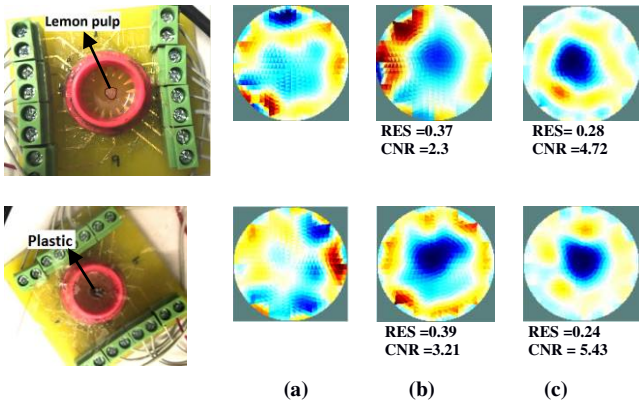

Figure2: Reconstructed images (a) Without amplification, (b) with instrumentation amplifier, (c) With Log amplifier

indicate that Log amplifier in the circuit certainly improves the spatial resolution and contrast to noise ratio.

References

[1] Yin X, Wu H, Jia J, Yang Y. A Micro EIT Sensor for Real-time and Non-destructive 3-D Cultivated Cell Imaging. *IEEE Sensors Journal.* Jul 1;18(13):5402-12,2018
[2] Yu C, Yue S, Wang J, Wang H. An effective measured data preprocessing method in electrical impedance tomography. *The Scientific World Journal*. 2014;2014
[3] Reynolds, W.E. The Use of a Logarithmic Amplifier in Data Processing of Analog Signals, Technical report IRL 1017, 1965
[4] Sun T, Tsuda S. Single cell imaging using electrical impedance tomography. *4th IEEE International Conference on Nano/Micro Engineered and Molecular Systems*(pp. 858-863) 2009
[5] Yasin M, Böhm S, Gaggero PO, Adler A. Evaluation of EIT system performance. *Physiological measurement,* 2011
[6] Bera TK, Nagaraju J. Studies and evaluation of EIT image reconstruction in EIDORS with simulated boundary data. *Second International Conference on Soft Computing for Problem Solving* (SocProS 2012), Springer, p. 1573-1581, New Delhi. December 2014

Investigation of measurement errors in miniature frequency-difference EIT measurement

Hancong Wu[1], Pierre O Bagnaninchi[2] and Jiabin Jia[1]

[1]School of Engineering, The University of Edinburgh, Edinburgh, UK, jiabin.jia@ed.ac.uk

[2]MRC Centre for Regenerative Medicine, The University of Edinburgh, Edinburgh, UK

Abstract: Measurement errors of the miniature frequency-difference EIT for cell culture monitoring are analysed and compensated in this study. Images reconstructed with the conventional method and with the compensated method are compared.

1 Introduction

Electrical impedance tomography (EIT) provides real-time imaging for cell culture without dyeing or sample destruction. However, only time-difference EIT are commonly used in cellular research so far. The variation of measurement errors at different frequencies reduces the accuracy of frequency-difference EIT in biological applications. This study investigated the measurement errors in the miniature frequency-difference EIT for cell culture monitoring. Equivalent circuit model was analysed and the effects of the leakage current on the measurements were evaluated. The method to eliminate the effect of leakage current was investigated.

2 Methods

2.1 Equivalent circuit analysis

The equivalent circuit of a single channel measurement of EIT is illustrated in Fig.1. Due to the capacitive coupling between the voltmeter terminals to the virtual ground, the leakage current is diverted from the measuring electrodes to the ground, which causes measurement errors on the voltage measurements [1, 2]. By applying Kirchhoff's law to the equivalent circuit, the approximate voltage measurement can be expressed as (1):

$$V=((Z_4-Z_3)+Z_m+\frac{Z_3Z_3+Z_3Z_x-Z_4Z_4-Z_4Z_y}{Z_x})I_3 \quad (1)$$

where $Z_3=R_3//C_3$, $Z_4=R_4//C_4$, $Z_x=1/j\omega C_x$ and I_3 is the current at the Kirchhoff's loop.

Since the contact impedance and coupling capacitance changes with the frequency, conventional weight frequency-difference EIT (wfdEIT) method cannot completely compensate the measurement errors. Previous studies showed that background calibration could help to improve the measurements [3, 4], so the calibrated frequency-difference EIT (cfdEIT) is developed for cell culture imaging:

$$\Delta V=((V_{m-2}-(V_{r-2}-V_{r-1}))-V_{m-1})/V_{m-1} \quad (2)$$

where V_{m-1} and V_{m-2} are the voltage measurements for samples at frequency f_1 and f_2. V_{r-1} and V_{r-2} are the voltage measurements for homogeneous reference at frequency f_1 and f_2. The conductivity of the culture medium is not necessarily the same as the reference.

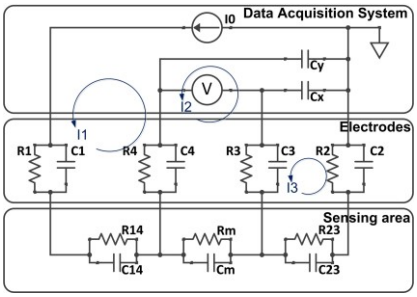

Figure 1: Equivalent circuit model for a single channel EIT measurement with adjacent current drive method.

2.2 Image reconstruction for 3D cell culture

Fig.2 shows that the reconstructed images with wfdEIT fail to indicate the correct location of the scaffolds due to measurement errors. However, reconstructed images with cfdEIT can distinguish the scaffold sample from its blank control because the cancer cells have a higher conductivity variation than the blank scaffold.

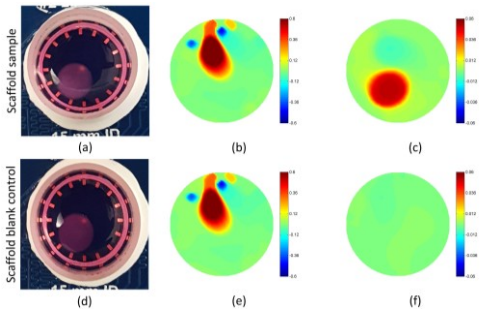

Figure 2: Reconstructed images of scaffold samples (b)(e) use wfdEIT and (c)(f) cfdEIT

3 Conclusions

The conductivity variation of scaffold sample is small and is susceptible to the measurement errors. The calibrated frequency-difference EIT is able to resist the errors and improve the image quality.

References

[1] B. Veal, P. Baldo, A. Paulikas, and J. Eastman, Journal of The Electrochemical Society, vol. 162, pp. H47-H57, 2015

[2] M. R. Baidillah, A.-A. S. Iman, Y. Sun, and M. Takei, IEEE Sensors Journal, vol. 17, pp. 8251-8262, 2017

[3] H. Wu, W. Zhou, Y. Yang, J. Jia, and P. Bagnaninchi, Materials, vol. 11, p. 930, 2018

[4] Y. Jiang and M. Soleimani, IEEE Access, 2018

Impact of Accelerated Ageing on Electrode Coatings used in EIT

Adam Fitchett[1], Kirill Aristovich[1] and Christopher Chapman[2]

[1]Medical Physics and Biomedical Engineering, University College London, UK, k.aristovich@ucl.ac.uk

[2]Bioengineering, Imperial College London, UK

Abstract: EIT neural cuff electrodes must display stable long-term performance. We subjected three key EIT electrode coatings (PEDOT:pTS, IrOx and Pt) to accelerated ageing protocols to assess their degradation. All three materials showed notable degradation at elevated temperature and in the presence of reactive oxygen species.

1 Introduction

EIT has shown promise as a technique for use in implantable neural cuffs [1]. For such devices to perform a therapeutic function, they must show stable physical and electrical properties over the course of their use, which could potentially span decades. The most promising electrode-coating materials due to their electrical properties are Poly(3,4-ethylenedioxythiophene):p-toluene sulfonate (PEDOT:pTS), iridium oxide (IrOx) and platinum black (Pt). But although all 3 have been previously used in an acute setting, their chronic stability has never been quantified in application to the specific EIT cuff design. The purpose of this work was to assess and compare the stability of each coating via accelerated ageing protocols.

2 Methods

2.1 Design & Fabrication of Arrays

Cuff electrode arrays suitable for chronic testing were fabricated and coated according to methods previously described [2]. Each array consisted of a stainless-steel foil sandwiched between layers of silicone and had three oblong contacts with dimensions 0.35 mm by 1.6 mm (Fig.1D). A total of 27 arrays were made, nine coated with each of the three materials.

2.2 Accelerated Ageing

Three arrays of each material underwent ageing for four weeks under one of three ageing conditions: (1) saline at 25 °C, (2) saline at 85 °C, and (3) 2 mM H_2O_2 at 25 °C.

Saline was chosen to simulate the ambient chemical conditions inside the human body. H_2O_2 simulated the effects of reactive oxygen species released by immune cells following implantation. Elevated temperature simulated the passage of time (approximately 2 years is simulated in 1 month at 85 °C).

2.3 Characterisation of Performance

The electrical properties of all arrays were characterised at regular intervals with electrochemical impedance spectroscopy (EIS) and cyclic voltammetry (CV).

Scanning electron microscopy (SEM) was performed at the end of each experiment to directly examine coating delamination.

3 Results

After 4 weeks in saline at 25 °C, no significant change in average impedance at 1kHz is seen with any of the three materials (Fig.1A, $p > 0.5$, unpaired two-tail t-test). All three materials do show a general upward trend in average impedance at 1 kHz after being in saline at 85 °C as well as with 2 mM H_2O_2. At 85 °C, the impedance of PEDOT:pTS and IrOx reached values a factor of 5 higher than at t = 0 days, and for Pt this was a factor of 10 (Fig.1B, $p < 0.0001$). With H_2O_2, impedance for all three materials after 4 weeks increased by approximately a factor of 3; this change was significant for PEDOT:pTS and IrOx (Fig1.C, $p < 0.01$) but not for Pt (Fig1.C, $p = 0.35$). PEDOT:pTS showed the lowest peak average impedance at 85 °C, reaching 4.1 kΩmm^{-2}, with IrOx and Pt reaching 4.6 kΩmm^{-2} and 7.7 kΩ mm^{-2} respectively.

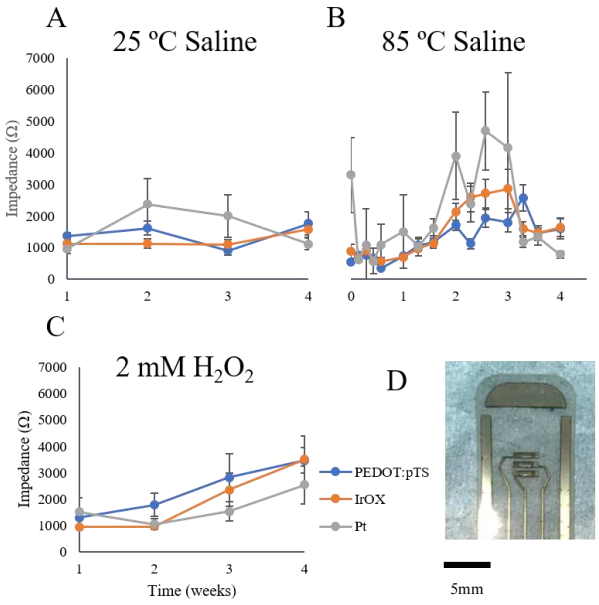

Figure 1: *A-C: Average impedance at 1 kHz under three ageing conditions: (A) 25 °C saline (B) 85 °C saline (C) 25 °C 2 mM H_2O_2. n = 9 for each material under each condition. Error bars indicate 1 SE. D: Close up of uppermost part of one of the tested electrode arrays.*

4 Conclusion

None of the three materials has displayed a clear advantage over the other two in these experiments. The excellent acute properties of PEDOT:pTS and its marginally better performance at 85 °C suggest it is the most promising of the three as a coating for chronic EIT electrode use. However, its degradation in the presence of reactive oxygen species remains an issue. IrOx also shows good performance, but its attractiveness over PEDOT:pTS is limited by how much harder it is to apply.

Non-linear difference reconstruction method for monitoring of cerebral haemorrhage

Jussi Toivanen[1], Asko Hänninen[1], Tuomo Savolainen[1], Ville Kolehmainen[1]

[1]Department of Applied Physics, University of Eastern Finland ville.kolehmainen@uef.fi

Abstract: We present a non-linear difference imaging algorithm for monitoring of progression of cerebral haemorrhage using EIT. The method is based on a joint reconstruction formulation where the initial conductivity and the change in the conductivity are reconstructed simultaneously based on the voltage data before and after the change.

1 Introduction

EIT has significant potential as a tool for bedside monitoring of progression of cerebral haemorrhage at intensive care unit. This application would have significant impact in the treatment process since it would alleviate the need of repeated transfer of the critically ill patient to CT imaging. In this talk, we propose a non-linear difference reconstruction approach for EIT monitoring of the cerebral haemorrhage. The approach allows using a region of interest constraint for the conductivity change (e.g. haemorrhage is constrained inside the skull) and structured regularization when anatomical prior information is available, for example, from a CT scan which is taken when the patient is admitted to the hospital.

2 Methods

Let σ_1 denote the conductivity before the change, and $\sigma_2 = \sigma_1 + \delta\sigma$ denote the conductivity after the change. One feature of this parameterization is that it offers a straightforward way to restrict the conductivity change $\delta\sigma$ to a region of interest (ROI), if temporal changes are known to occur only in a subdomain inside the body. Let

$$\mathrm{supp}(\delta\sigma) = \Omega_{\mathrm{ROI}} \subseteq \Omega$$

denote the region of interest and denote the conductivity change within Ω_{ROI} by $\delta\sigma_{\mathrm{ROI}}$. Then, we write

$$\delta\sigma = \mathcal{K}\delta\sigma_{\mathrm{ROI}},$$

where $\mathcal{K}$ is an extension mapping $\mathcal{K} : \Omega_{\mathrm{ROI}} \to \Omega$ such that

$$\mathcal{K}\delta\sigma_{\mathrm{ROI}} = \begin{cases} \delta\sigma_{\mathrm{ROI}} & x \in \Omega_{\mathrm{ROI}} \\ 0 & x \in \Omega \setminus \Omega_{\mathrm{ROI}} \end{cases} \quad (1)$$

and the conductivity σ_2 after the change can be modelled

$$\sigma_2 = \sigma_1 + \mathcal{K}\delta\sigma_{\mathrm{ROI}}. \quad (2)$$

Using (2), the EIT problem is formulated as a joint reconstruction of $(\sigma_1, \delta\sigma_{\mathrm{ROI}})$ by minimizing the functional [1]:

$$\begin{aligned} F(\sigma, \delta\sigma_{\mathrm{ROI}}) &= \|V_1 - U(\sigma_1)\|^2 + \|V_2 - U(\sigma_1 + \delta\sigma_{\mathrm{ROI}})\|^2 \\ &+ \alpha_1 B(\sigma_1) + \alpha_2 C(\delta\sigma_{\mathrm{ROI}}) \end{aligned} \quad (3)$$

where V_1 is the measured data for σ_1 and V_2 the data for $\sigma_1 + \mathcal{K}\delta\sigma_{\mathrm{ROI}}$, $B(\sigma_1)$ is a (structured) TV regularization functional and C is a suitable regularization functional, such as TV or smoothness regularization, for $\delta\sigma_{\mathrm{ROI}}$. The implementation of $C(\sigma_1)$ is based on the parallel level sets approach [2], and it allows straightforward inclusion of anatomical prior information.

3 Results

Figure 1 shows a 3D reconstruction from experimental data which was measured from a 3D printed UCL head tank phantom [3]. The regularization functionals B and C were isotropic TV regularization functionals.

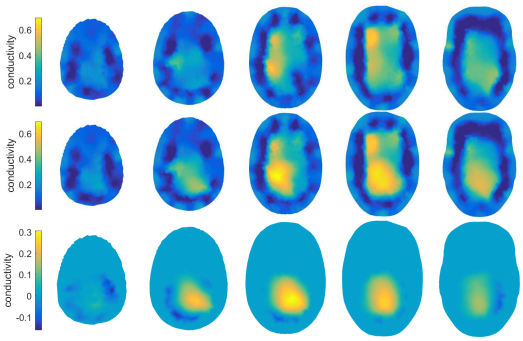

Figure 1: Horizontal slices of a 3D reconstruction. Top row: σ_1, Middle: σ_2, Bottom: $\mathcal{K}\delta\sigma_{\mathrm{ROI}}$

4 Acknowledgements

This work was supported by the Jane and Aatos Erkko foundation, and the Academy of Finland, Centre of Excellence in Inverse Modelling and Imaging.

References

[1] Dong Liu, Ville Kolehmainen, Samuli Siltanen, and Aku Seppänen. A nonlinear approach to difference imaging in EIT assessment of the robustness in the presence of modelling errors. *Inverse Problems*, 31(3):035012, feb 2015.

[2] Ville Kolehmainen, Matthias J. Ehrhardt, and Simon R. Arridge. Incorporating structural prior information and sparsity into eit using parallel level sets. *Inverse Problems and Imaging*, 13(2):285–307, 2019.

[3] James Avery, Kirill Aristovich, Barney Low, and David Holder. Reproducible 3d printed head tanks for electrical impedance tomography with realistic shape and conductivity distribution. *Physiological Measurement*, 38(6):1116–1131, may 2017.

3D EIT imaging with Green's functions

Christos Dimas[1], Nikolaos Uzunoglu[2], Paul P. Sotiriadis[3]

[1]Dept. of Electrical and Computer Engineering, National Technical University of Athens, Greece chdim@central.ntua.gr

Abstract: A theoretical approach that uses Green functions in order to perform 3D EIT imaging of low-conductivity disturbances is briefly described. Applying the Green's function solution in an integral governing equation, a sensitivity matrix is constructed, from which the solution is obtained.

1 Introduction

Although 2D imaging is applied in the majority of EIT medical applications, there exist numerous effects associated with the examination domain's depth and volume. This creates the necessity to perform 3D imaging even if only a single plane's properties are of interest. Here, we propose an alternative approach that uses the Green function vector theorem.

2 Methods

2.1 The Green function

The fundamental mathematical background for the 2D case has been introduced in [1]. If $\boldsymbol{r} = (x, y, z)$ is the observation point, $\boldsymbol{r'} = (x', y', z')$ an internal "source" point and $\boldsymbol{r}_+$, $\boldsymbol{r}_-$ the current source electrode vectors (point-electrode model), then the EIT equation is:

$$\nabla\sigma\nabla V + \sigma\nabla^2 V = I[\delta(\boldsymbol{r} - \boldsymbol{r}_+) - \delta(\boldsymbol{r} - \boldsymbol{r}_-)] \quad (1)$$

If $\Omega \in R^3$ is the examination domain and assuming that no currents flow through the boundaries, application of the Green's integral theorem gives:

$$V(\boldsymbol{r}) = \iiint_\Omega G(\boldsymbol{r}, \boldsymbol{r'}) \frac{\nabla\sigma(r')}{\sigma(r')} \nabla V(\boldsymbol{r'}, \boldsymbol{r}_+, \boldsymbol{r}_-) d\Omega + V_{ref}(\boldsymbol{r}, \boldsymbol{r}_+, \boldsymbol{r}_-) \quad (2)$$

The Green function $G(\boldsymbol{r}, \boldsymbol{r'})$ verifies the Poisson PDE $\nabla^2 G(\boldsymbol{r}, \boldsymbol{r'}) = -\delta(x-x')\delta(y-y')\delta(z-z')$ along with the non-current flow Neumann boundary condition, $\nabla V \boldsymbol{r} = 0$. The solution can be found either analytically for canonical or conformal geometries or numerically for more complex cases. In this work, we are interested in applications for maligant detection at female breast inserted in a cylindrical domain filled with conductive water; thus, we emphasize in a cylindrical geometry Ω_c with radius R_o. Multiple electrode planes are attached to the cylinder. The analytic solution on Ω_c includes a source term $G_o(\boldsymbol{r}, \boldsymbol{r'}) = \frac{1}{2\pi|\boldsymbol{r}-\boldsymbol{r'}|}$ and a correction term, approximated by the method of images: $G_1(\boldsymbol{r}, \boldsymbol{r'}) = \frac{1}{2\pi|\boldsymbol{r}_{im}-\boldsymbol{r'}|}$, where $\boldsymbol{r}_{im}$ is the symmetric of $\boldsymbol{r}$ with respect to $\partial\Omega_c$. [2]

2.2 System formulation and solution

Due to the singular behavior of G on the electrodes we set two assumptions: Firstly, the electrodes are not placed at $\partial\Omega_c$, but in a small inner distance ($|R_o - \epsilon|$). Secondly, (2) is solved in an inner area of interest $A \subset \Omega_c$ which does not include the electrodes. Furthermore, a linearization $\nabla V \simeq \nabla V_{ref}$ is performed around the background conductivity σ_{ref}. The conductivities are expressed globally with an exponential-type base (n even):

$$ln(\sigma(\boldsymbol{r'})) = \sum_{i=1}^{N}\sum_{j=1}^{M}\sum_{k=1}^{L} a_{ijk} e^{-\frac{[(x'-x_i)^n + (y'-y_j)^n + (z'-z_k)^n]^{\frac{1}{n}}}{D^2}} \quad (3)$$

where $\boldsymbol{r_{ij}} = (x_i, y_j, z_k)$ is a central voxel point. A is discretized in a $M \times N \times L$ voxel area and (2) is numerically solved, leading to an equation system $Sa = V_{ref}(\boldsymbol{r}) - V(\boldsymbol{r})$, $a = [a_{ij}]$. S is a sensitivity matrix, with similar behavior to a Jacobian matrix. The system can be solved with state-of-the-art inverse problem approaches (Gen. Tikhonov reg., priors).

3 Results

Simulation tests were performed using MATLAB. The forward model was created with the NETGEN feature of EIDORS. A result is shown in Fig. 1 (NOSER prior):

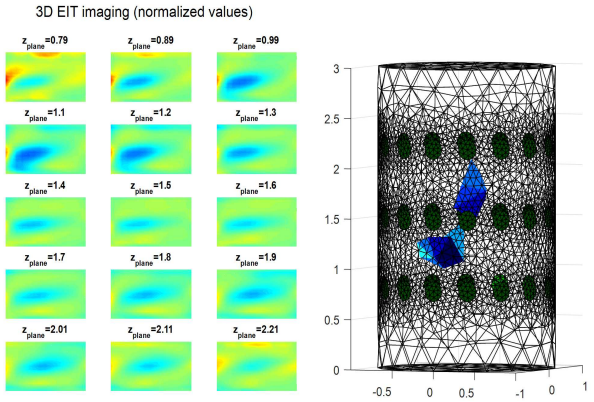

Figure 1: 3D image reconstruction for 2 small pertrurbations

4 Conclusions

In this paper, we proposed an algorithm that performs 3D imaging using Green's integral theorem. Results seem promising, with improvements such as extension for the complete electrode model and iterative approaches for more intense conductivity changes to be in the works.

5 Acknowledgements

This research is co-financed by Greece and the European Union (European Social Fund- ESF) through the OperationalProgramme "Human Resources Development, Education and Lifelong Learning" in the context of the project "Strengthening Human Resources Research Potential via Doctorate Research" (MIS-5000432), implemented by the State Scholarships Foundation (IKY).

References

[1] C Dimas, N Uzunoglu, P Sotiriadis *Conf 19th EIT*, p.51, Edinburgh, UK, Jun 2017

[2] G Barton *Elements of Green's functions and propagation* IOP Publishing: Oxford, 1989

B-spline based shape reconstruction to EIT in the presence of non-homogeneous background

Dong Liu[1], Danping Gu[2], Danny Smyl[3], Jiansong Deng[2], Jiangfeng Du[1]

[1]Department of Modern Physics, University of Science and Technology of China, dong.liu@outlook.com
[2]School of Mathematical Sciences, University of Science and Technology of China
[3]Department Civil and Structural Engineering, University of Sheffield, Sheffield, UK

Abstract: We evaluate the recently proposed B-spline based shape reconstruction approach [1] to EIT in the presence of non-homogeneous background. Simulation studies are conducted and results show that the B-spline based approach tolerates to modeling errors caused by the non-homogeneous background to some extent.

1 Introduction

The EIT image reconstruction problem is a nonlinear ill-posed inverse problem. Utilizing prior information is critical in addressing the EIT reconstruction problem. The idea of accounting for shape information based regularization in the reconstruction is gaining increasing interest within the scientific community [2]. Recently, a novel B-Spline based shape reconstruction approach for absolute EIT using the finite element method (FEM) [1] is introduced and has achieved good results [1]. In this approach, the conductivity distribution to be reconstructed is assumed to be piecewise constant, such that the background is generally treated as an ideal homogeneous state. However, in real situations, e.g., EIT lung monitoring, the conductivity of heart is completely different to the background. For this reason, in this work, more realistic values for the heart and aorta are assigned, leading to a non-homogeneous background and consequently modeling errors to the reconstruction problem. The objective of this work is to study the feasibility of the B-Spline based shape reconstruction approach in the presence of such modeling errors.

2 Methods

Given the complete electrode model and an additive Gaussian noise model, the observation model of EIT can be written in the form

$$V = U(\sigma) + e, \tag{1}$$

where vector V consists all the measured voltages, $U(\sigma)$ is the FEM solution to the forward problem, and e is additive Gaussian noise with mean e^* and covariance matrix Γ_e.

2.1 Boundary expression using B-spline curves

As mentioned in the Introduction, the conductivity distribution σ in the measurement domain was assumed to be piecewise constant. It offers a nice chance to reformulate the problem of the conductivity reconstruction as an inverse problem for a special geometrical representation of embedded objects, by using a shape description function, such as the uniform cubic B-spline curve (UCBS) used in [1].

Let P denote the coordinates of control points, and N denotes the matrix composed of basis functions of UCBS. Then we can express the UCBS curve in a matrix form as

$$C = NP. \tag{2}$$

Then, perturbing the control points will result in a change of the UCBS curve, which is treated as the boundary of the (unknown) embedded inclusions, such that the space of unknown boundary is mapped into the space of unknown control points' coordinates P. Then, the observation model in (1) can be expressed as

$$V = U(\sigma(x, P)) + e. \tag{3}$$

Now, the shape reconstruction problem is equivalent to solving the following minimization problem:

$$[\hat{P}, \hat{\sigma}_0, \hat{\sigma}_1] = \arg\min\{\|L_e(V - U(\sigma))\|^2 + \|L_p(P - P^*)\|^2 + \sum_{j=0}^{1} \|L_\sigma(\sigma_j - \sigma_j^*)\|^2\},$$

where P^* is a vector of a priori value of P and σ_j^* are predetermined constant values.

3 Results

Fig.1 shows the results of three different simulated cases. Here, we only apply two UCBS curves to model the lung's boundary, i.e., the inclusions marked as red color in Fig.1 are considered as auxiliary inclusions in the background and treated as modeling errors to the reconstruction problem. Despite the presence of the non-homogeneous background, the B-spline based approach recovers the inclusions' shape and tracks the sharp corners of the inclusions relatively well. This result demonstrates that the B-spline based approach tolerates to the modeling errors caused by the non-homogeneous background to some extent.

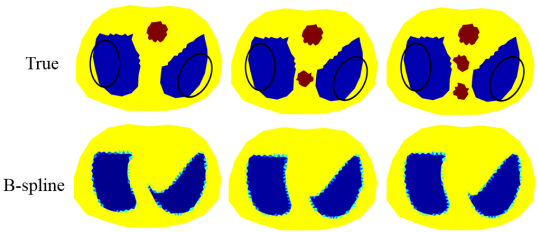

Figure 1: B-spline based reconstructions with non-homogeneous background.

References

[1] D. Liu, D. Gu, D. Smyl, J. Deng and J. Du "B-spline based sharp feature preserving shape reconstruction approach for electrical impedance tomography ," *IEEE Transactions on Medical Imaging(Early Access)*,2019

[2] D. Liu, A. K. Khambampati, and J. Du "A parametric level set method for electrical impedance tomography," *IEEE Transactions on Medical Imaging*, vol. 37, no. 2, pp. 451–460, 2018.

Jacobian Matrix Prediction in Wearable EIT Sensor Using K-Nearest Neighbour (K-NN) Algorithm.

PN Darma, MR Baidillah, MW Sifuna and M Takei.

Graduate School of Science & Engineering, Chiba University, Chiba, Japan, panji.nursetia@chiba-u.jp

Abstract: This paper investigates the possibilities of prediction Jacobian matrix in a wearable EIT sensor using K-Neighbour (K-NN) Algorithm. 8 electrode of wearable EIT sensor connected with stretch and angle detectors is used to generate different boundary shapes of phantoms and 105380 samples of Jacobian matrix elements with different geometries are used to generate training data. The results of true Jacobian matrix **J** and predicted Jacobian matrix **J'** compared using cross correlation *CC* show high correlation between the **J** and **J'**.

1 Introduction

There has been significant development in Electrical Impedance Tomography (EIT) with wearable sensors and miniaturized data acquisition systems (DAS) using Field Programmable Gate Array (FPGA) microcontroller. These developments open the opportunity for applying EIT in internet of thing healthcare monitoring. In wearable EIT, the Jacobian matrix is calculated whenever the boundary shape change to attain higher accuracy of EIT image reconstruction. However, 70% and 25% of computing time is spent for calculating Jacobian matrix and forward solving which is difficult to achieve in current FPGA due to limitation of memory and processor capacity. Therefore it is necessary to accelerate Jacobian matrix computation in FPGA based wearable EIT sensor to enable realtime healthcare monitoring process.

2 Methods

Let $\mathbf{J}=[J_{11}, J_{12},\ldots, J_{21}, J_{22},\ldots,J_{mn},\ldots,J_{MN}\ ]$ $\mathbf{J}\epsilon\mathbb{R}^{M\times N}$ is EIT Jacobian matrix with M measurement number and N mesh element, $\mathbf{T}=[\mathbf{I}_1, \mathbf{I}_2, \ldots,\mathbf{I}_{m\times n\times t}, \ldots,\mathbf{I}_{M\times N\times T}]$ $\mathbf{T}\epsilon\mathbb{R}^{I\times MNT}$ is training sample, $\mathbf{I}=(m,x_n,y_n,J_{mn})$ input variable with m measurement number, x_n and y_n Cartesian coordinate of J_{mn} Jacobian matrix. The predicted Jacobian matrix J' of predictive variable **I'** is expressed as

$$J'(I') = \frac{\sum_{I\in T(I')} J(I).w(-d^2)}{\sum_{I\in T(I')} w(-d^2)} \quad (1)$$

where **J'**(**I'**) is Jacobian matrix prediction of predictive variable **I'**, and **T**(**I'**) is a set of k training data which are closest to the input prediction, $w(-d^2)$ is weighting function and $d = \|\mathbf{I} - \mathbf{I}'\|_2$ is Euclidean distance between prediction variable and training variable.

3 Results

Fig. 1 shows the comparison between true Jacobian matrix **J** and predicted Jacobian matrix **J'** and Fig. 2 shows cross correlation evaluation which have average cross correlation value *CC* 0.98 and 0.97 for phantoms 1 and 2 respectively.

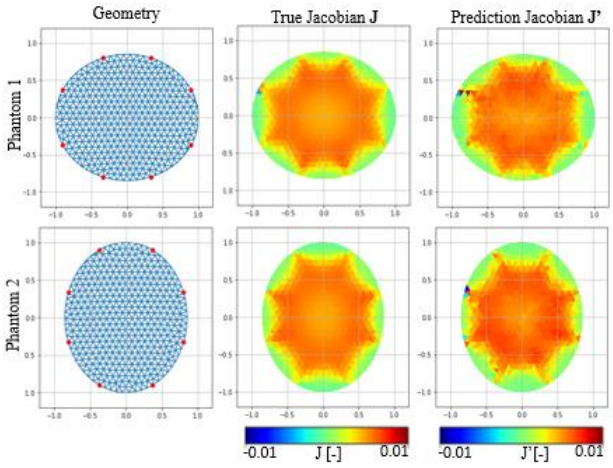

Figure 1. Comparison between true Jacobian matrix **J** and predicted Jacobian matrix **J'.**

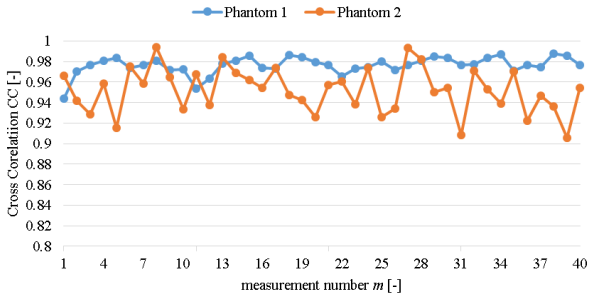

Figure 2. The cross correlation evaluation *CC*.

4 Conclusions

This paper demonstrates the feasibility study of Jacobian matrix prediction in FPGA based wearable EIT sensor. The Jacobian prediction results show high correlation with true Jacobian matrix. The findings open possibilities of real-time healthcare monitoring.

References

[1] MR Baidillah, A Iman, Y Sun, M Takei, *IEEE Sensors J*, 17(24): 8251-826.

[2] Xu Z, Yao J, Wang Z, Liu Y, Wang H, Chen B and Wu H 2018 Development of a Portable Electrical Impedance Tomography System for Biomedical Applications *IEEE Sens. J.* **18** 8117–24.

Fused-data TREIT using an 8-electrode biopsy needle and soft priors

Ethan K. Murphy[1], Xiaotian Wu[1], Alicia C. Everitt[1], and Ryan J. Halter[1,2]

[1]Thayer School of Engineering, Dartmouth College, Hanover, NH, USA, ethan.k.murphy@dartmouth.edu

[2]Geisel School of Medicine, Dartmouth College, Hanover, NH, USA

Abstract: We have incorporated an 8-electrode biopsy needle and spatial priors into our fused-data Transrectal Electrical Impedance Tomography (fd-TREIT) framework. This has improved accuracy in gelatin and ex vivo bovine tissue phantoms. An ex-vivo prostate study is ongoing to validate our approach in a clinically setting.

1 Introduction

Detecting prostate cancer non-invasively is clinically challenging. Low threshold PSA-based screening has a high sensitivity, but low specificity due to numerous benign conditions elevating PSA levels [1]. Men with elevated levels of PSA are typically subject to an image-guided biopsy protocol for more accurate diagnosis. Unfortunately, transrectal ultrasound (TRUS)-guided biopsies miss 10-30% of all cancers [1]. A number of ex-vivo studies have shown that electrical properties exhibit significant differences between benign and cancerous prostate [2]. We have previously developed an fd-TREIT system for prostate imaging that fuses tetra-polar impedance data recorded from 18 sonolucent electrodes adhered to a TRUS probe and 4 electrodes integrated near the tip of a biopsy needle. Here we added 1) an additional 4 electrodes onto the biopsy needle and 2) incorporate spatial priors into our reconstruction approach. Recent experiments have shown that only the biopsy-probe electrodes are needed, which significantly reduces computational costs. The fusion approach has been evaluated on ex vivo tissue and a series of realistic gelatin prostate phantoms. An ex vivo prostate study is ongoing.

2 Methods

Ex vivo bovine tissue (Fig. 1) and gelatine phantoms with two graphite-gel inclusions (Fig. 2A-B) were evaluated using 9 and 12 biopsy fd-TREIT measurements. Magnetic Resonance (MR) images were used to segment the prostate and gelatine inclusion and for validation purposes. EM-tracking using an NDI Aurora V2 system provided localization and pose of the TRUS probe, biopsy needle, and phantom for each EIT measurement which enabled registration with MR images.

The fd-TREIT approach was based on a standard Gauss-Newton algorithm using a regularization scheme optimized for open domains [3]. Soft-prior prostate and inclusion boundaries from the MR images were used in the gel phantom experiments [4]. The fusion process utilizes a single finite element method (FEM) mesh (180k nodes, 990M elements) that only models the biopsy needle. The mesh was transformed for each state and related to a fixed inverse mesh using the dual-mesh method. The inverse mesh is constructed by fusing regions of sensitivity from each measurement. Using a parallel implementation, 5-step absolute reconstructions are solved in approximately 12 minutes, which is a 30x speed-up from our earlier efforts using both TRUS and biopsy electrodes.

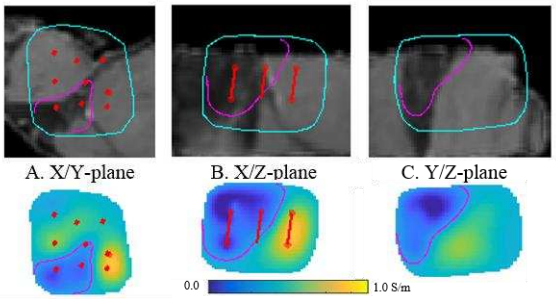

Figure 1: Absolute reconstruction on a meat phantom. The EIT ROI is overlayed on the MR slices (cyan), needle locations are shown in red and a magenta contour of the EIT image roughly separates the adipose and muscle tissue.

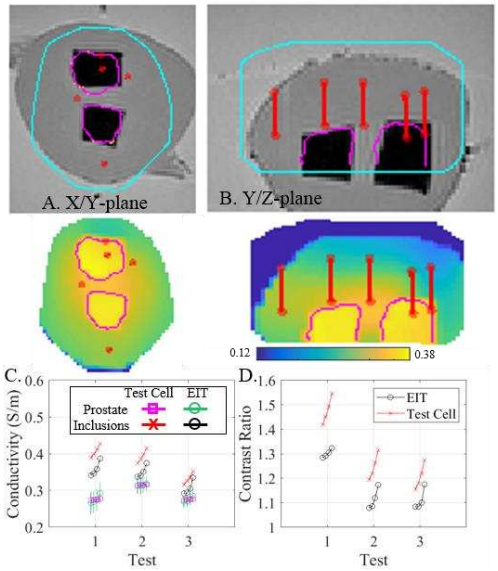

Figure 2: Absolute reconstruction of gelatin prostate phantom with graphite-gel inclusions (A-B/Test 1) and average conductivity values at 10-80 kHz of prostate and inclusion (C) and inclusion ratio (D) for 3 Tests. Remaining formatting is similar to Fig. 1. A best scalar matching the prostate test cell and EIT reconstructions was used.

3 Conclusions

An 8-electrode biopsy needle with soft-prior constrained fd-TREIT framework provides significant improvement in image accuracy compared to prior work in fd-TREIT.

4 Acknowledgements

Supported in part by DoD CDMRP W81XWH-15-1-0571.

References

[1] Campbell's Urology, ed, P. Walsh. 2007, Saunders: Philadelphia
[2] R. J. Halter, IEEE Bio. Eng., 10.1109/TBME.2007.897331, 2007.
[3] E.K. Murphy, IEEE Med. Imag.,10.1109/TMI.2016.2520907, 2016.
[4] E.K. Murphy, et al., Phys. Meas. 10.1088/1361-6579/aa691b, 2017.

Transfer function of regional respiratory system mechanics determined from EIT images during pressure-controlled ventilation

A. Dupré[1], M-R. Benissa[1], B. Müller[2], A.D. Waldmann[2], M. Kallio[3], M. Rahtu[3], R. Yerworth[4], T. Becher[5], M. Miedema[6], S.Nordebo[7], D. Khodadad[7], I. Frerichs[5], R. Bayford[8], P.C. Rimensberger[1,9]

[1]Department of Paediatrics, University of Geneva, Switzerland, antoine.dupre@alumni.epfl.ch
[2]SenTec AG, EIT Branch, Switzerland [3]PEDEGO Research Unit, University of Oulu and Oulu University Hospital, Finland
[4]University College London, UK [5]University Medical Centre Schleswig-Holstein, Germany [6]University of Amsterdam and Vrije Universiteit Amsterdam, Netherlands [7]Linnaeus University, Sweden [8]Middlesex University, UK
[9]Neonatalogy and Intensive Care Unit, University Hospital of Geneva, Switzerland

Abstract: This paper describes a robust frequency-domain technique to assess respiratory system transfer function and regional time constants from electrical impedance tomography (EIT) images and estimated input pressure waveforms delivered by the ventilator during pressure-controlled ventilation (PCV).

1 Introduction

Accurate breath detection [1] provides inspiration and expiration times to produce time-differentiated EIT impedance images from which tidal variation from which tidal variation and other clinically relevant parameters can be obtained [2]. Changes in impedance of the lung tissue correlate with changes in alveolar gas volume. In presence of heterogeneous lung disease, continuous information on regional respiratory system mechanics might be clinically useful to target homogeneous ventilation. We present a method for determination of respiratory time constants from ventilator breaths acquired during PCV.

2 Methods

A patient of gestational age of 35.5 weeks and postnatal age of 7.3 weeks, weighing 3608 g was treated in a neonatal intensive care unit within the clinical study (NCT02962505) of the CRADL project. EIT images were obtained using the CRADL study EIT system (SenTec AG, former SwissTom AG, Landquart, Switzerland). The patient was monitored by EIT at 47.68 frames per second for 72 hours. Each tomographic image with a 32x32 pixel resolution was reconstructed using the GREIT algorithm [3]. Pressure-controlled ventilation (PCV) is a mode of mechanical ventilation supporting all breaths, either triggered by the patient or initiated by the ventilator. Selected sequences contain exclusively periodic ventilator breaths. Thereby, the PCV signal applied during the patient examination can be approximated as a periodic pulse waveform characterised by the respiratory rate RR and the inspiration-to-expiration time ratio $I{:}E$.

In the one-compartment lung model, the respiratory system is approximated as a serial resistance and compliance. The corresponding transfer function $H(f)$ is a RC low-pass filter [4], with time constant τ_{rs}:

$$H(f) = \frac{S_{EIT}(f)}{S_p(f)} = \frac{1}{1+i\cdot 2\pi f \tau_{rs}} \qquad (2)$$

3 Results

From Equations (1) and (2), a 3-parameter model for EIT image pixel signals can be fitted:

$$S_{EIT}(f) = \alpha \cdot sinc(\beta \cdot f) \cdot \frac{1}{1+i\cdot 2\pi f\cdot \tau} \qquad (3)$$

Breath detection algorithm [1] provides a starting value for $\beta = \frac{1}{RR\left(2+\frac{1}{I:E}\right)}$ improving convergence of the fit using the least-square methods. α is a scaling parameter related to tidal impedance change and τ is the time constant of the transfer function (expressed in seconds). The fitting parameters for experimental measurements are shown in **Figure 1**.

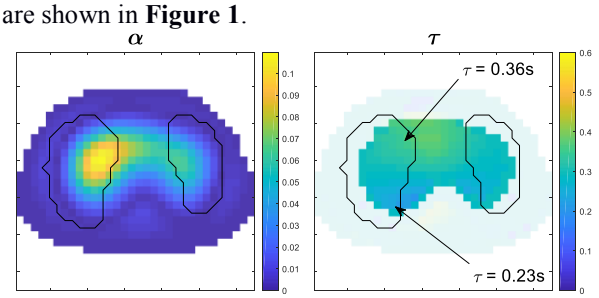

Figure 1: Fitting parameters α (left) and τ (right) of EIT image pixel signals. The colour bars indicate the scale of tidal impedance change and regional time constants.

4 Conclusions

This paper provides insight on the frequency-domain representation of the EIT images and the transfer function of the respiratory system, complementing the time-domain analysis [4,5]. The easily automatable method provides pixel-by-pixel estimates of regional respiratory time constants.

5 Acknowledgements

The indirect contribution of CRADL partners to this research is very much appreciated. This project has received funding from the European Union's Horizon 2020 Research and Innovation Programme under the grant agreement No. 668259. This work was supported by the Swiss State Secretary for Education, Research and Innovation (SERI) under contract number 15.0342-1. The opinions expressed and arguments employed herein do not necessarily reflect the official views of the Swiss Government.

References

[1] Khodadad et al. *Physiol Meas*, 39:094001, 2018
[2] Frerichs et al. *Thorax*, 72:83-93, 2017
[3] Adler et al. *Physiol. Meas.* 30(6):S35-55, 2009
[4] Pikkemaat et al. *Appl. Cardiopulm Pathophysiol,* 16:212-225, 2012
[5] Karagiannidis et al. *Critical Care* 22:221, 2018

Estimating Upper Airway Behaviour during Obstructive Sleep Apnea using EIT Imaging

Ghazal Ayoub[1], Hang Dang[2], Tong In Oh[2] and Eung Je Woo[2]

[1]Department of Biomedical Engineering, Graduate School, Kyung Hee University, Yongin, Korea
[2]Department of Medical Engineering, Graduate School, Kyung Hee University, Seoul, Korea, tioh@khu.ac.kr

Abstract: Electrical impedance tomography (EIT) can visualize the occlusion of upper airway non-invasively. In this study, we presented the ability of EIT to characterize upper airway collapsibility during sleep apnea events. A novel algorithm was applied on measured EIT data to reconstruct time difference images and extract quantitative information of the upper airway behaviour during respiratory events.

1 Introduction

Obstructive sleep apnea (OSA) is the most common sleep-disorder associated with increased likelihood of hypertension, stroke, diabetes, and other comorbidities. Plethysmography (PSG) is the conventional method of OSA diagnosis. There are many treatment methods of OSA with oral appliance, surgery, and positive airway pressure. Currently, there exist unmet clinical need to select an individualized treatment modality. The information about the obstruction pattern of the upper airway during obstructive apnea events can guide the selection of OSA treatment. The aim of this work is to provide a novel method to describe the behaviour of upper airway during OSA events.

2 Methods

We recruited OSA patients for simultaneous PSG and EIT (KHU Mark2.5, IIRC, Korea) test [1]. EIT data was recorded using 16 electrodes attached on the lower face around retroglossal space of upper airway.

2.1 Pre-processing

Both EIT and PSG data were segmented at the time of respiratory events occurrence. The measured EIT data influenced not only by upper airway occlusion but also with blood flow circulation, respiratory motions, and head motions. Therefore, we used independent component analysis (ICA) to extract the voltage component related to upper airway closing and opening. After getting the upper airway component, a full set of 208 voltage channels were recovered using source consistency algorithm [2].

2.2 Postprocessing

Time difference EIT images were reconstructed using the fidelity-embedded regularization (FER) algorithm [3]. Based on reconstructed images, the upper airway region of interest (ROI) was defined with threshold equalled 40% of the maximum pixel values. The waveform of upper airway conductivity $\Delta\sigma_U(t)$ was extracted as a sum of pixels within the ROI. The upper airway ROI was fitted to ellipse shape. The behaviour of airway was estimated based on features extracted from the $\Delta\sigma_U(t)$ waveform and from parameters of fitted ellipse such as axial ratio and rotation angle.

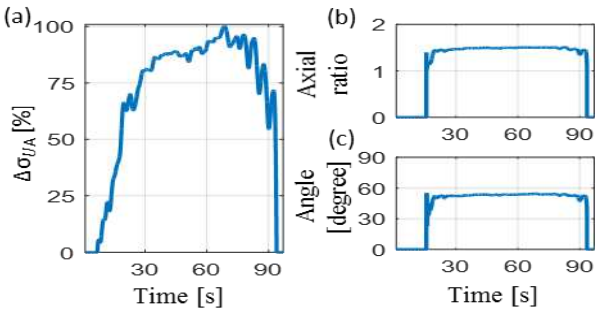

Figure 1: Obstructive sleep apnea event. (a) upper airway conductivity change, (b) axial ratio, (c) rotation angle of upper airway ROI.

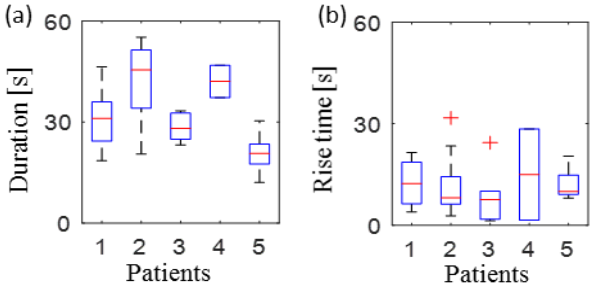

Figure 2: Feature extracted from OSA events of five patients. (a) duration, (b) rising time of OSA events.

3 Results

Figure 1 represents an example of the conductivity change, axial ratio, and rotation angle during an obstructive apnea event. The behaviour of the upper airway was specific for each patient. Figure 2 shows the duration and rising time for 5 patients during several obstructive apnea events.

4 Conclusions

EIT imaging of upper airway can provide a quantitative information of upper airway behaviour during OSA events.

5 Acknowledgements

This work was supported by a grant of the Ministry of Health and Welfare (HI17C0984) in Republic of Korea.

References

[1] H. Wi, H. Sohal, L. M. Alistair, E. J. Woo and T. I. Oh *IEEE Trans Biomed Circuits Syst.* 8:119-128, 2014.
[2] T. Zhang, G. Y. Jang, T. I. Oh, K. W. Jeung, H. Wi, and E. J. Woo, *SIAM Appl. Math* submitted, 201
[3] K. H. Lee, E. J. Woo, J. K. Seo *IEEE. Trans. Med. Imaging* 37: 1970-1977, 2018.

EIT Imaging on 3D Thorax Model for Assessing Lung Injury

Qi Wang[1], Jianming Wang[1]and Jiabin Jia[2]

[1]School of Electronics and Information Engineering, Tianjin Polytechnic University, Tianjin, China, wangqitju@163.com

[2]School of Engineering, The University of Edinburgh, Edinburgh, UK

Abstract: The global inhomogeneity (GI) index based on 3D EIT reconstruction is used to evaluate lung injury. Simulations based on 3D thorax model revealed that this method can accurately reflect the state of lung injury compared with 2D GI calculation method. Even mild damage of lung injury can be adequately detected.

1 Introduction

Global inhomogeneity (GI) has been used for the diagnosis of lung injury based on 2D EIT images, which is not suitable for the diagnosis and monitoring of mild lung injury [1]. In this paper, the GI parameter for 3D EIT reconstruction is proposed to assess the extent of lung injury. The forward and inverse problems of EIT were solved based on true 3D thorax model, considering the geometric structure of the human thorax. Simulation experiment was conducted to verify the accuracy of the proposed method.

2 Methods

2.1 EIT forward problem for true 3D thorax

The true 3D thorax model was constructed according to the human thorax structure, which was extracted from sequential CT images. To accurately extract useful information from the CT images, each CT image was processed based on threshold segmentation and contour line extraction. As shown in fig. 1(a), in order to obtain 3D reconstruction results, six electrode layers were placed on the thorax model. Each layer had 16 electrodes. In order to simulate different severity of lung injury, eight lung models were established based on the true 3D thorax, as shown in fig.1(b). Two conditions were discussed: The first condition represents the lung at end-expiration, and the second condition represents the lung at end-inspiration. The condition at end-expiration is modelled by setting the conductivity of lung tissue to σ_{exp} =120 mS/m. Other tissues not belonging to the lung are set to σ_{bkg} =480mS/m. End-inspiration is simulated by changing the conductivity of lung tissue to σ_{insp} =60 mS/m. The conductivity of lung injury does not change in both static lung conditions and remained at σ_{injury} =120 mS/m.

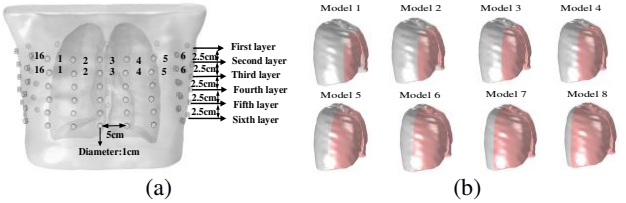

(a) (b)

Figure 1: Simulation model. (a)The true 3D thorax model with 3D electrode structure. (b) Eight different degrees of lung injury models. The red parts of the lung denote lung injury. The severity of lung injury increases from Model 1 to Model 8.

2.2 3D EIT inverse problem

To guarantee the authenticity of the image boundary. inverse problem is performed within subdivision of each layer. According to the GI calculated based on 2D image [2], this paper proposes a method for calculating GI based on 3D EIT reconstructed images,

$$\frac{\sum_{j=1}^{M}\sum_{i=1}^{N}\left|\delta\sigma_{ij}-mean\left(\delta\sigma_{lung\ ij}\right)\right|}{\sum_{j=1}^{M}\sum_{i=1}^{N}\delta\sigma} \qquad (1)$$

where $\delta\sigma_{ij}$ is the conductivity of the *i*th pixel in the *j*th layer, $\delta\sigma_{lung\ ij}$ is the conductivity change belonging to the lung, N_j is the number of pixels in the *j*th layer, M is the number of image layers.

3 Results

Fig.2 (a) shows the 3D reconstructed images with eight different severities of the lung injury. All of the images are reconstructed by the Conjugate Gradient (CG) method. The GI values are calculated according to equation (1) and the methods in reference [3], respectively. The normalized GI values for different severities of lung injury are shown in fig.2 (b).

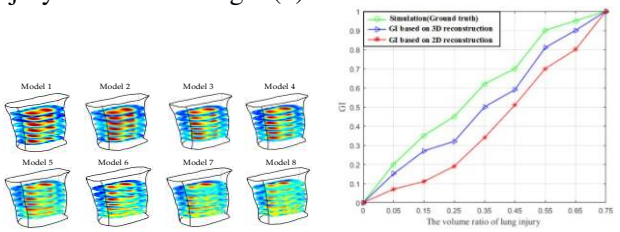

(a) (b)

Figure 2: The results. (a) Reconstructed images with different severity of lung injury. (b) GI values for eight severities of lung injury based on different methods.

From fig.2, we can see that 3D thorax images are more objective and provide more comprehensive physiological information than single 2D image slices. Compared with the traditional method, GI based on 3D reconstructed images are closer to the ground truth; it can more accurately reflect the condition of lung than 2D EIT, even low levels of lung injury.

4 Acknowledgements

This work was supported in part by the National Natural Science Foundation of China (61872269).

References

[1] B. Schullcke, Z. S. Krueger, and B. Gong, *Journal of Clinical Monitoring and Computing*, vol. 32, no. 4, pp. 753–761, 2018.

[2] Z. Hao, S. Yue and B. Sun, *Computer Assisted Surgery*, vol. 22, no. 1, pp. 326-338, 2017.

[3] J. Wagenaar and A. Adler, *Physiological Measurement*, vol. 37, no. 6, pp. 922-937, 2016

PEEP setting with EIT during one-lung ventilation in elderly patients undergoing thoracoscopic surgery

Kun Liu[1], Chengya Huang[1], Meiying Xu[1], Jingxiang Wu[1] and Zhanqi Zhao[2,3]

[1] Department of Anesthesiology, Shanghai Chest Hospital, Shanghai Jiao Tong University, wu_jingxiang@sjtu.edu.cn
[2] Department of Biomedical Engineering, Fourth Military Medical University, Xi'an, China
[3] Institute of Technical Medicine, Furtwangen University, Villingen-Schwenningen, Germany

Abstract: EIT guided PEEP settings on lung mechanics and oxygenation were superior to a fixed PEEP 5 cmH_2O, examined in 100 elderly patients scheduled for elective thoracoscopic surgery and one lung ventilation. Other outcomes e.g. lung complications rate and length of hospital stays did not differ.

1 Introduction

Elderly patients are often accompanied by pulmonary dysfunction, which is a high risk for thoracic surgery [1]. It is reported that the incidence of pulmonary complications in the elderly over 65 years after thoracic surgery is about 28% [2]. Intraoperative anesthesia and ventilation management may be critical. At present, the commonly used lung protect strategy is small tidal volume (6-8ml/kg) combined with certain level of positive end-expiratory pressure (PEEP) [3]. How to optimize the setting of PEEP during one lung ventilation is still controversial, and whether a fixed PEEP is suitable for all patients, especially in the elderly, is unclear.

The aim of the study was to examine the influence of positive end-expiratory pressure (PEEP) setting with electrical impedance tomography (EIT) versus 5 cmH_2O on lung mechanics and oxygenations in elderly patients undergoing thoracoscopic surgery.

2 Methods

One hundred patients over 65 years and scheduled for elective thoracoscopic surgery were randomly allocated into the control group and the EIT group. Other inclusion criteria included: one lung ventilation planned; postoperative hospitalization at least 2 days; American Association of Anesthesiologists score Ⅱ-III; Complete pulmonary function examination report available before operation.

Each group underwent volume-controlled ventilation (tidal volume 6 ml/kg) combined with a PEEP either fixed to 5cmH_2O or individually determined with EIT. In the EIT group, PEEP value was titrated with the regional compliance method [4] from 15 cmH_2O to 1 cmH_2O (steps of 2 cmH_2O). The primary outcomes were driving pressure (ΔP), dynamic respiratory system compliance (C_{dyn}) and ratio of arterial oxygen partial pressure to fractional inspired oxygen (PaO_2/FiO_2) at the time points of two lung ventilation (T1), one lung ventilation 0.5 h (T2), one lung ventilation 1 h (T3) and the end of operation (T4). The secondary outcomes included mean airway pressure (P_{mean}), mean arterial pressure (MAP), vasopressin drug dosage, partial pressure of carbon dioxide ($PaCO_2$), PH, lung complications and the length of hospital stays.

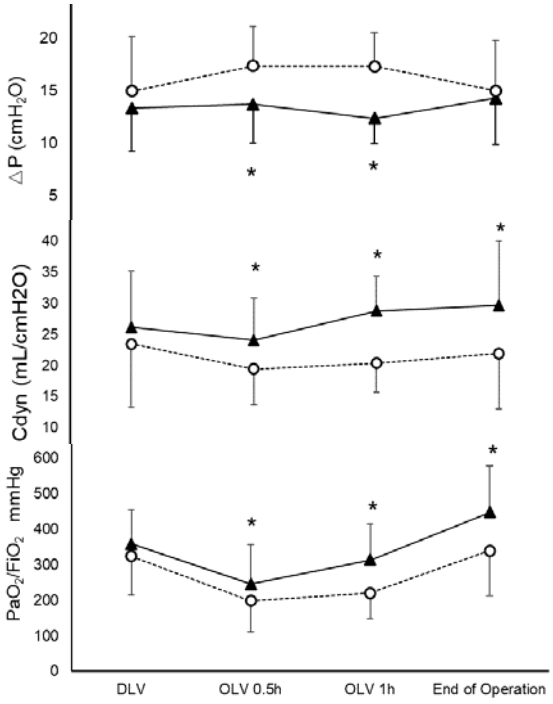

Figure 1: Comparison of driving pressure (ΔP), dynamic respiratory system compliance (Cdyn) and PaO_2/FiO_2 between EIT (solid triangle) and control group (circle) at different time points (DLV, two lung ventilation; OLV, one lung ventilation). * significant difference between groups. Means and standard deviations were presented.

3 Results

The optimal PEEP set by EIT was significantly higher (range from 9-13 cmH_2O). Primary outcome parameters can be found in Fig. 1. P_{mean} was higher in EIT group. No significant differences were found in other parameters including MAP, lung complications and length of hospital stay between two groups.

4 Conclusion

In elderly patients undergoing thoracoscopic surgery, PEEP setting with EIT may effectively improve oxygenation and lung mechanics. However, the study could not demonstrate any further significant outcome differences in this patient group.

References

[1] Y Yutaka et al. *Lung Cancer*, 125:192-197, 2018
[2] S Wang et al. *J Thorac Dis*, 9:5143-5152, 2017
[3] MO Meade et al. *JAMA*, 299:637-45, 2008
[4] EL Costa et al. Intensive Care Med, 35:1132-1137, 2009

Dynamic compliance underestimates PEEP requirement assessed by Electric Impedance Tomography

SJH Heines, U Strauch, MCG van de Poll, PMHJ Roekaerts, DCJJ Bergmans

Department of Intensive Care, Maastricht University Medical Centre+, the Netherlands, S.Heines@mumc.nl

Abstract: Electrical impedance tomography enables calculation of alveolar collapse (CL) during a PEEP trial. We selected the PEEP with a CL of <5% and compared it to the PEEP at best dynamic compliance (Cdyn). PEEP and increase in end expiratory lung impedance was smaller when using Cdyn for PEEP titration.

1 Introduction

With electrical impedance tomography (EIT) it is possible to detect alveolar overdistension (OD) and CL making it possible to select a level of PEEP based on a percentage of CL during a decremental PEEP trial[1]. A commonly used bedside PEEP titration is the best Cdyn during a decremental PEEP trial[2]. Furthermore, changes in end expiratory lung impedance (EELI) reflect changes in end expiratory lung volume. It can be used to quantify the effect of alveolar recruitment and derecruitment. The larger the decrease in EELI the larger the amount of derecruitment. The present study describes the difference in PEEP level and in increase of EELI when PEEP is titrated based upon the two above mentioned methods (EIT guided versus Cdyn guided PEEP titration).

2 Methods

In 15 patients with acute hypoxic respiratory failure (AHRF) with a PaO_2/FiO_2-ratio <200 and 20 postoperative cardiothoracic surgical patients (CTS) we used EIT for PEEP titration during an incremental-decremental PEEP trial. Patient characteristics are presented in Table 1. Optimal PEEP was selected and compared when CL was <5% (EIT guided PEEP) or when Cdyn was highest in the decremental trial. Furthermore, we compared the increase in EELI between optimal PEEP from EIT versus Cdyn by subtracting EELI of the decremental PEEP trial from EELI of the incremental trial with the same PEEP level.

2.1 Statistics

Data are expressed as a number (%) for categorical variables and as mean ±SD for continuous variables. Difference in PEEP and increase in EELI between the EIT and Cdyn guided PEEP were compared using paired sample *t*-test.

2.2 Results

There was a significant larger increase of EELI (p=.003) and a higher PEEP (p=.000) when using the EIT method compared to Cdyn for PEEP titration (Fig 1). The increase of EELI did not gain if PEEP was set another 4 cmH_2O higher than EIT guided PEEP (p=.618).

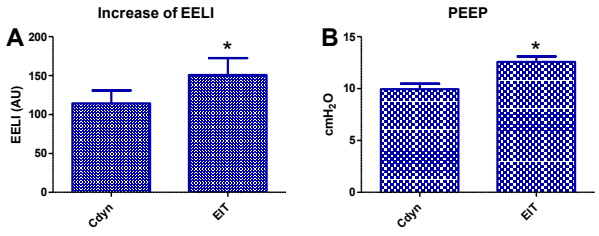

Figure 1: Significant difference in changes of EELI (A) and optimal PEEP (B) based on Cdyn versus EIT. (*p<0.05)

2.3 Discussion

When using solely Cdyn for PEEP titration, CL could already be present while Cdyn is still increasing if at the same time an amount of OD is present. This could explain the reason why the increase in EELI is smaller with Cdyn PEEP titration compared to the EIT method. Increasing PEEP further upon EIT guided PEEP, did not result in more increase in EELI, meaning EIT guided PEEP was sufficient to prevent derecruitment where Cdyn was not. EIT can visualise regional OD and CL, this may help the physician in the decision making on ventilator settings in an individual patient.

3 Conclusions

The advantage of EIT is that it can identify the level of PEEP where derecruitment begins, even if global Cdyn still increases due to some relief of OD, which can also be visualised with EIT. Using solely Cdyn may lead to an underestimation of the optimal PEEP level.

4 Acknowledgements

Not applicable.

References

[1] E Costa, J Borges, A Melo *Intensive Care Med* 35(6):1132-7, 2009
[2] F Suarez-Sipman, S Bohm, G Tusman *Crit Care Med* 35(1):214-21, 2007

Table 1: Patient characteristics. Data are presented as means ±SD, unless stated otherwise. (*$p<0.05$).

	Patients (%)	Age, years (SD)	Sex (M/F)	APACHE II (SD)	PaO_2/FiO_2-ratio
CTS	20 (57)	68 (8)	16/4	14 (3)	328 (76)
AHRF	15 (43)	58 (18)	7/8	27 (8)	116 (36)

Optimal positive end-expiratory pressure determination by electrical impedance tomography and P/V loop in acute respiratory distress syndrome patients

Hui-Ju Hsu[1,2*] David Hung-Tsang Yen[2],Hou-Tai Chang[1],and Zhanqi Zhao[3,4]

[1] Division of Chest Medicine, Far Eastern Memorial Hospital, Taipei, Taiwan, *j0917toro1002@yahoo.com.tw

[2] Institute of Emergency and Critical Care Medicine, National Yang-Ming University, Taiwan

[3] Department of Biomedical Engineering, Fourth Military Medical University, Xi'an, China

[4] Institute of Technical Medicine, Furtwangen University, Villingen-Schwenningen, Germany

Abstract: Patients with acute respiratory distress syndrome were randomized in two groups. Optimal positive end-expiratory pressure was titrated with EIT and Maximal Hysteresis in pressure/volume loop in each group respectively. Outcome parameters were compared.

1 Introduction

The mortality rate of ARDS is high (35–46% from mild to severe) [1]. The acute phase is usually accompanied with moderate to severe hypoxemia. Positive end-expiratory pressure (PEEP) may improve oxygenation but at the same time may induce barotraumas. The best PEEP selection method is still under debate. The aim of the study was to compare EIT-based PEEP selection method (EIT group) with a ventilator embedded method based on PV loop (G5 group).

2 Methods

This randomized control trials study was conducted from April 2017 to February 2019 in the ICU of FEMH (FEMH-106094-E). Patients with moderate to severe ARDS according to Berlin criteria were included. The exclusion criteria were clinical contraindications applying EIT or high PEEP level. All patients were total sedated to prevent any spontaneous breathing and ventilated under volume-control mode (IBW/6ml/kg) and FiO_2 100%. The G5 group used Hamilton G5 to measure the PV loop. The lungs were inflated with an increase pressure of 3 cmH_2O/sec from 5 cmH_2O to 40 cmH_2O. The pressure was kept constant at 40 cmH_2O for 1 second. Subsequantly, the lungs were passively deflated down to 5 cmH_2O. PEEP with maximal hysteresis (volume difference in the PV loop) was defined as optimal. In the EIT group, optimal PEEP was defined according to the regional compliance method published elsewhere [2]. The methods are illustrated in Fig. 1.

Parameters including optimal PEEP, airway pressures, compliance (Crs), and PEEP, APACHE II, PaO_2/FiO_2, ICU day, MV day, MV free day, resistance of the respiratory system (R) were measured and recorded.

3 Results

Totally 87 patients were included so far. Preliminary results are presented in Table 1.

4 Conclusion

PEEP titration guided with EIT is feasible and may be superior than the PEEP selected by the Hamilton G5 ventilator based on PV loop.

Table 1: Comparison of outcomes between the EIT and control groups

Demographics	G5 group (n=45)	EIT group (n=42)	*P* value
Survival n	19 (42.2%)	29 (69%)	<0.05
Optimal PEEP (cmH_2O)	17.4 ± 1.7	16.2 ± 2.6	<0.05
PaO_2/FiO_2 24hr later	196.3 ± 95.8	214.2 ± 90.7	0.38
MV free day (within28 Days)	2.6 ± 4	3.7 ± 4.5	0.23

References

[1] E Rezoagli, *et al.Ann Transl Med*,5:282-93,2017

[2] E Costa, *et al. Intensive Care Med*,35: 1132-37, 2009

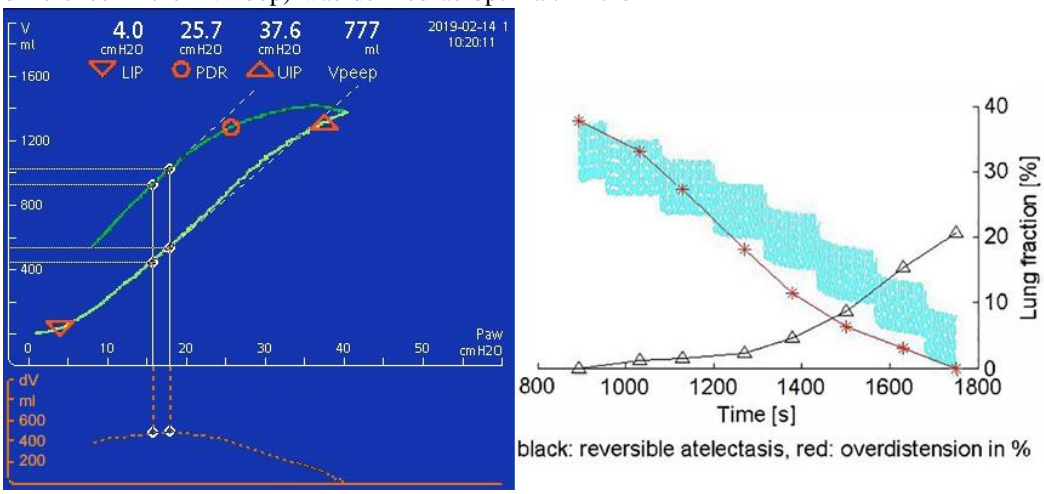

Figure 1: PEEP titration with G5 ventilator using maximal hysteresis in PV loop (Left) and EIT-based regional compliance (Right).

Cardiac Eigen Imaging: Isolating Cardiac Activity in Thoracic EIT

Saaid H. Arshad[1], Ethan K. Murphy[1], Joshua M. Callahan[2], James T. DeVries[2], Kofi Odame[1], and Ryan J. Halter[1,2]

[1]Thayer School of Engineering, Dartmouth College, Hanover, NH
[2]Dartmouth-Hitchcock Medical Center, Lebanon, NH

Abstract: Cardiac Eigen Imaging (CEI) is proposed as a novel method to isolate cardiac activity in thoracic electrical impedance tomography (EIT). The method is developed, tested, and compared to a standard approach, regular-cardiac gated averaging (RCGA), on 20 heart-failure patients. CEI obtains a correlation of 0.81 with SV, an improvement over RCGA, which obtains 0.70 at best.

1 Introduction

Stroke volume (SV) is the volume of blood pumped out by the heart every beat and is an important indicator of cardiovascular health [1]. Current methods of monitoring SV are not reliable in long-term, continuous monitoring settings, making it challenging for clinicians to deliver proactive healthcare. Electrical impedance tomography (EIT) has the potential to non-invasively monitor SV over long periods of time. Here we present a novel method called Cardiac Eigen imaging (CEI) as an improvement over a standard approach, regular cardiac gated averaging (RCGA).

2 Methods

2.1 Patient Data Collection

Data was collected from 20 patients scheduled for echocardiography under an IRB-approved study. EIT data was recorded immediately before the echocardiography procedures using a 32-channel SwissTom Pioneer Set with electrodes positioned at the nipple plane between the 3rd and 4th intercostal space. Pulse oximeter (PO) and ECG-based heart-rate data was collected using a BIOPAC MP150 data acquisition system. Data was collected on patients sitting up as they were regularly breathing. Reconstructions are computed with a standard Gauss-Newton EIT algorithm using the dual-mesh method.

2.2 Regular Cardiac-Gated Averaging

RCGA uses heart-rate (HR) data to define end-diastole (ED) and end-systole (ES) in a heart-cycle, and then uses that information to define the equivalent points temporally in the EIT data. It is defined as:

$$\Delta\overline{\boldsymbol{v}}_{\mathrm{RCGA}} = \frac{1}{\mathrm{N_C}}\sum_{\mathrm{c}=1}^{\mathrm{N_C}}\left(\boldsymbol{v}_{\mathrm{ED,c}} - \boldsymbol{v}_{\mathrm{ES,c}}\right) \quad (1)$$

where $\Delta\overline{\boldsymbol{v}}_{\mathrm{RCGA}}$ is the average voltage measurement vector from RCGA, $\mathrm{N_C}$ the total number of heart cycles recorded over the imaging period, $\boldsymbol{v}_{\mathrm{ED,c}}$ is a frame of voltage data at ED for cardiac cycle c, and $\boldsymbol{v}_{\mathrm{ES,c}}$ is a corresponding ES frame from the same heart cycle. This creates an average signal representative of the voltage change due to SV which is then reconstructed into an image representative of the conductivity change due to SV.

2.3 Cardiac Eigen Imaging

CEI uses the Singular Value Decomposition (SVD) along with an *a priori* canonical image representing cardiac activity to isolate cardiac activity in EIT data. After applying the SVD on preprocessed EIT data, the first three left singular vectors and their linear combinations are compared with the canonical image:

$$s_i = \frac{\widehat{\mathbf{U}}_i^{\mathrm{P}\times 1}}{\|\widehat{\mathbf{U}}_i^{\mathrm{P}\times 1}\|} \cdot \frac{\widehat{\boldsymbol{\sigma}}_{can}^{\mathrm{P}\times 1}}{\|\widehat{\boldsymbol{\sigma}}_{can}^{\mathrm{P}\times 1}\|} \quad (2)$$

where $\widehat{\mathbf{U}}_i^{\mathrm{P}\times 1} \in [\Sigma_{1,1}U_1,\ \Sigma_{2,2}U_2,\ \Sigma_{3,3}U_3,\ \Sigma_{1,1}U_1 + \Sigma_{2,2}U_2,\ \Sigma_{2,2}U_2 + \Sigma_{3,3}U_3,\ \Sigma_{1,1}U_1 + \Sigma_{2,2}U_2 + \Sigma_{3,3}U_3]$. The singular vector or vector combinations that had the highest inner product with the canonical image, $\widehat{\boldsymbol{\sigma}}_{can}^{\mathrm{P}\times 1}$, is used as the basis image for that patient, with the vector aligned to be in the same direction as the canonical image. That is, the final CEI image is given by:

$$\widehat{\boldsymbol{\sigma}}_{i_{cardiac}}^{\mathrm{P}\times 1} = \mathrm{sign}(\boldsymbol{s}_{i_{cardiac}})\widehat{\mathbf{U}}_{i_{cardiac}}^{\mathrm{P}\times 1} \quad (11)$$

where $i_{cardiac} = \arg\max_{i\in[1\ 6]}(|\mathbf{s}|)$. For analysis, high-correlating pixels with Pearson correlation coefficients greater than 0.5 were compared between RCGA and CEI across patients.

3 Results and Conclusions

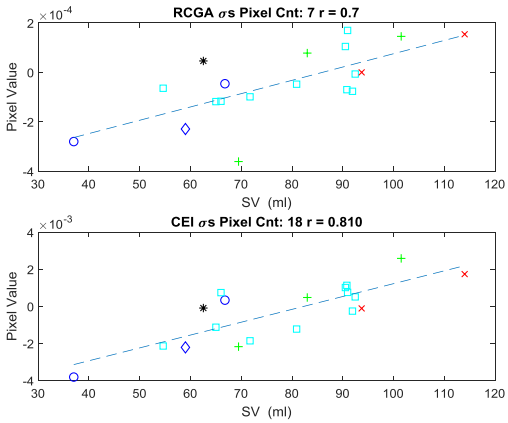

Figure 1: RCGA and CEI correlations with SV.

The RCGA images identify 7 highly correlating pixels with an average of r ~ 0.70. The CEI images have 18 highly correlating pixels that attain an average r ~ 0.81. CEI outperforms RCGA and represents a novel approach to SV assessment that does not rely on capturing high quality ECG or pulse ox signatures and can be performed during normal breathing patterns.

References

[1] Hall Critchley L A 2013 Artery Bypass (InTech)

Graphical User Interface for Patient Data Overview of long and continuous EIT monitoring for research analysis

A. Dupré[1], M-R. Benissa[1], B. Müller[2], A.D. Waldmann[2], R. Yerworth[3], T. Becher[4], M. Miedema[5], S.Nordebo[6], D. Khodadad[6], I. Frerichs[4], R. Bayford[7], P.C. Rimensberger[1,8]

[1]Department of Paediatrics, University of Geneva, Switzerland, antoine.dupre@alumni.epfl.ch
[2]SenTec AG, Switzerland [3]University College London, UK [4]University Medical Centre Schleswig-Holstein, Germany [5]University of Amsterdam and Vrije Universiteit Amsterdam, Netherlands [6]Linnaeus University, Sweden [7]Middlesex University, UK
[8]Neonatalogy and Intensive Care Unit, University Hospital of Geneva, Switzerland

Abstract: This paper describes the graphical user interface for patient data overview developed specifically for the CRADL project.

1 Introduction

Electrical Impedance Tomography (EIT) is an imaging technique allowing continuous measurement of regional distribution of ventilation in the lungs. The information immediately available to the clinicians at the bedside provides a relevant insight to guide therapy [1]. In some cases, post-clinical analysis or research will require the retrospective investigation of the important amount of continuously-monitored data by the medical teams.
The clinical study (NCT02962505) within the CRADL project monitored 200 neonatal and paediatric patients continuously for up to 72 hours. The huge amount of recorded data (over 1.9 billion EIT frames, i.e. 461 days) represents a challenge in terms of user-friendly visualisation and interpretation. A graphical user interface (GUI) for patient data overview (PDO) has been specifically developed to display the data for research-oriented clinicians.

2 Method

The GUI was developed with the Matlab AppDesigner module. Once compiled into an executable, it requires the Matlab Runtime Compiler software to be used. The software uses about 700MB of RAM.
The EIT data, containing already reconstructed images, was pre-processed and thereby significantly compressed. Videos were converted using mp4 compression. Essentially, frame-by-frame EIT signals were discarded or converted to breath-by-breath signals. As a drawback, compression has to be reprocessed in case of modifications in the breath detection algorithm [2].
The initial CRADL data set represents 25 TB. The compression of EIT data is an active subject of research [3]. However, after pre-processing, the data used for clinical research represents 220 GB and can be stored locally (50 GB of which represent the video files recorded simultaneously with the EIT data to validate clinical events retrospectively).

3 Results

Three levels of visualisation have been implemented in the software. The first tab displays general patient information (ID, gender, weight, reason for inclusion, etc.). The second tab displays the timeline, i.e. the set of EIT files ordered chronologically with essential information to help the user to navigate to the event of interest (Figure 1). The third tab displays EIT-derived signals and video for the selected file (Figure 2).
User Declared Events (UDE) complement Clinically Declared Events (CDE) declared on the monitor during measurements (mode of ventilation, body position, clinical interventions, etc). A large number of project partners contributes to the analysis and clinical interpretation of the data. A cloud-based collaborative feature (hosted on dedicated space of a secured FTP server) has been developed in order to share the UDE.

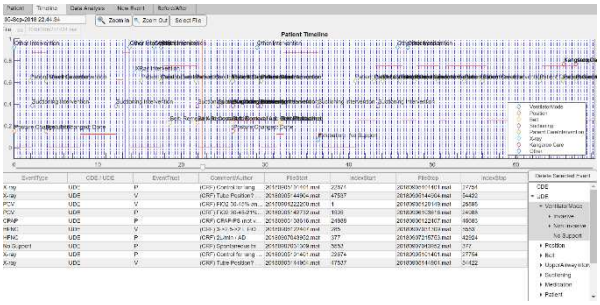

Figure 1: Screenshot of the PDO-GUI – Patient Timeline tab featuring the set of EIT files in the patient folder.

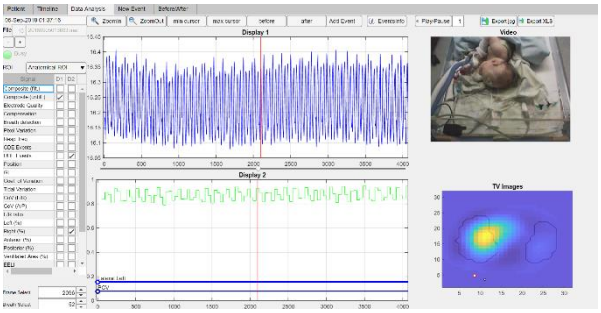

Figure 2: Screenshot of the PDO-GUI – Data Analysis tab with various EIT-derived signals, UDE, video, etc.

4 Acknowledgements

This project has received funding from the European Union's Horizon 2020 Research and Innovation Programme under the grant agreement No. 668259.
This work was supported by the Swiss State Secretary for Education, Research and Innovation (SERI) under contract number 15.0342-1. The opinions expressed and arguments employed herein do not necessarily reflect the official views of the Swiss Government.

References

[1] Frerichs et al. *Thorax*, 72:83-93, 2017
[2] Khodadad et al. *Physiol Meas*, 39:094001, 2018
[3] Shiraz et al., *Physiol Meas*, 40:034010, 2019

EIT Meshing and Forward Solution Using HPC

Thomas Dowrick[1], James Avery[2], Roland Guichard[3], David Perez-Suarez[3] and David Holder[4]

[1]Wellcome/EPSRC Centre for Surgical and Interventional Sciences, University College London, UK, t.dowrick@ucl.ac.uk
[2]Department of Surgery and Cancer, Imperial College London, London, W2 1NY, United Kingdom
[3]Research Software Development Group, University College London
[4]Medical Physics and Biomedical Engineering, University College London

Abstract: EIT forward simulations of high resolution meshes in the human head/rat brain (>10M elements) are very computationally intensive, requiring in excess of 5 hours for large protocols and electrode counts.
An ARCHER eCSE project has been undertaken to translate UCL's EIT-MESHER and EIT-PEITS code to the ARCHER supercomputer service, facilitaing rapid deployment of large numbers of complex simulations, and producing HPC tools that can be used by the EIT community.

1 Introduction

The UCL-MESHER [1] software provides a method for generating high quality meshes from segmented and labelled CT/MRI scans, for use in EIT simulations (Figure 1). This is complemented by UCL-PEITS [2-3] which provides an efficient solver for the EIT forward solution, which makes use of MPI to utilise multiple cores during computation, reducing the overall solution time (Table 1). While both packages are available to the EIT community through an open-source license, usability and performance scaling issues were identified, which required additional software engineering experience to rectify. Complex simulations (>100 protocol lines on a >10 million element mesh) can take in excess of 10 hours on an 8 core workstation. By porting to the codebase to work on local or national scale supercomputing services, it will be possible to a) run with a greatly increased number of parallel cores, and b) despatch multiple jobs in parallel e.g. 10 different simulations each running on 10 cores.

2 Methods

Funding was received from the ARCHER supercomputer service to fund 2 months of development time by UCL's Research Software Development Group, with the following aims:

- Update code to use the latest versions of petsc/dune libraries.
- Containerise the software using Docker/Singularity to enable easier distribution among the community.
- Deploy the software on UCL's supercomputer service (LEGION) and eventually on ARCHER.
- Investigate the performance as the number of cores is scaled up.
- Investigate the performance of multiple jobs despatched in parallel.

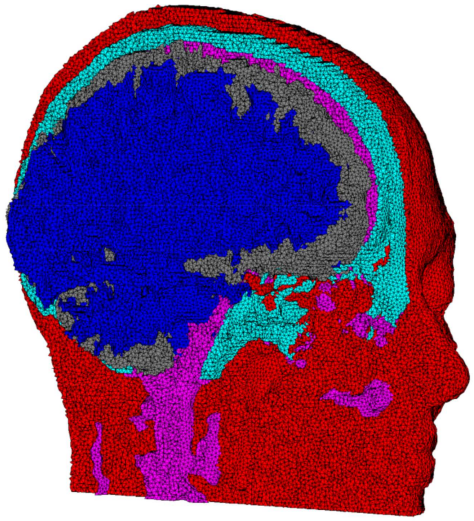

Figure 1: Layered cut through a 5-m element head mesh with scalp, skull, CSF, and gray and white matter, created using EIT-MESHER.

3 Acknowledgements

This was work funded by an ARCHER eCSE grant (eCSE13-11)

References

[1] https://github.com/EIT-team/Mesher
[2] https://github.com/EIT-team/PEITS
[3] A Fast Parallel Solver for the Forward Problem in Electrical Impedance Tomography, Markus Jehl, Andreas Dedner, Timo Bekte, Kirill Aristovich, Robert Klofmon, David Holder, IEEE Transcations on Biomedical Engineering, 2014

Table 1: Time in seconds taken by EIT-PEITS to compute one forward solution [3].

Mesh elements	**2 million**	**5 million**
1 process	18.5	399
2 processes	8.3	169
5 processes	3.6	77
10 processes	2.25	45.8
20 processes	0.6	22.3
40 processes	0.58	13.0
60 processes	1.3	9.6

Non-difference static EIT imaging using linear method

Kyounghun Lee[1,2]

[1]Sciospec Scientific Instruments GmbH, Germany k.lee@sciospec.de
[2]Department of Computational Science and Engineering, Yonsei University, South Korea imlkh84@gmail.com

Abstract:

The non-linear problem of reconstructing conductivity from EIT data can be considered as a linear problem of reconstructing the reciprocal of a weighted average of conductivity. This observation leads to a static EIT imaging using a linear method without need of reference data.

1 Introduction

Although difference EIT imaging techniques such as time- and frequency-difference imaging achieved success in some applications, it is still desirable to have a practical static method without reference data. We propose a robust static method and validates using human cheat data.

2 Methods & Results

For simplicity, we restrict our description to the case of a 16-channel EIT system using the neighboring data collection scheme. Let $V^{i,j}$ be the measured voltage between the electrode pair $(\mathcal{E}_i, \mathcal{E}_{i+1})$ subject to the jth injection current. For the voltages measured on the non-current carrying electrodes, the relation between σ and $V^{i,j}$ is expressed approximately as [1]:

$$V^{i,j} = \int_\Omega \sigma(\mathbf{r}) \nabla u_i^\sigma(\mathbf{r}) \cdot \nabla u_j^\sigma(\mathbf{r})\, d\mathbf{r}, \tag{1}$$

where u_j^σ is the electrical potential distribution corresponding to the jth injection current. Using the integration by parts, (1) can be expressed as

$$V^{i,j} = \int_\Omega \nabla v_i(\mathbf{r}) \cdot \nabla u_j^\sigma(\mathbf{r})\, d\mathbf{r}, \tag{2}$$

where v_i is the potential induced by the ith injection current with the unit conductivity ($\sigma = 1$). Note that if σ is homogeneous, that is, constant over Ω, $\frac{\nabla v_i \cdot \nabla u_j^\sigma}{\nabla v_i \cdot \nabla v_j} = \sigma$ over Ω. This motivates us to investigate the ratio $\rho_{i,j}^\sigma$:

$$\rho_{i,j}^\sigma(\mathbf{r}) := \frac{\nabla v_i(\mathbf{r}) \cdot \nabla v_j(\mathbf{r})}{\nabla v_i(\mathbf{r}) \cdot \nabla u_j^\sigma(\mathbf{r})} \tag{3}$$

Figure 1(Left) shows the distribution of reciprocal of $\rho_{i,j}^\sigma$ for circular shaped domain when an ellipse shaped anomaly, having κ as conductivity value, is located near injection electrodes with background conductivity value κ_0. The contrast of $\left(\rho_{i,j}^\sigma\right)^{-1}$ is very similar to that of σ near the current injection electrodes. Moreover, Figure 1(Right) shows that $\frac{1}{\rho_{i,j}^\sigma(\mathbf{r}_{\text{anomaly}})}\frac{1}{\kappa_0} - 1$ is proportional to $\frac{\kappa}{\kappa_0} - 1$. This implies that $\rho_{i,j}^\sigma(\mathbf{r}_{\text{anomaly}})$ is the reciprocal of a weighted average of conductivity values κ and κ_0 (or a weighted harmonic average of resistivities $1/\kappa$ and $1/\kappa_0$):

$$\rho_{i,j}^\sigma(\mathbf{r}_{\text{anomaly}}) = \frac{1}{w\kappa + (1-w)\kappa_0}, \tag{4}$$

where w is the weight and depends on the size of anomaly as shown in Figure 1(Right).

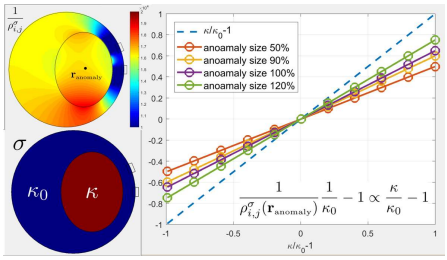

Figure 1: (Top left) The distribution of $\left(\rho_{i,j}^\sigma\right)^{-1}$ (Bottom left) The conductivity distribution (Right) The graph of $\frac{1}{\rho_{i,j}^\sigma(\mathbf{r}_{\text{anomaly}})}\frac{1}{\kappa_0} - 1$ over $\frac{\kappa}{\kappa_0} - 1$

Since the ratio $\rho_{i,j}^\sigma$ can be considered as the reciprocal of a weighted average of conductivity, it is desired to recover $\rho_{i,j}^\sigma$ from the data $V^{i,j}$ to identify anomaly. For this, we rewrite (2) as:

$$V^{i,j} = \int_\Omega \rho_{i,j}^\sigma(\mathbf{r})\, \nabla v_i(\mathbf{r}) \cdot \nabla v_j(\mathbf{r})\, d\mathbf{r}. \tag{5}$$

For simplicity, we neglect the dependency of $\rho_{i,j}^\sigma$ on i, j and consider the following minimizing problem:

$$\bar{\rho} = \arg\min_\rho \sum_{i,j} \left| V^{i,j} - \int_\Omega \rho(\mathbf{r}) \nabla v_i(\mathbf{r}) \cdot \nabla v_j(\mathbf{r})\, d\mathbf{r} \right|^2.$$

The minimizer $\bar{\rho}$ satisfies the system of linear equations after discretization $\Omega = \cup_k \Omega_k$:

$$\mathbf{V} = \mathbb{S}\bar{\boldsymbol{\rho}}, \tag{6}$$

where $\mathbb{S}$ is the sensitivity matrix, $\mathbf{V}$ is the voltage vector of $V^{i,j}$, and $\bar{\boldsymbol{\rho}}$ is the vector of $\bar{\rho}|_{\Omega_k}$. Although the problem (6) to recover $\bar{\boldsymbol{\rho}}$ is linear, it is difficult to solve because of high sensitivity near boundary. To alleviate this, we remove the portion of $\mathbf{V}$ correlated to the boundary sensitivity by utilizing the motion artefact filter [1]. Then, we solve (6) using FER method [1]. Figure 2 shows the reconstructed distribution of $\bar{\boldsymbol{\rho}}$ using lung ventilation data acquired from normal human using the proposed static method. The reconstructed value $\bar{\boldsymbol{\rho}}$ at lung region is bigger than the background. This is because $\bar{\boldsymbol{\rho}}$ is the reciprocal of conductivity.

References

[1] K Lee, E J Woo, J K Seo *IEEE Trans Med Imaging*, 37:1970-1977, 2018

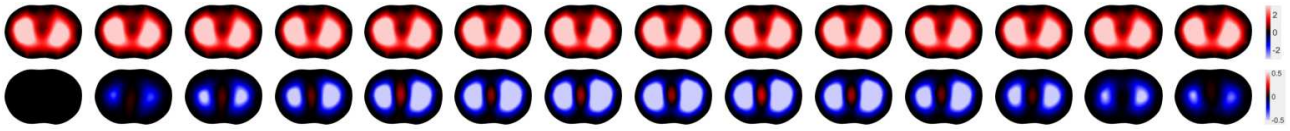

Figure 2: Comparison of static imaging (first row) with time-difference imaging (second row) by the proposed method

Transient Circuit Simulation of (Cole-Cole) Fractional-Order Models for Biomedical Instrumentation

Alistair Boyle

Systems and Computer Engineering, Carleton University, Canada, boyle@sce.carleton.ca

Abstract: In an ongoing process of interviewing designers of EIT and ERT instruments, realizing AC current sources that perform well *in situ* has been identified as a major source of instrument design challenges due to broadband switching transients. Circuit simulations often do not reflect performance on biological media.

1 SPICE Simulators

There are many closed source variants of the SPICE circuit simulator freely available or under commercial licenses. Examples include PSPICE (Cadence), HSPICE (Synopsys), LTspice (Linear Technology), and TINA-Ti (Texas Instruments). Two open source variants are ngspice (GPL), and the original code for spice3f5 (BSD) [1]. There are a host of alternatives with an equally broad selection of slightly incompatible or ill-defined SPICE dialects. Various SPICE implementations support an array of control constructs, measurement and plotting which automate common tasks. Circuits designed with SPICE tools, with some careful simulation work, can achieve admirable correlation with lab-measured results. In general, simulation tools accelerate the debug/test loop by enabling rapid iteration and exploration which minimizes hardware design costs.

The circuit simulation tools are capable of large and small signal steady-state, transient, and noise performance simulations on linear elements (RLC), mixed signal (integrated digital logic), complex semiconductor device models, and behavioural models. Many semiconductor products, such as op-amps and high-speed interfaces, have vendor-supplied SPICE models for use in analog design and signal integrity work.

SPICE models support integer exponents, for example ideal capacitors are modelled in the frequency domain as $1/\mathbf{j}\omega C$. A second-order filter has a transfer function with a denominator term $(\mathbf{j}\omega)^2$. Fractional exponents do not generally occur in common circuit analysis practice. This mismatch in simulator capability means that when a circuit (for example, an EIT current source) is connected to biological media, instead of a resistor phantom, performance often degrades to an unanticipated level.

2 Fractional-Order Models

Biological media can be characterized by multiple "dispersions" over frequency using a summation of multiple Cole-Cole models as a complex-valued permittivity $\hat{\epsilon}$ [2, 3]

$$\hat{\epsilon} = \epsilon_\infty + \sum_m \frac{\Delta\epsilon_m}{1 + (\mathbf{j}\omega\tau_m)^{(1-\alpha_m)}} + \frac{\sigma}{\mathbf{j}\omega\epsilon_0}$$

for the permittivity of free space $\epsilon_0 = 8.8542 \times 10^{-12}$ F/m, angular frequency $\omega = 2\pi f$, and $\mathbf{j} = \sqrt{-1}$. The high frequency permittivity ϵ_∞, low-frequency ionic conductivity σ, time constants τ_m, breadth $0 \leq \alpha_m \leq 1$, and the permittivity difference $\Delta\epsilon_m = \epsilon_m - \epsilon_\infty$ for a particular permittivity ϵ_m at $\omega\tau_m \ll 1$ define a complex permittivity which can be converted to complex conductivity σ^*

$$\sigma^* = \mathbf{j}\omega\epsilon_0\hat{\epsilon} = \sigma + \mathbf{j}\omega\epsilon_0\epsilon \quad \text{for} \quad \hat{\epsilon} = \epsilon + \frac{\sigma}{\mathbf{j}\omega\epsilon_0}$$
$$= \sigma + \mathbf{j}\omega\epsilon_0 \left(\epsilon_\infty + \sum_m \frac{\Delta\epsilon_m}{1 + (\mathbf{j}\omega\tau_m)^{(1-\alpha_m)}} \right)$$

and used in an FEM forward EIT computation.

This FEM can be reduced to an n-port RLC network over n electrodes [4] and simulated in SPICE tools as a linear passive subcircuit to calculate large signal steady-state solutions at a fixed frequency ω. For broadband behaviour over frequency ω, the non-integer exponent α_m leads to *fractional-order models*.

Modelling of fractional-order super-capacitor, lithium-ion, and photo-voltaic power performance (off-grid, mobile and low power devices), certain control systems, chaotic and biological systems modelling, and the design of fractional-order filters and ultra low voltage sensors suffer from a lack of support in circuit simulation tools [5].

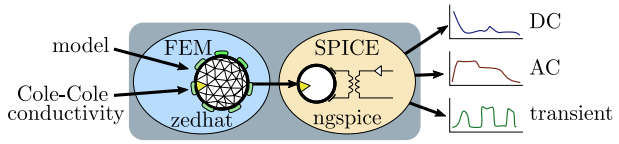

Figure 1: Proposed connection between EIT FEM modelling (zedhat) and SPICE circuit simulation (ngspice)

3 Solution Approaches

Common simulators do not have fractional-order elements (e.g. Constant Phase Elements) for building biological models. Two approaches have been suggested in recent publications: to fit RC networks to the complex impedance spectra [6] over a certain bandwidth, or to solve using nonlinear Modified Nodal Analysis (MNA) and convolution [7, 8].

We propose a code linking specialized EIT FEM software and SPICE circuit simulation (Figure 1). We invite discussion of the utility of such a tool building on an integration of FEM Cole-Cole models from the new `zedhat` software library.

References

[1] Quarles T. *Analysis of Performance and Convergence Issues for Circuit Simulation*. Ph.D. thesis, University of California, Berkeley, 1989
[2] Cole KS, Cole RH. *Journal of Chemical Physics* **9**(4):341–351, 1941
[3] Gabriel C. Tech. Rep. Report AI/OE-TR-1996-0004, Occupational and Environmental Health Directorate, Radiofrequency Radiation Division, Brooks Air Force Base, USA, 1996
[4] Boyle A, Adler A. In *EIT2018*. Edinburgh, UK, 2018
[5] Elwakil A **10**(4):40–50, 2010
[6] Freeborn T, Elwakil A, Maundy B. *Mathematical Problems in Engineering* **2016**(1):1–10, 2016
[7] Magin R, Ortigueira M, Podlubny I, et al. *Signal Processing* **91**(3):350–371, 2011
[8] Athanasiou V, Konkoli Z. *International Journal of Circuit Theory and Applications* **46**(5):1072–1090, 2018

Testing a conductive and flexible phantom of a neonatal torso for EIT

Serena de Gelidi[1], Andy Bardill[1], Nima Seifnaraghi[1], Yu Wu[2], Andreas Demosthenous[2], Erich Sorantin[3], Andrew Tizzard[1], Richard Bayford[1]

[1]Middlesex University, London, United Kingdom s.degelidi@mdx.ac.uk
[2]University College London, London, United Kingdom
[3]Medical University of Graz, Graz, Austria

Abstract: A novel conductive phantom has been produced in the shape and dimension of a simplified neonatal torso for EIT *in vitro* testing. In order to test its sensitivity, preliminary analyses have been carried out by reconstructing its EIT image when materials of different conductivity are filling the lung cavities.

1 Introduction

Phantoms are objects that offer a controlled testing environment to carry out experiments that mimic the clinical application of a device. Although the saline-filled cylindrical tanks are the most commonly used among the EIT community [1], they are not viable options for the development of a wearable device as they are always made of a insulating material. Therefore conductive phantoms of a skull, breasts and a pelvis have started to be prepared. As part of the CRADL project (http://cradlproject.org/), which is developing EIT technology as supportive method for monitoring the ventilation of the newborns, the need of a conductive and flexible phantom for *in vitro* testing of the neonatal prototypes arose. A previous study [2] generated a simplified neonatal torso printed out of carbon filled thermoplastic polyurethane Palmiga 95-250 (Creative Tools, Sweden). This work aims to obtain the EIT reconstruction of the phantom while highlighting the presence of different materials in the lung cavities, similarly to the introduction of objects in the classic cylindrical tank.

2 Methods

The belt prototype to test the phantom was made of 32 copper tape electrodes placed on a PVC substrate. Salt-free electrode gel (Spectra 360, Parker Laboratories, US) was applied on the interface between the belt electrodes and the phantom.

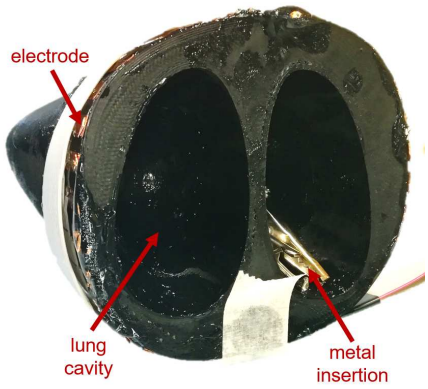

Figure 1: The neonatal phantom tested by means of a passive belt while the lung cavities are air filled and a small piece of metal is inserted.

The raw measurements were recorded by the Pioneer Set (SenTec AG, CH) and processed in a Matlab (The MathWorks, US) custom script by means of the GREIT algorithm [3] using the EIDORS v 3.9 toolbox. The image has been calculated as difference EIT with the reference measurement, during which the lung cavities of the idealized phantom were filled by the same material used to print the torso. Therefore, the reference domain is homogeneous. Aiming to test the possibilities of the phantom, materials of different conductivities were inserted in one cavity during different experiments. Hence, first a small piece of rubber was used to almost fill one cavity, while the other one was filled by air. In a different test, a small crocodile clip was swapped to the rubber insertion as shown in Figure 1.

3 Results

The EIT image reconstruction of the phantom featuring the rubber insertion shows limited difference in conductivity change compared to the case in which both lung cavities are filled just by air. Differently, the metal inclusion shown in Figure 1 generates an obvious localised positive change of conductivity.

4 Discussion

Preliminary results demonstrate that the conductive phantom offers the possibility to discriminate insertion of different materials similarly to the classic cylindrical tank. Such feature could be used to mimic certain lung diseases for the hardware development and for the training of clinicians. However, further tests are required to understand in which settings the reconstructed image reports correctly the position of the inclusion in the left or right lung, being the division between them physically narrow in the present simplified phantom. In order to take into account the deformation of the phantom, the EIT reconstructed image of the undeformed phantom will also be compared to the corresponding arbitrary deformed one. This study has the potential to generate a dynamic phantom to train clinicians for the EIT monitoring.

5 Acknowledgements

This work is supported by the CRADL project which has received funding from the European Union's Horizon 2020 research and innovation programme 2014-2018 under grant agreement No 668259.

References

[1] Grychtol B, Müller B, Adler A. *Physiol Meas*, 37:785–800, 2016
[2] de Gelidi S, Seifnaraghi N, Bardill A, Wu Y, Frerichs I, Demosthenous A, Tizzard A, Bayford R. *J Med Eng Phys*, Under review
[3] Adler A, Arnold J H, Bayford R, Borsic A, Brown B, Dixon P, Faes T J, Frerichs I, Gagnon H, Gärber Y, Grychtol B, Hahn G, Lionheart W R, Malik A, Patterson R P, Stocks J, Tizzard A, Weiler N, Wolf G K. *Physiol Meas*, 2009

Entirely EIT-Based Aortic Detection

Lisa Krukewitt[1], Fabian Müller-Graf[1], Karin H. Wodack[2], Sarah Bühler[2], Amelie Zitzmann[1], Stephan H. Böhm[1], Sascha Spors[3], Daniel A. Reuter[1]

[1]Department of Anesthesiology and Intensive Care Medicine, University Medical Center Rostock, Rostock, Germany
lisa.krukewitt@uni-rostock.de
[2]Department of Anesthesiology, Center of Anaesthesiology and Intensive Care Medicine, University Medical Center Hamburg-Eppendorf, Hamburg, Germany
[3]Institute for Communications Engineering, University of Rostock, Rostock, Germany

Abstract: We propose an algorithm to detect the aorta in EIT images during apnea based on pulse arrival time (PAT), intensity, and pulse shape. In data of four different pigs, the average distance between the aortic pixel found with this method and that found by bolus injection was 2.3 pixels in a 64×64 pixel image.

1 Introduction

While detection of the aorta in EIT images would be an important first step to EIT-based non-invasive monitoring of central haemodynamics, previously proposed methods for aorta detection relied either on the injection of a saline bolus [1] for spatial detection or the use of an aortic catheter as a trigger for a time-based algorithm [2]. We now propose an algorithm that relies solely on EIT during periods of apnea and thus requires neither reference nor invasive signals.

2 Methods

2.1 Study Protocol

We analysed data from four pigs used in a previous study [1] with two measurements during apnea for each animal. The data were acquired with the EIT Pioneer Set (Swisstom AG, Landquart, Switzerland) and the image reconstruction was done as described in [1]. The data were then filtered with a 20th order high pass finite impulse response (FIR) filter with a corner frequency of 0.1 Hz and a 10th order low pass FIR filter with a corner frequency 1.5 Hz above the heart rate.

2.2 Algorithm

We first selected an estimated heart region of 5×5 pixels. We defined heart pixels as pixels within the assumed anatomical location of the heart and having a higher spectral energy in the typical range of the heart rate between 1 Hz and 2 Hz than the surrounding pixels as shown in figure 1.

We then calculated the following for each of the 25 selected heart pixels: A cardiac cycle was defined as the time frame between two maxima of the EIT signal of the heart pixel. Calculating an ensemble average from data of the entire period of apnea yielded an average cardiac cycle for each pixel in the EIT image.

For each pixel, the intersecting tangent method [3] was used to determine the PAT of the impedance pulse, with the PAT of the heart pixel defined as $t = 0$ and all other pixels having a longer PAT.

The impedance pulse arrives at the aorta shortly after the heart, but before its arrival in other pixels. Therefore, we defined all pixels with a PAT shorter than 1/50 of a cardiac cycle to be potential aortic pixels. Furthermore, we expected the signal in the aorta to have a higher amplitude than that in surrounding tissue and thus excluded all pixels with an amplitude smaller than 70 % of the maximum signal of all possible aortic pixels. Lastly, since the impedance signal in aortic pixels has minimum towards the end of a cardiac cycle, we only allowed the pixels with the latest minimum to remain in the aortic region.

This process was then repeated for all other previously defined heart pixels. We then added all found aortic pixels to get a distribution of aortic pixels as shown in figure 1. To get one aortic pixel from this result, the center of gravity of this aortic pixel distribution was calculated. As a reference, we used the aortic pixels previously determined via bolus-injection in the same pigs as described in [1].

3 Results and Conclusions

For all eight measurements, we get a cohesive aortic region as shown in figure 1 for one animal. The center of gravity of this region has an average distance to the aortic pixel determined by bolus injection of 2.3 pixels with a standard deviation of 1 pixel in a 64×64 pixel image.

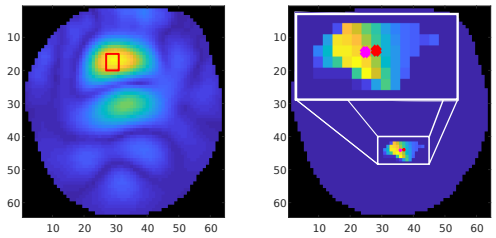

Figure 1: Left: Energy of the EIT signal at frequencies around the heart rate and selected heart region (red) for one animal. Right: Intensity distribution for detected aortic pixels for the same animal. Center of gravity of these pixels is marked in pink, aortic pixel detected via bolus injection in red.

Future work should focus on validation of this method in further animals and the application of the algorithm to patient data. If successful, this would enable the monitoring of central haemodynamics by EIT without the need for bolus injections or additional synchronised data.

References

[1] K Wodack, S Buehler, S Nishimoto, M Graessler, C Behem, A Waldmann, B Mueller, S Böhm, E Kaniusas, F Thürk, A Maerz, C Trepte, D Reuter *Physiol Meas*, 39:024022, 2018

[2] J Solà, A Adler, A Santos, G Tusman, F Sipmann, S Bohm *Medical & Biological Engineering & Computing*, 49:409–416, 2011

[3] C Chiu, P Arand, S Shroff, T Feldman, J Carroll *American Heart Journal*, 121:1460–1470, 1991

Combining Iterative Absolute EIT, Difference EIT and Control Theory to Optimise Mechanical Ventilation

Henry FJ Tregidgo[1] and William RB Lionheart[2]

[1]Medical Physics and Biomedical Engineering, University College London, UK h.tregidgo@ucl.ac.uk
[2]School of Mathematics, University of Manchester, UK

Abstract: We examine the combination of absolute and difference imaging to provide fast pseudo-absolute EIT reconstructions required for the recovery of local ventilation parameters. Parameters recovered from simulations are incorporated into an optimal control framework to demonstrate personalised optimisation of mechanical ventilation.

1 Introduction

Methods have been proposed to incorporate patient specific modelling into the automated control of mechanical ventilation through the use of EIT [1]. Through these methods it is possible to generate the H^1 minimal pressure profile to take ordinary differential equation (ODE) model of lungs from given initial state to specified target state while minimising the pressure gradients applied. Two limitations of this method are the requirement for absolute values of conductivity in ODE parameter recovery and the sensitivity of the generated pressure profiles to the target ventilation state.

In this paper we examine possible solutions to these limitations. To address the need for fast estimates of absolute conductivity, we investigate the accuracy of ODE parameters recovered through pseudo-absolute EIT reconstructions [2]. We also propose a framework to produce pressure profiles optimising regional recruitment while minimising gradients of pressure.

2 Pseudo-absolute Reconstruction

Pseudo-absolute EIT reconstruction assumes additional imaging modalities allow a segmented mesh of the thorax to be constructed [3, 4], which is used to perform a very low dimensional absolute reconstruction. The absolute values are then incorporated into the conductivity Jacobian for further difference imaging.

To test this algorithm's utility in automated ventilator control we generate simulated EIT reconstructions by coupling a compartmental ODE lung model to a segmented thorax mesh in EIDORS 3.9 [5]. We then examine the errors in ODE parameter recovery under errors in both mesh segmentation and signal measurement.

3 Optimised Control

The compartmental ODE model used in this paper can be written in the form

$$\dot{\mathbf{y}}(t) = A\mathbf{y}(t) + Bu(t), \tag{1}$$

where $\mathbf{y}(t)$ is a vector containing air volume of each lung compartment at time t, $u(t)$ is the applied pressure at time t, and A and B are matrices constructed from the elastances and airway resistances of each compartment. The H^1 minimal pressure profile taking this system from an initial inflation state $\mathbf{y_0}$ to a target inflation state $\mathbf{y_T}$ in time T can be generated using the formula

$$\mathbf{u} = \tilde{M}\left(\begin{bmatrix}\mathbf{y_T}\\ p_T\end{bmatrix} - \exp\left\{T\begin{bmatrix}A & B\\ 0 & 0\end{bmatrix}\right\}\begin{bmatrix}\mathbf{y_0}\\ p_0\end{bmatrix}\right) + p_0, \tag{2}$$

where p_0 and p_T are the initial and target pressures and $\tilde{M}$ is a specially constructed matrix of the form $\begin{bmatrix}M_y & M_p\end{bmatrix}$ [6, Chapter 4]. To generate an optimised pressure control we use eqn. 2 to formulate an optimisation for the control target

$$\mathbf{y}_T = \arg\min_{\mathbf{x}} \left[\mathbf{x}^* V^{-2}\mathbf{x} - \mathbf{r}^* V^{-1}\mathbf{x}\right], \tag{3}$$

$$\begin{bmatrix}M_y\\ -M_y\end{bmatrix}\mathbf{x} \leq \begin{bmatrix}\mathbf{p}_{\max}\\ -\mathbf{p}_{\min}\end{bmatrix} + \boldsymbol{f}(\mathbf{y}_0, p_0, p_T, T). \tag{4}$$

Here V is a diagonal matrix of weightings for each compartment so that $(V^{-1}\mathbf{x})$ is a vector of clinically meaningful ratios such as the ventilation perfusion ratio or filling factor, $\mathbf{r}$ is a vector containing the desired ratios, $\mathbf{p}_{\max}$ and $\mathbf{p}_{\min}$ are boundaries on allowable pressure and $\boldsymbol{f}$ is a vector valued function. This system can be solved to produce optimal target states and subsequently optimal pressure controls as illustrated in figure 1. We investigate the behaviour of these optimal controls under errors in parameter estimation as performed with pseudo-absolute EIT.

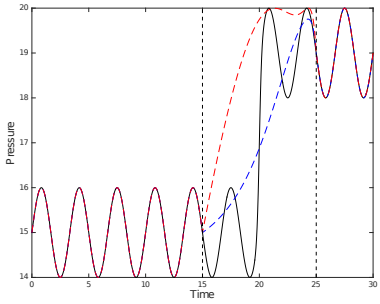

Figure 1: Comparison of H^1 minimal (blue) and optimised (red) PEEP steps to a demonstrative sinusoidal pressure profile (black).

4 Conclusions

Fast estimation of absolute conductivity values from EIT may allow construction of pressure controls optimised for recruitment while minimising damaging pressure gradients.

References

[1] Tregidgo HFJ, Crabb MG, Hazel AL, et al. *IEEE Transactions on Biomedical Engineering* **65**(11):2459–2470, 2018
[2] Tregidgo HFJ, Crabb MG, Lionheart W. In *Proc. 18th Int. Conf. Biomed. Applications of EIT*, 2. 2017
[3] Crabb M, Davidson J, Little R, et al. *Physiol Meas* **35**(5):863, 2014
[4] Grychtol B, Lionheart WR, Bodenstein M, et al. *Medical Imaging, IEEE Transactions on* **31**(9):1754–1760, 2012
[5] Adler A, Boyle A, Braun F, et al. In *Proc. 18th Int. Conf. Biomed. Applications of EIT*, 63. 2017
[6] Tregidgo HFJ. *Inverse problems and control for lung dynamics*. Ph.D. thesis, University of Manchester, 2017

Calculation of a Dynamic Regional Inflation Delay

Silke Borgmann[1,2], Johannes Schmidt[1,2], Sashko Spassov[1,2], Christin Wenzel[1,2], Stefan Schumann[1,2]

[1]Department of Anesthesiology and Critical Care, Medical Center – University of Freiburg
silke.borgmann@uniklinik-freiburg.de
[2]Faculty of Medicine, University of Freiburg, Germany

Abstract: We aimed at analysing a dynamic regional inflation delay (DRID) on a breath-by-breath basis. We show that using a proper filter, such calculation is feasible and regional lung damage can be visualized and localized in EIT images using DRID. This might improve the real time observation of regional ventilation delay which is associated with lung damage.

1 Introduction

The analysis of regional ventilation delay was initially calculated to illustrate the time dependency of certain lung regions during a single slow inflation maneuver [1]. Since the temporal resolution provided by EIT is excellent, adaptation of such an approach to determine the regional delay of inflation during an inspiration for monitoring the lung under sustained mechanical ventilation is promising. This way, the lung damage could be visualized in real time giving the medical personnel the chance to counteract or compensate for degenerative changes.

However, realization of this scenario is challenging. Estimation of regional delay depends crucially on finding the exact starting point of inspiration (SI) in each pixel. The original algorithm for a single low flow maneuver, was quite straight forward, since a distinct pattern in the global and individual impedance curves can be easily detected. By contrast, during regular tidal motion, the SI is often masked by—sometimes considerable—noise. Further, the signal strength of tidal variation of each pixel depends highly on the pixel's location. As a result, proper filtering of individual pixel signals becomes necessary.

2 Methods

Unifying the seemingly adverse requirements on filtering poses a challenge which we chose to tackle using the Matlab signal processing toolbox (MATLAB R2016a, The Mathworks Inc., Natick, MA). In our first approach we used a predefined Butterworth filter for all pixels. This did not deliver accurate responses of SI detection for all pixels. Especially peripheral pixels SIs were prone to misclassification.

However, using a rectangular filter with predefined cut-off frequencies that included only the first three harmonics of the breathing frequency improved the SI detection. We applied this setting to two test sets of data originating from lung healthy and lung injured pigs under different means of mechanical ventilation (volume controlled ventilation).

3 Results and Discussion

The breath-by-breath calculated DRID provided a very good visualization and localization of the lung injury (Fig. 1) for the first data set. Also the effects of different ventilation methods could be visualized impressively [2]. However, using a rectangular filter was not easily adaptable to the second data set, and we found that cut-off frequencies needed to be modified for each pixel. Hence, our current work in progress focuses on applying individual filtering to each pixel. To achieve this, we currently explore digital signal processing techniques to unify the somewhat adverse filtering needs of individual pixels. First results reduced misclassification from 20% to 3.5%.

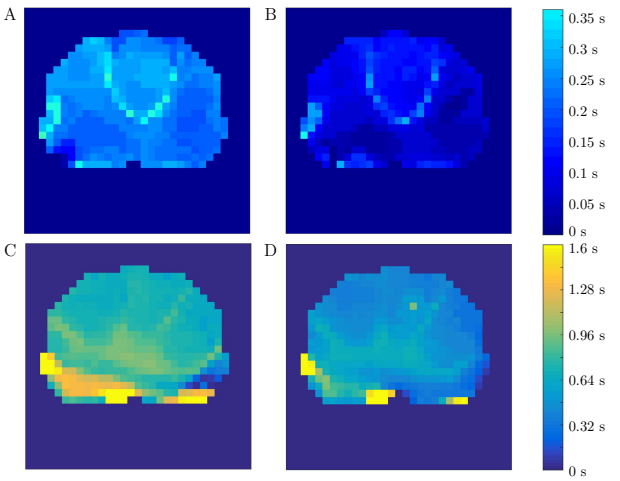

Figure 1: Calculated DRID for different ventilation settings and different states of the lung. (A) Healthy pig lung under conventional volume controlled ventilation (VCV). (B) The same lung under VCV using flow controlled expiration (FLEX). (C) Injured lung under VCV. (D) The same injured lung under VCV using FLEX. The areas with higher delay correspond to the location of the lung injury.

4 Conclusions

Generating a rectangular filter for each pixel in an EIT frame based on a predefined cut-off frequency provided a reasonable approach to determine DRID on a breath-by-breath basis. The resulting visualization map was well associated with lung injury. A real-time calculation of DRID could provide monitoring of the state of the lung, allowing the medical personnel to intervene, if the lungs show early signs of degenerative changes.

References

[1] T Muders, H Luepschen, J Zinserling et al. *Crit Care Med*,40:903–911, 2012

[2] S Borgmann, J Schmidt, U Goebel, J Haberstroh, J Guttmann and S Schumann *Crit Care*,22:245–254, 2018

Platelet Aggregation Measurement with Electrical Impedance Spectroscopy

Jianping Li[1], Huilu Bao[1], Nen Wan[1], and Jianming Wen[1]

[1] Institute of Precision Machinery, Zhejiang Normal University, Jinhua 321004, Zhejiang Province, China, lijp@zjnu.cn

Abstract: The platelet aggregation in whole blood has been measured with electrical impedance spectroscopy. In order to modify the conventional platelet aggregation measurement in whole blood, the red blood sedimentation is considered into the measurement.

Keywords: platelet, blood, impedance, red blood cell sedimentation

1 Introduction

Platelet aggregation has been related to many serious human diseases, such as thrombosis, diabetes, and uraemia [1].Hence, it is of great significance for patients to measure the platelet aggregation in time. Generally, two methods are utilized for the platelet aggregation: optical nephelometry method and electrical impedance spectroscopy method [2]. The optical nephelometry method is more widely to be applied, since it is more accurate. However, it needs the centrifuge to get the platelet rich plasma (PRP), which takes more time and more costs. The electrical impedance spectroscopy method utilizes the whole blood for measurement, hence, it is more convenient. But, the accuracy is still the problem, since the red blood cells sedimentation also influences the impedance signal of blood.

2 Methods

2.1 Experimental setup

During the experiments, the blood was put into a container with two electrodes, the impedance analyzer was utilized to measure the impedance signals of the blood, and all the data was saved and processed by the PC.

2.2 Experimental conditions

Fresh porcine blood with 1/10 tri-sodium citrate solution (3.28%) from the slaughterhouse was used for the experiments. At first, the whole blood with ADP medicine (for platelet aggregation) was tested to obtain the impedance change. And then, only fresh whole blood was measured. Every 5 minutes, the impedance signals was measured and recorded. The excitation current i for the impedance analyser was fixed at 0.1 mA. The measurement frequency was from f_1=100 kHz to f_2=300 MHz (101 points, log scale). The impedance Z^* was obtained, and analyzed by the Nyquist Plot [3].

2.3 Experimental results

Figure 1 shows the impedance change of the blood in one hour. Here, Z' is the real part of impedance Z^*, while Z'' is the imaginary part of impedance Z*. It can be seen in Figure 1(a) that the impedance of the blood with ADP increases with time. This is the so called electrical impedance spectroscopy method for platelet aggregation measurement. However, we can find that without ADP, the impedance of blood also increases with time, as is shown in Figure 1(b). This is mainly thought to be caused by the red blood cells sedimentation. In other words, the conventional electrical impedance spectroscopy method for platelet aggregation is greatly influenced by the red blood cells sedimentation. Hence, in the real application, the influence of red blood cells sedimentation should be considered.

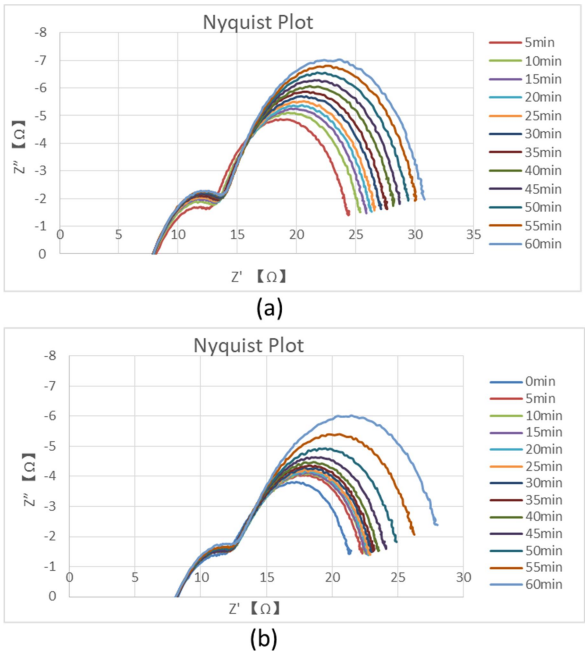

Figure 1: Impedance change of blood: (a) with ADP, (b) without ADP

3 Conclusions

This study investigates the influence of red blood cells sedimentation during the platelet aggregation measurement with whole blood. It is advised that if more accurate result from the electrical impedance measurement is wanted, the influence of red blood cells sedimentation should be considered.

References

[1] Alemu, Y., Girdhar, G. M., Sheriff, J., Jesty, J., Einav, S., & Bluestein, D. *Asaio Journal*, 56(5), 389-396, 2010.

[2] Dyszkiewicz-Korpanty, A. M., Frenkel, E. P., & Sarode, R., *Clin Appl Thrombosis/hemostasis*, 11(1), 25, 2005.

[3] Li, J., Sapkota, A., Kikuchi, D., Sakota, D., Maruyama, O., & Takei, M.. *Biosensors & Bioelectronics*, 112, 79, 2018.

Preliminary study of the effect of injection and measurement patterns ('skip') on separating EIT bladder volume measurement data

Eoghan Dunne, Adam Santorelli, Martin O'Halloran and Emily Porter

Translational Medical Device Lab, National University of Ireland Galway, Ireland, e.dunne13@nuigalway.ie

Abstract: In this study, we analyse the effect of different injection and measurement patterns on a 2D simulation configuration to improve the bladder volume measurement data separability. We found that the patterns affect the separability of EIT bladder volume measurement data and that the best pattern selection metric is hardware limited.

1 Introduction

Electrode injection and measurement patterns have been previously researched to distinguish different conductivity distributions and to improve EIT sensitivity and results [1-3]. In bladder volume studies, we utilise the time-difference EIT measurements during bladder filling to determine the bladder volume or bladder state [4-6].

Before measurement, the injection and measurement patterns are selected. In systems such as the Swisstom Pioneer Set (Swisstom.com), the injection and measurement patterns are equal and have a fixed number of electrodes between each of the injection electrodes and between each of the measurement electrodes called a 'skip'. In this paper, we investigate the effect of modifying this skip on the separability of different bladder volume data and determine if there is an optimum skip for this application.

2 Methods

The finite element model (FEM) outlined in [6] was used to generate data for this study (using EIDORS 3.9 [7] and Netgen 6.1 [8]). The FEM consisted of 32 electrodes arranged in a 2D configuration. Two different bladder volumes of 80 ml and 160 ml were used, with a urine conductivity of 2 S/m. In this study, we analyse all skips from 0 to 14. For each skip, two voltage frames consisting of 928 voltages were generated (injection measurements removed), one for each bladder volume.

To test the separability resulting from measurements with each skip, we used a metric we define as the Absolute Mean Separability (AMS). The AMS is the absolute difference between the mean of the larger bladder voltage frame and the mean of the small bladder voltage frame. This metric can be linked to the Voltage Change Ratio (VCR) used in the 4-electrode method [9] by normalising the AMS by the mean voltage of the frame of the small bladder. We also employ the VCR as a performance metric in this paper.

3 Results & Discussion

Figure 1 illustrates the effect of skip-selection on the separability of EIT data. In ideal circumstances, the AMS could be maximised by using a skip of 14. However, based on the absolute VCR graph, the absolute VCR is maximal at a skip of 8, which may improve separability for classification if the measurement system has a low noise floor. Thus, the decisions of the skip metric and skip are dependent on the hardware resolution.

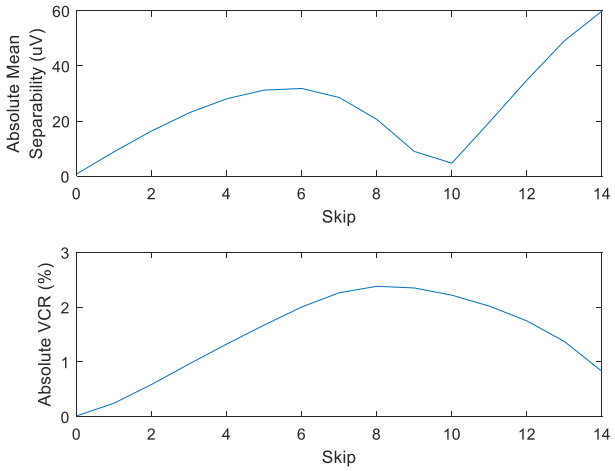

Figure 1: *(top)* AMS and *(bottom)* Absolute VCR for each skip.

4 Conclusions

In this study, we have carried out a preliminary investigation of how the skip affects the separability of EIT bladder volume measurement data for a 2D electrode configuration. We found that the bladder volume separability is dependent on the skip used. Hardware limitations such as the noise floor of a system may determine which metric is chosen to identify the skip with the best separability.

This work has the potential to improve EIT voltage data and image-based bladder state classification by improving separability of the measurement data.

5 Acknowledgements

This research was supported by funding from the European Research Council under the European Union's Horizon 2020 Programme/ ERC Grant Agreement BioElecPro n. 637780 and the charity RESPECT and the People Programme (Marie Curie Actions) of the European Union's Seventh Framework Programme (FP7/2007-2013) under REA Grant Agreement no. PCOFUND-GA-2013-608728. The research was also supported by the Irish Research Council under the fund GOIPD/2017/854.

References

[1] D Isaacson, *IEEE Trans Med Imaging*, 5:91:95, 1986
[2] B Grychtol, B Müller, A Adler, *Physiol Meas*, 37:785–800, 2016
[3] A Adler, P Gaggero, Y Maimaitijiang *Physiol Meas*, 32:731–744, 2011
[4] T Schlebusch, et al., *Physiol Meas* 35:1813-1823, 2014.
[5] E Dunne, et al., *Sci Rep,* 8:5363, 2018
[6] E Dunne, et al., *Physiol Meas*, 39:124001, 2018
[7] A Adler, et al. *Physiol Meas,* 27:S25–42, 2006
[8] J Schöbel, *Comput Visual Sci,* 1:41-52, 1997
[9] Y Li, et al., *BioMed Eng Online*, 18:34, 2019

Electrical Impedance Tomography in Soft Robotics

James Avery[1], Mark Runciman[2], Darya Shulakova[1], George Mylonas[2], and Ara Darzi[1]

[1]Dept. Surgery & Cancer, Imperial College London, UK, james.avery@imperial.ac.uk

[2]HARMS Lab, Imperial College London, UK

Abstract: Soft, compliant robots offer many benefits compared to conventional rigid devices, particularly in minimally invasive surgery. In this work we tackle the fundamental challenge of shape sensing in soft robotics, through the combination of full EIT methods and SOFA soft body simulations.

1 Introduction

Controlling soft systems is challenging given the deformability of the compliant structures, and the difficulty in integrating shape or pose sensing. Many proposed sensing methods either compromise the desirable mechanical properties or require line of sight. Soft tactile and pose sensors have been proposed wherein shape related electrical impedance changes are imaged using Electrical Impedance Tomography. However, these elastomer sensors are often not suitable for minimally invasive surgery (MIS), as they have low packing efficiencies or are not biocompatible. Further, the imaging methods do not take advantage of full EIT methodology, often neglecting the complete electrode model, or using back projection during reconstruction. Here we propose the use of conductive elastomers and EIT as a low-profile shape sensor, to reconstruct the bending angle of a continuum actuator.

2 Methods

A model of simple cable driven continuum actuator, of comparable dimensions to a single module of the STIFF-FLOP surgical manipulator [1], was created in the SOFA Soft Robotics plugin [2]. This design simulates a soft cylindrical silicone rubber (PDMS) manipulator, with three internal independent tendons to control the tip position. The behaviour of the soft body is simulated using the SOFA package, which requires *a priori* knowledge of the constraints of the system, and the material properties and a FEM defining the system. Due to the complexity of the calculations, and the target of real-time calculation a model (SOFA-FEM) of c. 2000 elements was used. Using this model, the manipulator shape was simulated along the complete actuation range at five time steps (Fig 1A).

To produce deflection related impedance change, it was assumed that the PDMS was made electrically conductive, e.g. through the addition of PEDOT, Carbon black, Gold Nanowires etc. The conductivity was assumed to be constant 0.4 S/m, i.e. no piezoresistive effects, and thus any voltage changes are due to the geometric changes only. Electrodes were placed at the fixed base and the tip of the actuator at specific nodes in the SOFA-FEM. These models were then globally refined, and further locally refined around the electrodes in COMSOL, to create c. 50,000 element EIT-FEMs (Fig 1A). Using the five FEMs the voltages were simulated using SuperSolver (https://github.com/EIT-team/SuperSolver), assuming the use of a six-injection Frequency Division Multiplexed EIT system [3]. Images were reconstructed using Zeroth Order Tikhonov.

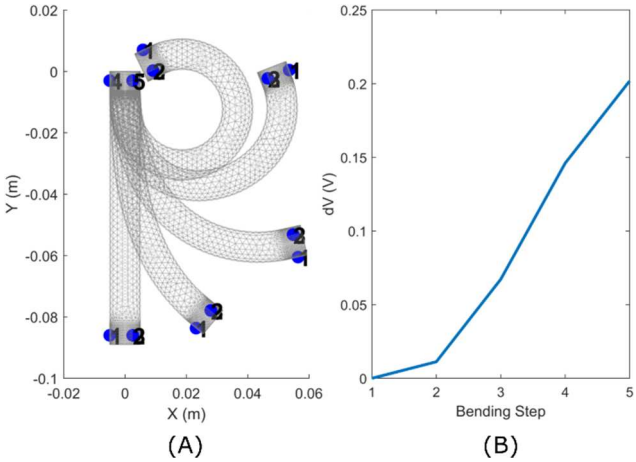

Figure 1: (A) EIT-FEM of continuum actuator at five bending steps, electrodes highlighted in blue (B) corresponding mean EIT voltage change from baseline during actuation.

3 Results

The results at each step show clear separable voltage changes (Fig 1B). However, the imaging results did not show distinctive modes in the apparent conductivity changes, merely a changing of intensity.

4 Conclusions

The low electrode count used in this model is based on current manufacturing limits, and the results suggest a voltage-based machine learning approach is more appropriate for estimating the bending angle than imaging. Work is on going to incorporate more electrodes into the prototype device and experimentally validate the results.

5 Acknowledgements

This work was supported by the NIHR Imperial BRC.

References

[1] M Cianchetti, et. al. *Soft Robotics*, 1:2, 2014

[2] E Coevoet, A Escande, C Duriez, *IEEE Robotics and Automation Letters,* 2:1413-1419, 2017

[3] Avery et. al, *IEEE International Conference Robotics and Automation,1904.02429* 2019

EIT of Muscle Contraction in the Forearm: A Preliminary Study

Ethan K. Murphy[1], Saaid Arshad[1], Seward B. Rutkove[2], and Ryan J. Halter[1,3]

[1]Thayer School of Engineering, Dartmouth College, Hanover, NH, USA, ethan.k.murphy@dartmouth.edu
[2]Beth Israel Deaconess Medical Center, Boston, MA, USA
[3]Geisel School of Medicine, Dartmouth College, Hanover, NH, USA

Abstract: To date, there are no good tools to assess muscle contraction in real time, outside of the evaluation of force, which provides only a non-specific output. Here, we evaluate Electrical Impedance Tomography (EIT) data during a muscle contraction in preparation for studies in patients with neuromuscular diseases.

1 Introduction

The assessment of muscle contraction in real time remains a remarkably challenging problem. Standard methods such as force output are nonspecific and do not provide any information on the geometrical or stress-related changes within the muscle itself. Standard imaging modalities such as MRI and CT are generally slow and inconvenient or, like ultrasound, are challenging to quantify. Needle electromyography only evaluates the depolarization of the muscle fibres and not the contraction itself. EIT could potentially be applied in this way to assist in holistically evaluating changes in the muscle structure and strain during a contraction. It is anticipated that in disease, the normal contractile patterns will be disrupted, causing atypical stresses in the muscle which may produce irregular alterations in the EIT signal. Here we explore real-time, 3D imaging of the forearm during flexing and extending of individual fingers.

2 Methods

Data collection is ongoing and data presented is on one volunteer. 32-electrodes are arranged on the forearm, as in Fig. 1A and data is collected using the 32-channel SwissTom Pioneer Set at 100 kHz using 2-skip patterns. The experiment involves flexing or extending one finger (or thumb) at a time. For each finger the volunteer first engages (light flex) for 1 second and then hard flex for 1 second. The test is repeated 3 times for each finger flexing and extending. 3D EIT images are produced (Fig. 2) by differencing the hard flex minus the engaged data frames. We chose the engaged frame as a reference as opposed to a relaxed frame to minimize artefacts from forearm shape-changes between frames. 2D images of the middle slice are qualitatively assessed and local maxima from each test are highlighted to evaluate consistency. Flexing was performed by pressing fingers against a 1L bottle of water (gave resistance and allowed for compression) and extensions were performed against the opposing hand. It is noted, that it is challenging to flex one finger without involuntarily flexing other fingers, thumb, and/or wrist.

3 Results

The EIT images are presented in Fig. 2, which show 1) the local maxima are generally consistent across images, 2) most of the finger flexing results are very similar (3rd, 4th, and 5th digits), and 3) direct anatomical interpretation appears challenging. Prior results have mainly used bulk electrical impedance myography measurements with some cases showing increases and in other decreases in muscle impedance due to contraction [1]. Overlaid (black) in Fig. 2 are the finger flex (row 1) and extension muscles (row 2), which are often associated with yellow regions (conductivity increase). There are other yellow regions, which in certain cases may be associated with a wrist extension (row 1) or flex (row 2) see red outlines.

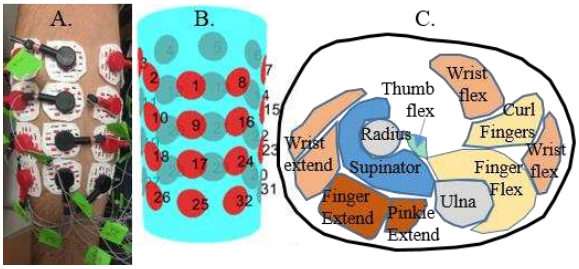

Figure 1: A. View of the 4 rows of 8 electrodes (attached with adhesive), B. corresponding 3D mesh used for imaging, and C. anatomical cross-section of the upper forearm.

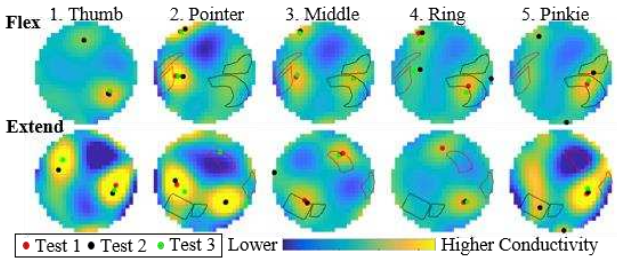

Figure 2: EIT images of flexed (or extended) minus engaged for each finger. Images are from test 1, while local maxima from test 2 and 3 are shown as black and green dots. Black outlines are finger flex (row 1) or extension muscles (row 2) and red outlines are wrist extension (row 1) and flex (row 2) muscles.

4 Conclusions

The consistency of these results appears very promising. Ongoing data collection should reveal if these regions are consistent across individuals. Although the exact nature of what underlies these alterations is unknown, further study of this novel approach to muscle imaging may be valuable for clinical diagnostic assessment and for assessing the effects of therapy.

5 Acknowledgements

This work was partially supported by CDMRP funding W81XWH- 15-1-0572.

References

[1] B. Sanchez, Neurotherapeutics, 10.1007/s13311-016-0491-x

Using EIT to assess Pulmonary Function in ALS Patients

Seward Rutkove[1], Ethan Murphy[2], Courtney McIlduff[1], Fu Zhang[1], Hilda Gutierrez[1], Badria Munir[1] and Ryan Halter[2,3]

[1]Beth Israel Deaconess Medical Center, Boston, MA, USA srutkove@bidmc.harvard.edu
[2]Thayer School of Engineering, Dartmouth College, Hanover, NH, USA, ethan.k.murphy@dartmouth.edu
[3]Geisel School of Medicine, Dartmouth College, Hanover, NH, USA

Abstract: This preliminary work investigates whether Electrical Impedance Tomography (EIT) can assess pulmonary function in Amyotrophic Lateral Sclerosis (ALS) patients. Five healthy volunteers and three ALS patients were studied, and positive correlations were found between forced vital capacity (FVC) and an EIT metric.

1 Introduction

ALS is a progressive neuromuscular disorder, having an incidence of 1-2/100,000 people a year with no cure, and an average life expectancy after diagnoses of 2 to 5 years, [1] with people dying from respiratory insufficiency. Pulmonary function tests (PFTs) are routinely used to help assess progression of the disease as well as the time to institute supportive therapies, including bi-level pulmonary assisted pressure (BiPAP) [2]. EIT is a non-invasive imaging modality that has shown good success in pulmonary monitoring, and may be able to provide important assessment of pulmonary function in ALS patients, especially in those who are unable to participate in the test due to concomitant weakness of mouth closure. Additionally, there is a need for a sensitive marker for disease progression for use in clinical trials [3]. Here, we investigate EIT's potential for serving as such a biomarker.

2 Methods

Data has been collected on 3 ALS patients at Beth Israel Deaconess Medical Center (BIDMC) under an IRB-approved study. EIT data was recorded using a 32-channel SwissTom Pioneer Set during normal breathing and during a pulmonary function test (PFT). The electrodes were positioned at the nipple plane between the 3rd and 4th intercostal space with the patient in a sitting upright position. Data was recorded at 195 kHz using 4-skip patterns. Tidal images were produced (end-inspiration minus end-expiration) and the Negative Conductivity Area was used as the metric for analysis. The primary PFT metric investigated was FVC. As a comparison, normal breathing data were recorded from 5 healthy volunteers, although no PFT test was available for this cohort. The cumulative number of breathes used in the study were 17, 11, and 4 for the ALS patients and 10, 12, 8, 9, and 12 for the healthy volunteers.

3 Results

Quantitative results are shown in Fig. 1 and average tidal images are shown in Fig. 2 for the healthy volunteers and ALS patients. There is a general trend of a higher negative conductivity area for the healthy cohort as compared to the ALS patients (Fig. 1A) and a positive correlation between negative conductivity area and FVC (% predicted) from the PFTs. Qualitatively, there appears to be more of a cardiac signal in the ALS patients, which may be apparent because of the smaller amplitude breathing signal (shallower breaths).

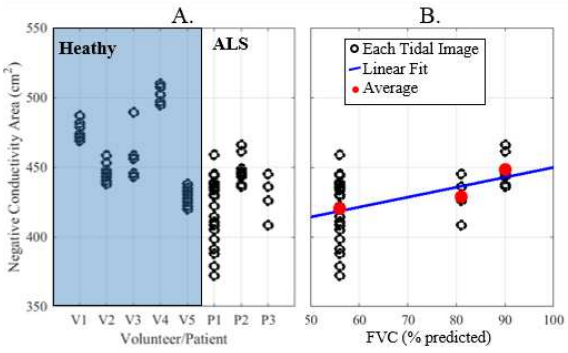

Figure 2: A. Negative conductivity area for each tidal-image of healthy volunteer and ALS patients, and B. Scatter plot of the negative conductivity area versus the FVC (% predicted), showing on average a positive correlation (n=3,R^2=0.56,p=0.3).

4 Conclusions

While preliminary, these initial findings suggest that EIT may be a promising method to assess pulmonary function and may be able to serve as an important biomarker in future ALS clinical studies.

5 Acknowledgements

This work was partially supported by CDMRP funding W81XWH- 15-1-0572.

References

[1] Website, http://www.alsa.org, as of 29/4/2019.
[2] J. Cederbaum, J of Neurological Sciences, 10.1016/S0022-510X(99)00210-5
[3] S. Rutkove, Amyotrophic Lateral Sclerosis, 10.3109/17482968.2012.688837

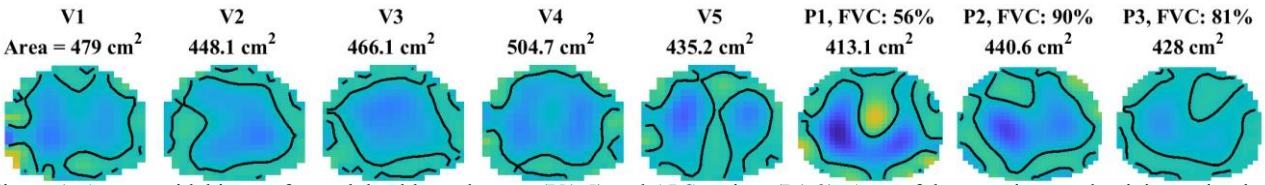

Figure 1. Average tidal image for each healthy volunteer (V1-5) and ALS patient (P1-3). Area of the negative conductivity region is noted and contours at zero are shown.

Regional differences in small airways function indicated by EIT

Sabine Krueger-Ziolek[1], Bo Gong[1], Ullrich Müller-Lisse[2] and Knut Möller[1]

[1]Institute of Technical Medicine, Furtwangen University, 78054 Villingen-Schwenningen, Germany, krue@hs-furtwangen.de

[2]Department of Clinical Radiology, LMU Hospital of the University of Munich - Inner City Campus, 80336 München, Germany

Abstract: A two-term exponential model was used to fit relative impedance changes measured during forced expiration in a spontaneously breathing cystic fibrosis patient and a lung healthy control to exemplarily show intra-/intersubject variations in ratios of fit coefficients which may indicate differences in small airways function.

1 Introduction

Functional EIT images representing relative impedance changes corresponding to spirometric lung function parameters, such as forced expiratory volume in 1 second (FEV_1), forced vital capacity (FVC) or mean forced expiratory flow between 25% and 75% of FVC are frequently used to detect and evaluate ventilation distribution inhomogeneities in patients with obstructive lung diseases [1].

In this feasibility study, a new method using a two-term exponential model to fit relative impedance changes measured during FVC manoeuvres is introduced which may provide additional information about lung function. Since the second term of the model mostly represents the last half of the forced expiration (mainly affected by the small airways), we hypothesised to find intra-/interpatient differences in small airways function.

2 Methods

2.1 Study protocol and data processing

EIT data from a cystic fibrosis (CF) patient (male, 32 years, 71 kg, 178 cm, $FEV_{1(Ref)}$: 58%) and a lung healthy (HL) subject (male, 27 years, 107 kg, 194 cm, $FEV_{1(Ref)}$: 104%) measured during FVC manoeuvres were analysed retrospectively. The whole study protocol is described in detail in [2]. EIT data acquired at the 5th intercostal space with a frame rate of 30-40 Hz were reconstructed with a linearized Newton-Raphson algorithm. Lung regions were defined by pixel values > 20% of the maximum value of the respective functional regression coefficient image [3].

2.2 Data analysis

A two-term exponential model (equation 1) was used to fit relative impedance changes measured during a forced expiration from total lung capacity to reserve volume (Figure 1, right).

$$f(t) = ae^{bt} + ce^{dt} \quad (1)$$

Fitting was performed in MATLAB (R2017a, The Mathworks® Inc., Natick, USA) using the '*fit*' function, specifying the model type as '*exp2*'. Global (whole scan) and regional (pixel) relative impedance changes were fitted. Additionally, global and regional ratios of the fit coefficients *c* and *a* were calculated.

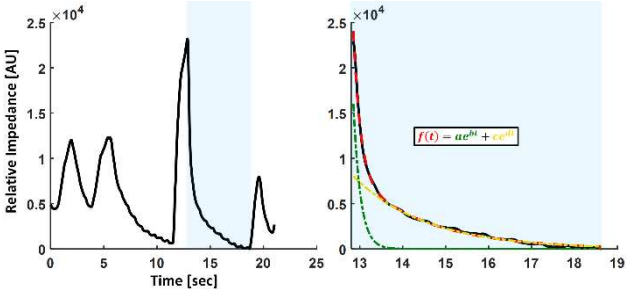

Figure 1: Relative impedance changes recorded during lung function testing (left). Two-term exponential model fitting relative impedance changes measured during the FVC manoeuvre (right).

Global *c*/*a* of the CF patient was 0.25, whereas the lung healthy control had a ratio of 0.12.

Functional EIT images showing regional ratios of *c* and *a* were generated for both subjects (Figure 2). Overall, the CF patient exhibited more lung regions (84% > mean of regional *c*/*a* of HL) with increased *c*/*a* compared to the control (28% > mean of regional *c*/*a* of HL).

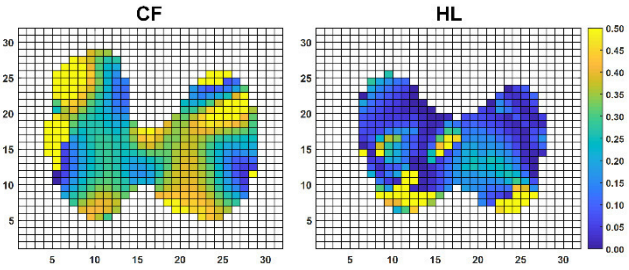

Figure 2: Regional ratios of the fit coefficients *c* and *a* of a cystic fibrosis patient (CF, left) and a lung healthy control (HL, right).

3 Conclusions

The two-term exponential model can be used to fit relative impedance changes measured during forced expiration. Intra- and intersubject variations in regional *c* and *a* ratios may indicate differences in small airways function.

4 Acknowledgements

This work was partially supported by the German Federal Ministry of Education and Research (MOVE, Grant 13FH628IX6).

References

[1] B Vogt, Z Zhao, P Zabel, *Am J Physiol Lung Cell Mol Physiol*, 311:L8-L19, 2016

[2] S Krueger-Ziolek, B Schullcke, Z Zhao *Respir Physiol Neurobiol*, 233:25–32, 2016

[3] S Pulletz, HR van Genderingen, G Schmitz *Physiol Meas*, 27:S115-S127, 2006

Regional lung pressure analysis from EIT

Bo Gong[1], Sabine Krueger-Ziolek[1], Serge Heines[2], Knut Moeller[1]

[1]Institute of Technical Medicine (ITeM), VS-Schwenningen, Germany, bo.gong@hs-furtwangen.de

[2]Intensive Care, Maastricht University Medical Centre+, Maastricht, Netherlands

Abstract: Electrical impedance tomography (EIT) has been applied on mechanically ventilated patients. In this study, we combine data which are simultaneously measured from EIT and the mechanical ventilator to reconstruct the lung pressure with a regional aspect.

1 Introduction

Canonical lung mechanical models, using the measurement data from the ventilator, focus on the global lung mechanical properties. Regional lung ventilation, which may be heterogenous, can be extracted from EIT images. However, limited studies address modelling regional lung mechanical properties using regional ventilation information derived from EIT.

2 Methods

The mechanical ventilation and EIT measurements were deployed on an ARDS patient in ICU. Pressure controlled mechanical ventilation under BIPAP mode with an automatic tube compensation (ATC) was applied on this patient. The patient was placed in supine position. EIT data were recorded with a frame rate of 20 Hz by the device PulmoVista 500 (Draeger). Time-difference EIT images were reconstructed using the GREIT algorithm [2].

2.1 Image processing

The reconstructed 2D EIT images have a pixel resolution of 64 X 64. It has been shown that the regional impedance changes obtained from EIT measurements are proportional to regional lung volume changes [3]. Normalized by the global lung volume derived from ventilator measurements, each of these pixel values represents regional lung volume changes. The derivative of this regional volume data with respect to time provides the regional airflow.

2.2 Reconstruct lung pressure

In this section, we outline a method to reconstruct the regional pressure data using regional impedance /volume information. A simplified single-compartment lung mechanical model (first order equation of motion) can be described by the following equation:

$$P(t) = E \cdot V(t) + R \cdot \dot{V}(t) + P_0 \qquad (1)$$

which represents the relations between pressure $P(t)$, PEEP value P_0, lung volume $V(t)$, and the air flow $\dot{V}(t)$. The parameter E represents the elastic property of the lung tissue. The parameter R represents the airway mechanical resistance counteracting air-flow. When the air-flow equals zero, for example, at the begin and the end of inspiration, the flow term $R \cdot \dot{V}(t)$ vanishes. Employing the pressure and volume values at such special cases, the regional lung tissue elastance parameter E can be determined [1].

The lung volume changes during the passive expiration phase in the single-compartment model have been described by the following differential equation:

$$0 = E \cdot V(t) + R \cdot \dot{V}(t). \qquad (2)$$

We can get the time constant $\tau = E/R$ by fitting the volume data during the expiration using an exponential function. Together with the lung tissue elastance E calculated from the inspiration phase, the airway resistance R, can be obtained under the assumption that inspiratory and expiratory R are equal. The regional pressure value during the whole breath (Fig. 1 (c)) can be reconstructed using equation (1).

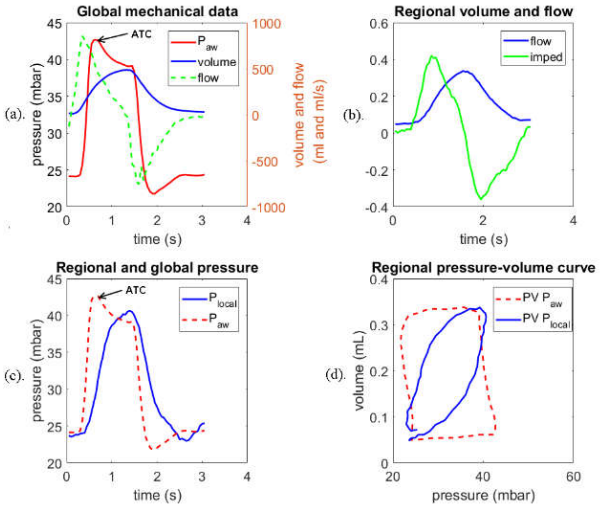

Figure 1:(a). Global airway pressure, volume and flow data. (b). The volume and flow at a pixel region. (c) The reconstructed regional pressure data associated to this pixel. (d). The pressure-volume curve with respect to airway and regional pressure.

3 Results and conclusion

This work provided a method to reconstruct the regional pressure during mechanical ventilation. Different patterns between airway and regional pressure can be observed. As indicated from Fig. 1 (c), the pressure peak induced by ATC, shown in airway pressure P_{aw}, cannot be found in the reconstructed regional pressure data.

4 Acknowledgements

This work was supported by the BMBF grant no. 13FH628IX6 (MOVE).

References

[1] JH Bates, *Lung mechanics: an inverse modeling approach.* Cambridge University Press, 2009

[2] A Adler, *et al*, *Physio Meas*, 30.6, S35, 2009

[3] CJ Roth, *et al*, *Physio Meas*, 36.6: 1211, 2015

Effect of small-volume fluid bolus administration on end-expiratory lung impedance in ventilated neonates

L Sophocleous[1], T Becher[2], T Papadouri[3], C Karaoli[3], M Kallio[4], M Miedema[5], A H van Kaam[5], A Waldmann[6], S Nordebo[7],D Khodadad[7], R Yerworth[8], A Dupré[9], R Bayford[10], I Frerichs[2]

[1]KIOS Research Centre, Dept. of Electrical and Computer Engineering, University of Cyprus, Nicosia, Cyprus, louiza.sophocleous@gmail.com, [2]Dept. of Anaesthesiology and Intensive Care Medicine, University Medical Centre Schleswig-Holstein, Campus Kiel, Kiel, Germany, [3]Neonatal Intensive Care Unit, Arch. Makarios III Hospital, Nicosia, Cyprus, [4]PEDEGO Research Group, University of Oulu and Dept. of Children and Adolescents, Oulu University Hospital, Oulu, Finland, [5]Dept. of Neonatology, Amsterdam University Medical Centers, Amsterdam, Netherlands, [6]SenTec AG, Landquart, Switzerland, [7]Dept. of physics and electrical engineering, Linnaeus University, Växjö, Sweden, [8]Dept. of medical physics and biomedical engineering, University College London, London, United Kingdom; [9]Dept. of Paediatrics, University of Geneva, Switzerland,[10]Dept. of Natural Sciences, Middlesex University, London, United Kingdom

Abstract: We assessed the effect of small volume fluid bolus administration in neonates on tidal volume variation and end-expiratory lung impedance. We found no significant changes before and after intervention.

1 Introduction

The measurement of pulmonary bioimpedance using electrical impedance tomography (EIT) can provide continuous assessment of regional lung function in critically ill neonates and infants [1]. End-expiratory lung impedance (EELI) and tidal impedance variation (differences between inspiration and expiration, TI) are commonly used parameters in pulmonary EIT applications. EELI has been found to be highly affected by fluid administration [2]. More specifically, a decrease in EELI after fluid administration of 500ml crystalloid solution has been observed in critically ill adults [3]. A similar effect has been documented in experimental animals [4]. We aim to assess possible changes in EELI and TI after small volume fluid administration in critically ill neonates.

2 Methods

This sub study was performed within the framework of a larger multicentre observational study called **C**ontinuous **R**egional **A**nalysis **D**evice for neonate **L**ung (CRADL). Rapid normal saline fluid administration of 2ml (0.9% crystalloid saline fluid) has been documented, as routine clinical practice in one of four neonatal intensive care units (NICU) within the CRADL study. Normalized to body weight, the fluid dose given was 1.15 ml/kg. In other centres, 10 ml/kg of normal saline fluid administration was used as fluid bolus intervention. EIT measurements were performed using BB^2 device (SenTec AG, Landquart, Switzerland). The tidal images were generated using a breath detection algorithm optimised for neonatal use [5]. From the tidal images we calculated the global mean TI and mean EELI values for 1 min in two time intervals, 5 min before fluid administration (T_{-5}) and 5 min after (T_{+5}). Values were compared using Wilcoxon matched pairs test, p values <0.05 were considered statistically significant.

3 Results

For the analysis of 1.15 ml/kg fluid administration, we assessed 32 documented events from 12 ventilated patients. Patients had mean weight of 1732±993 g (mean±SD). There was no significant change in the values of EELI and TI between T_{-5} and T_{+5}.
For the analysis of 10 ml/kg fluid administration, we assessed 10 documented events from 10 ventilated patients with mean weight of 1773±647 g (mean±SD). No significant change was observed in EELI and TI between the studied intervals. All values of EELI and TI are summarized in table 1.

4 Conclusions

With this systematic approach, no significant differences were observed in EELI and TI values between intervals before and after 1.15 ml/kg and 10 ml/kg fluid administration. Further investigation and a larger sample size of documented events is needed for conclusive results on the 10 ml/kg fluid administration.

5 Acknowledgements

This project has received funding from the European Union's Horizon 2020 research and innovation programme under grant agreement No 668259.

References

[1] Frerichs et al. *Thorax*, 72:83-93, 2017
[2] Bodenstein et al. *Physiol Meas*, 33:1225-1236, 2012
[3] Becher et al. *Am J Respir Crit Care Med*,201812-2252LE, 2019
[4] Sobota et al. *Sci Rep*, 9:5775,2019
[5] Khodadad et al. *Physiol. Meas*, 39:9,2018

Table 1: Descriptive statistics and p-values for tidal impedance variation (TI) and end-expiratory lung impedance (EELI) at two time points, 5 min before fluid administration (T_{-5}) and 5 min after (T_{+5}).

Volume of fluid administration	EIT parameter	T_{-5}	T_{+5}	p-value
2 ml	EELI	22.08 (20.45-23.71)	22.26 (20.50-24.02)	0.63
	TI	0.48 (0.41-0.54)	0.51 (0.41-0.61)	0.64
10 ml	EELI	20.07 (16.05-24.09)	19.88 (15.00-24.77)	0.33
	TI	0.41 (0.30-0.51)	0.43 (0.31-0.55)	0.72

EIT measurement of pulmonary artery pressure in neonatal lambs

Fabian Braun[1], Martin Proença[1], Michaël Sage[2], Jean-Paul Praud[2], Mathieu Lemay[1], Andy Adler[1,3], Étienne Fortin-Pellerin[2]

[1]CSEM, Neuchâtel, Switzerland, [2] Université de Sherbrooke, Canada, [3] Carleton University, Ottawa, Canada

Abstract: Pulmonary artery pressure (PAP) is inversely related to the pulse arrival time (PAT) of the EIT signal in the lungs. The goal of this study is to evaluate whether PAT-based EIT measures can accurately monitor directly-measured PAP in newborn lambs. Early results show good correlations and trending ability, although the technique is sensitive to belt placement and signal quality.

1 Introduction

While non-invasive measurements of arterial pressure are routine, few techniques exist to measure PAP. We are motivated by the value in (especially premature) neonatal medicine, where hypoxic vasoconstriction of immature pulmonary arteries is a key clinical challenge. While PAP can be measured with ultrasound, it requires a high level of expertise, is not possible in all patients, and cannot provide continuous readings. Recently, the EIT-measured PAT has been shown to correlate well with ultrasound measures in healthy adults [1]. Our goal in this study is to evaluate EIT-based PAP measures against invasive measures in neonatal lambs.

2 Methods

Healthy (2–4 days old, 2.57 ± 0.49 kg) lambs were anesthetized, ventilated, and placed in prone position, while EIT data were acquired with a 32-electrode belt (protocol details in [2]). A Swan-Ganz catheter was placed in the pulmonary artery and pressure waveforms and ECG signals were acquired and synchronized to the EIT data. Data were analyzed using the algorithm of [1]; briefly, in each 2-minute window, an average PAT in the lung region was calculated from an ECG-gated average EIT image sequence. PAP was estimated from the PAT values using linear regression.

3 Results and Discussion

At the time of writing, data were acquired in eight animals with four more experiments planned. Four data sets were rejected due to electrode errors or missing data. Representative data for one animal are shown (Fig 1), illustrating good correspondence between PAP measures, except in the last phase of the protocol, in which the epinephrine caused a decreased duration of the pre-ejection period. Overall, correspondence between PAP measures was high, with an average correlation $r = -0.810$ (range $-0.762 - -0.872$).

We consider these initial results to be very promising and hope to be able to report similar results with the full experimental set. A non-invasive, continuous, EIT-based measure of PAP would provide vital clinical data for the management of many newborns. For example, such PAP monitoring would help titrate iNO treatment in real time, helping especially avoid the risk of right ventricular failure and shock.

References

[1] M Proença *et al* Physiol Meas, 37:713–726, 2016
[2] Sage *et al*, Frontiers Physiology, 9:1723, 2018.

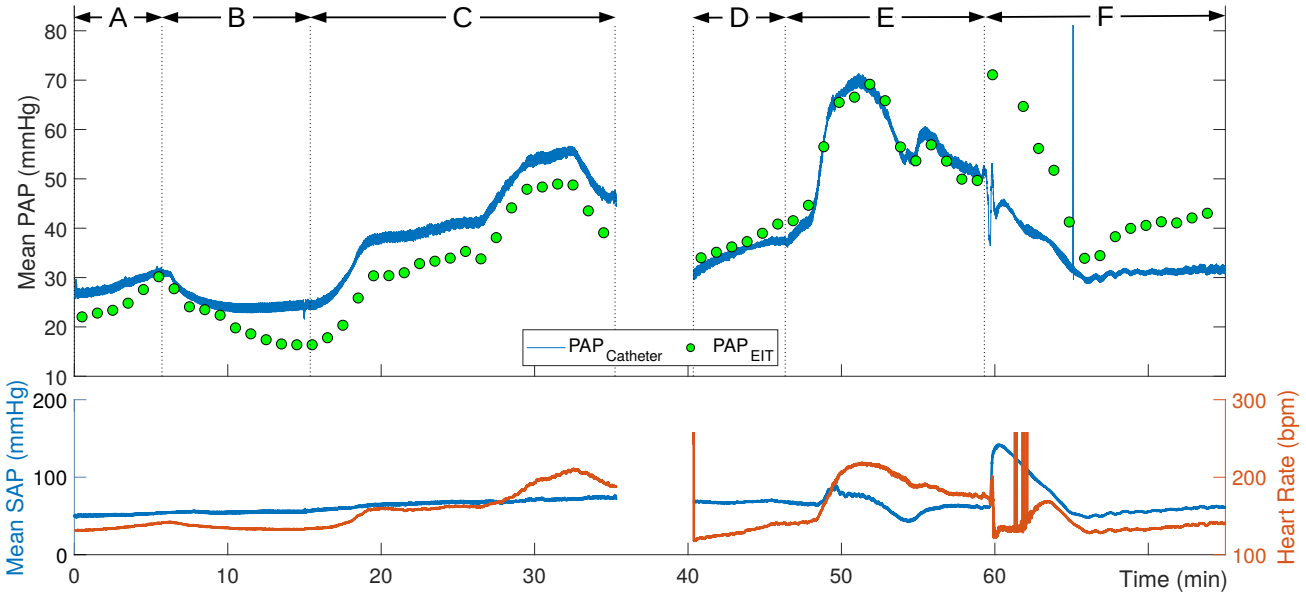

Figure 1: PAP and PAP_{EIT} (top row) and systemic arterial pressure (SAP) and HR data (bottom row) for a representative animal. A: FiO_2=21% B: FiO_2=100%, C: FiO_2=12–14%, D: FiO_2=21%, E: FiO_2=12–14%+hypoventilation, F: FiO_2=100%+epinephrine.

Identification and Quantification of Regional Lung Strain using EIT

Fabian Müller-Graf[1], Lisa Krukewitt[1], Alexander März[1], Emiliano Gogniat[2], Gerardo Tusman[3], Stephan H Böhm[1] and Daniel A Reuter[1]

[1] Department of Anaesthesiology and Intensive Care Medicine, University Medical, Center Rostock, Rostock, Germany
fabian.mueller-graf@uni-rostock.de

[2] Department of Intensive Care Medicine, Hospital Italiano de Buenos Aires, Buenos Aires, Argentina

[3] Department of Anesthesiology, Hospital Privado de Comunidad, Mar de Plata, Argentina

Abstract: We proposed an EIT-based algorithm for the visualisation and quantification of lung strain. We used a porcine model of lung injury and calculated strain as regional tidal volume (Vt) per end-expiratory lung impedance (EELI) normalized to PEEP 15 cmH_2O. Strain occurred in ventral lung areas especially at lower PEEP.

1 Introduction

Acute respiratory distress syndrome (ARDS) is a life-threatening lung injury where EIT is able to display regional ventilation and thereby may help to develop lung protective ventilation strategies [1]. Amato showed how high driving pressure is the main predictor of ventilator-associated death in ARDS patients. Especially low PEEP levels with concomitant atelectasis in dorsal lung sections causing a 'reduced functional lung' size and therefore needing injurious high driving pressures for maintaining sufficient ventilation. This functionally reduced lung, if ventilated with normal tidal lung volumes, is prone to overdistension of the remaining ventilated tissue [2]. Therefore, we developed an EIT-based algorithm capable of detecting lung areas with high relative strain, a factor known to cause lung injury.

2 Methods

We analysed data from eight pigs with an ARDS model induced by washing out lung surfactant with 30 ml/kg body weight of isotonic saline solution per lavage and by superimposing 2 hours of injurious mechanical ventilation with high tidal volumes and low PEEP. Pigs were supine and treated with a volume-controlled mode of ventilation with tidal volumes of 10 ml/kg body weight and randomly assigned PEEP levels ranging from 0 to 30 cmH_2O (5 cmH_2O steps) at a respiratory frequency of 24/min and a I:E ratio of 1:2 meanwhile 2D-EIT data were recorded by a 32 electrode EIT Pioneer Set (SenTec AG, Landquart, Switzerland). Images were reconstructed using a modified GREIT algorithm.

For analysing a representative area of the lungs, we defined the lung's Region of Interest (ROI) as all pixels showing a tidal impedance change of >10% of the maximum amplitude at PEEP 15 cmH_2O.

Regional strain was calculated pixelwise dividing EIT derived regional tidal volume (Vt) by end-expiratory lung impedance (EELI) for each pig and for each PEEP level. These data were referenced to PEEP at 15 cmH_2O, where atelectasis is known to be minimal and compliance maximal in pigs subjected to the same model [3].

$$relative\ strain = \frac{Vt}{EELI} \Big/ \frac{Vt_{PEEP15}}{EELI_{PEEP15}}$$

Total strain was calculated as average strain of the whole ROI for all pigs at each individual PEEP level.

3 Results and Conclusions

Figure 1 shows a series of strain images. We demonstrated how high strain occurs mainly at lower PEEP levels. This strain was located primarily in the ventral lung regions. Astonishingly, higher PEEP levels did not increase the strain in lungs, in contrast, it was diminished. These findings are supported by Amato's multilevel mediation analysis, showing that higher driving pressures, which are required at lower PEEP levels for maintaining ventilation, were associated with death in ARDS patients [2]. The combination of high strain at low PEEP can be interpreted as a consequence of the accumulation of atelectasis in the dorsal lung at this low PEEP, thereby reducing functional lung size [2]. This gives rise to the assumption that EIT-based calculation of regional strain might help in detecting a reason for the high driving pressures seen at low PEEP.

EIT detected and estimated local lung strain. Further investigations are needed to determine on a biological level whether the described lung sections actually become injured.

References

[1] Frerichs I, Amato MB, van Kaam AH, Tingay DG, Zhao Z, Grychtol B, Bodenstein M, Gagnon H, Böhm SH, Teschner E, Stenqvist O, Mauri T, Torsani V, Camporota L, Schibler A, Wolf GK, Gommers D, Leonhardt S, Adler *A Thorax*, 72(1):83-93, 2017

[2] Amato MB, Meade MO, Slutsky AS, Brochard L, Costa EL, Schoenfeld DA, Stewart TE, Briel M, Talmor D, Mercat A, Richard JC, Carvalho CR, Brower RG *N Engl J Med*, 372(8):747-55, 2015

[3] Suarez-Sipmann F, Böhm SH, Tusman G, Pesch T, Thamm O, Reissmann H, Reske A, Magnusson A, Hedenstierna G *Crit Care Med*, 35(1):214-21, 2007

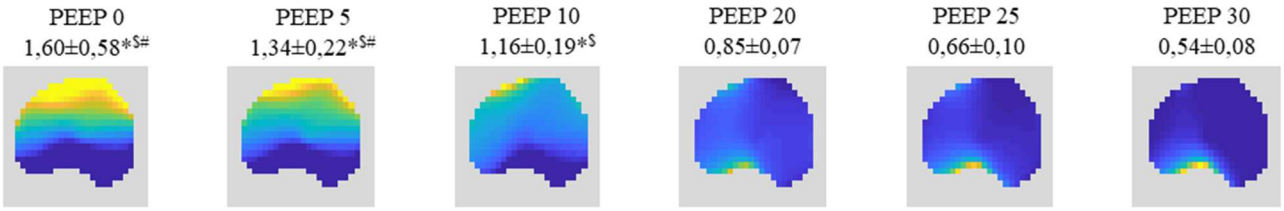

Figure 1: Relative regional strain (yellow = high strain, blue = low strain). Total strain given as mean ± standard deviation for whole lung of all pigs at each PEEP level. * P < 0,05 vs. PEEP 30; $ P < 0,05 vs. PEEP 25; # P < 0,05 vs. PEEP 20.

Bi-Frequency Symmetry Difference (BFSD) EIT in Stroke Diagnosis

Barry McDermott[1], Martin O'Halloran[1] and Emily Porter[1]

[1]Translational Medical Device Lab, National University of Ireland, Galway, b.mcdermott3@nuigalway.ie

Abstract: BFSD-EIT can detect deviations in the inherent normal symmetry of the head due to, for example, the presence of a bleed or clot in stroke. We assess the potential of BFSD-EIT to robustly detect lesions under a series of modelling errors and calculate tolerable error levels before lesion detection is confounded.

1 Introduction

Detection of static lesions, such as is the case for an intracranial bleed or clot in stroke, is an ongoing challenge for EIT [1], [2]. We present a novel technique (described in [3]) based on the symmetrical nature of the head across the sagittal plane. The presence of a lesion results in deviations in this symmetry. Identification of these deviations enables detection of the lesion, with subsequent determination of the nature of the lesion achieved using *a priori* knowledge of conductivity (and contrast) changes of tissues between frequency points. In this numerical study, an anatomically accurate 4-layer model was used with or without either a bleed or clot at different locations within the brain. Measurement frames from two symmetrically equal but opposite injection/ measurement protocols (taken at carefully selected frequency points) are differenced to detect deviations in symmetry (if present). The performance is assessed using images and metrics. Next, the model is exposed to a battery of modelling errors with performance assessed at different levels of error. The proposed Global Left Hand Side (LHS) & Right Hand Side (RHS) Mean Intensity (GMI) metric is particularly robust to modelling errors, and can be used to detect, identify and locate lesions as well as describe the effect of errors.

2 Methods

Models were generated with various levels of error assessing the impact of noise, errors in electrode positioning, contact impedance, assumed conductivity of tissues, the assumed anatomy of the head, and a frequency dependent background. The metric used to assess performance was the GMI: The average intensity over all the voxels on each side (LHS & RHS) of the sagittal plane.

The performance of the BFSD-EIT technique and the GMI metric were compared with those of an error-free model. The results are summarised as follows.

∗The SNR of the system used to record measurements should be at or above a rating of 80 dB.

∗Errors in electrode positioning have a severe effect on performance but a high degree of tolerance is seen if symmetry is maintained between symmetric partner electrodes (up to ± 30 mm).

∗Errors in contact impedance of electrodes (up to ± 50% of the assumed impedance) have little or no effect on performance.

∗Errors in the assumed conductivity of the tissue voxels (up to ± 50% of the reference value) have little or no effect on performance.

∗Errors in the assumed anatomy of the head affect performance. Asymmetrical anatomy can mask the presence of lesions. If the tissues have a frequency dependent change in conductivity this challenge may be overcome. Errors in the assumed geometry of the head (i.e. the boundary) with a variance of 10% cause only a slight decrease in performance.

∗A frequency dependent background has the potential to confound disambiguation if frequency points f are not carefully chosen. The pattern of contrast change at the selected f points between lesion and background must differ for bleed and clot.

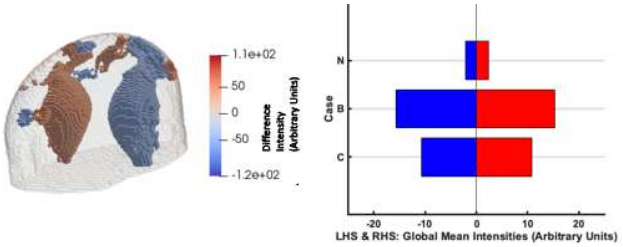

Figure 1: Left: A BFSD-EIT image for a 10 ml LHS bleed. Right: GMI metric results for no lesion (N); 10 ml LHS bleed (B); 50 ml LHS clot (C) (all at 25 Hz).

3 Conclusions

This set of numerical studies point to BFSD-EIT being feasible for use in the stroke diagnosis problem, provided potential error sources are respected and within parameters of tolerance. The technique is potentially applicable to other domains where symmetry may be exploited, stroke representing a particularly challenging problem and perhaps a "hardest case" for the algorithm. Future work is planned where the algorithm will be applied to both phantom and human data, with the hope that strong numerical performance is carried into more realistic scenarios.

4 Acknowledgements

The research leading to these results has received funding from the European Research Council under the European Union's Horizon 2020 Programme/ ERC Grant Agreement BioElecPro n.637780, and from the Hardiman Research Scholarship, NUIG.

References

[1] A Adler, A Boyle, *IEEE Transactions on Biomedical Engineering* 64(11):2494–2504,2017

[2] A Romsauerova, A McEwan, L Horesh, *Physiological Measurement* 27(5):S147-S161,2006

[3] B McDermott, M O'Halloran, E Porter, *Physiological Measurement* 39(4): 044007,2018

Imaging slow impedance changes in focal epilepsy model in porcine brain with EIT and depth electrodes

Anna Witkowska-Wrobel[1], Kirill Aristovich[1], Abbe Crawford[2], Jamie Viscasillas[2], Thaleia-Rengina Stathopoulou[2], Justin Perkins[2] and David Holder[1]

[1]Medical Physics and Biomedical Engineering, University College London, UK, anna.wrobel@ucl.ac.uk
[2]Royal Veterinary College, Hawkshead Lane, North Mymms, Hatfield, Hertfordshire AL9 7TA, UK

Abstract: This study presents for the first time the feasibility of imaging slow impedance changes during each seizure in a chemical model of epilepsy in swine brain using intracranial electrodes. This novel work shows that EIT has potential as a real-time imaging method during seizures.

1 Introduction

Electrical Impedance Tomography (EIT) might be used to image neuronal depolarization over milliseconds or slower changes over seconds related to blood flow/cell swelling; both require intracranial electrodes for brain imaging. Patients with refractory focal epilepsy requiring surgery may have implanted multiple intracranial electrodes to localise seizure onset by recording the EEG, but this has limited sensitivity. We propose that the coverage and sensitivity could be improved by EIT of slow changes with these intracranial electrodes [1]. **The purpose** of this work was to evaluate this in a chemical epilepsy model in the anesthetised pig. Whereas fast neural EIT requires averaging over several minutes, slow EIT may employ frequency division multiplexing [2] to acquire all current injection pairs needed simultaneously and, by so, produce real-time imaging.

2 Methods

Data were collected with a parallel EIT system of 32 current sources at 8-10kHz, spaced 50Hz apart, BW 10Hz, and simultaneous recording on 64 channels, able to address any pre-selected electrode combinations. It allows EIT recording of slow neural activity with 0.1sec resolution in real-time without averaging. Images were reconstructed using 9M forward and 1M inverse FEMs, using subject-specific CT images. A craniotomy ~5x2cm size was made over the left somatosensory cortex. A subdural grid electrode (4x8 contacts, 5mm spacing), and 3 to 4 depth electrodes (10 contacts, 0.86mm diameter, 2.29mm length, 5mm spacing, AdTech, platinum), were placed directly on the cortex, towards the midline, recording from near the hippocampus, amygdala and thalamus. A cannula for seizure induction was positioned at the centre of the grid and ~30mm deep into the brain. Focal seizures were induced with a single 20µl Procaine Benzyl-Penicillin (BPN, Depocillin 300mg/ml) injection into the brain. A post-mortem head CT scan was taken to create accurate FEM meshes and locate the electrodes and cannula.

3 Results and conclusions

In 5 pigs, there were 115 reproducible recurrent focal/focal and secondary generalised seizures and 90 generalised, occurring every 3 to 10min, lasting 25.7±14sec (mean±SD). There was an impedance increase of 1.4±1mV (6±4%) in focal and 2.8±1.5mV (8±5%) in generalised seizures. It was delayed from EEG onset of 14±9sec (Fig.1).

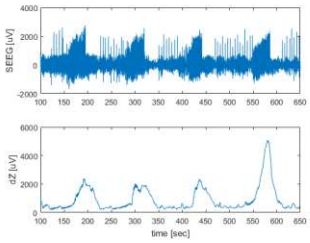

Figure 1. Maximum impedance change (bottom) occurring during four seizures seen in EEG (top). In this example, impedance rose ~13sec after the EEG onset. The last seizure quickly generalised, which is reflected by the difference in magnitude of dZ.

EIT produced images of the seizure in real time. The maximum impedance increase localised within 11±9mm of the tip of the BPN cannula in 50 seizures reconstructed so far (e.g. Fig.2).

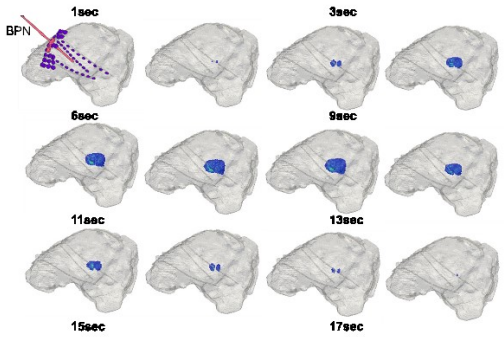

Figure 2. Focal seizure start and spread as reconstructed with EIT. The change is localised in proximity of BPN injection.

Work is in progress to analyse further the images, to establish the accuracy and evaluate the specificity and selectivity of EIT when limited number of intracranial electrodes is used. In parallel, a human study is in progress on epilepsy patients using the same electrodes.

4 Acknowledgements

Research supported by DARPA.

References

[1] A. Witkowska-Wrobel, K. Aristovich, M. Faulkner, J. Avery, and D. Holder, “Feasibility of imaging epileptic seizure onset with EIT and depth electrodes,” Neuroimage (173) 2018.
[2] J. Avery, T. Dowrick, M. Faulkner, N. Goren, and D. Holder, “A Versatile and Reproducible Multi-Frequency EIT System,” Sensors (17) 2017.

Towards Unconstrained *In Vivo* Transcranial Electrical Stimulation (TES) Field Measurements using DT-MREIT

Saurav Z. K. Sajib[1], Munish Chauhan[1], Oh In Kwon[2], Rosalind J. Sadleir[1]

[1]School of Biological and Health Systems Engineering, Arizona State University, Tempe, Arizona, USA
Rosalind.Sadleir@asu.edu
[2]Department of Mathematics, Konkuk University, Seoul, 05029, Korea

Abstract: Existing MREIT reconstruction techniques require injection of two independent currents for unique conductivity reconstructions Here, we demonstrate an algorithm using an artificial neural network-based algorithm that can be used to reconstruct electromagnetic parameters using flux density data from only one current injection.

1 Introduction

While current density can be estimated from one set of MREIT data, stable conductivity reconstruction requires two independent current administrations [1, 2]. Lee et al. [3] used one current profile data to reconstruct conductivity image from known conductivity values at the boundary using the KVL in a mimetic discretized network. However, the performance of the reconstructed images was limited due to streaking artifacts caused by noise propagation along equipotential lines [3]. Therefore, MREIT or DT-MREIT techniques could not be used to reconstruct tissue conductivities during standard tES/DBS studies. We used additional B_z data obtained from computational models and a radial basis function artificial neural network (RBF-ANN) correction in this work to demonstrate the feasibility of conductivity reconstruction using one experimental current injection.

2 Methods

Reconstructions were performed with the aid of mimetic algorithms, simulations of magnetic flux density from complementary electrode montages, combined with machine learning.

2.1 Gel Phantom

A 55-mm diameter phantom consisting of chicken breast muscle oriented in x (left), y (right) and z-directions (top), and potato (bottom), embedded in an 1.0 S/m conductive gel made of agarose was used for imaging (Figure 1, insets). Data were measured using the ASU-BNI 7.0 T Bruker scanner. A 10 mA MREIT imaging current was used. Two sets of B_z data were collected over five slices, with an image matrix size of 128×128. Diffusion tensor data of the same five slices were then collected using a single-shot spin-echo echo planar imaging (SSSE-EPI) pulse sequence with b of 1000 sec/mm^2 and six diffusion directions. Data were acquired with TR/TE=2500/32.67 ms. Other parameters were the same as for MREIT image sequences.

2.2 Reconstructions and Comparisons

An overdetermined system was built comprising overlapping KVL equations, which was then solved for scale factors (η) on internal nodes. To overcome streaking artifacts, an RBF-ANN was trained using 1000 numerical models (agar: 0.1-1, chicken: 0.2-1.25 potato: 0.01-0.3 S·/mm^3) with conductivity assumed piece-wise constant in each ROI. To verify reconstruction performance, relative L^2 errors were measured between the proposed and standard two current injection method [5].

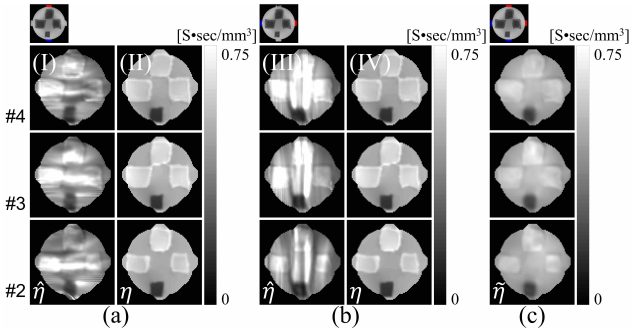

Figure 1: Reconstructed scale factor images of the central three slices of phantom object. (a) and (b) show reconstructed scale factors found using vertical or horizontal current injection respectively. I (and III) shows solution of the dual-loop matrix system. II (and IV) shows images of ANN-corrected scale factors.(c) Scale factor images recovered from data measured from both current injections.

3 Conclusions

In case of a biological tissue phantom we found that use of these methods reduced relative errors between single-current and two-current DT-MREIT results to around 10%. These results suggest that incorporation of machine learning approaches may make it easier to recover electrical conductivity tensors and electric field measures *in vivo* without the need for multiple current administrations.

4 Acknowledgements

This work was supported by NIH grant RF1MH114290 to RJS.

References

[1] E J Woo, J K Seo, "Magnetic resonance electrical impedance tomography (MREIT) for high-resolution conductivity imaging," *Physiol Meas.*, 29(10), R1-26 (2008).

[2] M Chauhan, A Indahlastari, A K Kasinadhuni, M Schar, T H Mareci and R J Sadleir, "Low-frequency conductivity tensor imaging of the human head in-vivo using DT-MEIT: first study," *IEEE Trans. Med. Imaging* 37 (4), 966-76 (2018).

[3] T H Lee, H S Nam, M G Lee, Y J Kim, E J Woo and O I Kwon, "Reconstruction of conductivity using dual-loop method with one injection current in MREIT," *Phys. Med. Biol.* 55 (24), 7523-39 (2010).

[4] Oh, T. I. *et al*. Improved current source design to measure induced magnetic flux density distributions in MREIT. *J. Biomed. Eng. Res.* **27** 30–7 (2006).

[5] Sajib, S. Z. K. *et al*. Regional absolute conductivity reconstruction using projected current density in MREIT. *Phys Med Biol.* **57** 5841-59 (2012).

Analysis of noise in EIT recordings of fast neural activity

Sana Hannan[1], Enrico Ravagli[1], Kirill Aristovich[1] and David Holder[1]

[1]Medical Physics and Biomedical Engineering, University College London, UK. (email: sana.hannan.14@ucl.ac.uk)

Abstract: A noise analysis was undertaken to determine the principal source of noise in fast neural EIT recordings obtained using epicortical electrodes on the rat brain. Results indicate that physiological noise is larger in EIT recordings in the brain than in the nerve and thus may be attributed to spontaneous EEG activity.

1 Introduction

EIT is capable of imaging fast electrical activity during evoked neural activity and epileptiform discharges with a resolution of <300 µm and 2 ms through the cerebral cortex of the anaesthetised rat, using epicortical electrode arrays [1, 2]. In addition, it can be used for the functional localisation of evoked compound activity in peripheral nerve fascicles [3]. The critical limitation of fast neural EIT in its current state of development relates to the need for averaging in order to reduce noise and achieve an adequate SNR for imaging. However, averaging is not possible for certain proposed applications of this technique, for example, in the presurgical evaluation of patients with epilepsy for localising the seizure onset zone. As such, alternative methods of improving the effective SNR should be investigated to increase the applicability of fast neural EIT. The purpose of the current work was to determine whether the principal source of noise in EIT recordings of fast neural EIT relates to the hardware used for data acquisition or the physiological noise from the spontaneous EEG activity in the brain**.**

2 Methods

2.1. Fast neural EIT recordings in the brain

Adult female Sprague-Dawley rats were anaesthetised with isoflurane; anaesthesia was maintained with an isoflurane-fentanyl combination. After performing a craniotomy, a 57-electrode array, fabricated from stainless steel and silicone rubber, was implanted on the cortical surface. Baseline impedance recordings were obtained, by injecting a 50 µA sine-wave at 1.7 kHz, *in vivo* and post-mortem. The impedance signals were demodulated at two different bandwidths, ±500 Hz and ±200 Hz, around the carrier frequency using a fifth-order Butterworth filter.

2.2. Fast neural EIT recordings in the sciatic nerve

Anaesthesia was induced and maintained with urethane. The right sciatic nerve was isolated and a 14-electrode cylindrical array, fabricated from stainless steel and silicone rubber, was placed around it. Baseline impedance recordings were obtained *in vivo* and post-mortem by injecting a 60 µA sine-wave at 6 kHz. The impedance signals were demodulated at a bandwidth of ±2 Hz.

3 Results

For impedance measurements in the brain, the baseline noise level in *in vivo* recordings was 1.61 ± 0.41 µV when using a bandwidth of ±500 Hz. This was significantly higher than the noise level in post-mortem recordings, 0.74 ± 0.21 µV ($p < 0.01$, $n = 154$ traces, $N = 3$ rats). When using a ±200 Hz bandwidth, the post-mortem and *in vivo* noise levels were 0.38 ± 0.11 µV and 0.54 ± 0.19 µV, respectively, and were also significantly different ($p < 0.01$). In contrast, preliminary recordings in a single rat sciatic nerve indicate no observable difference in baseline noise levels between the post-mortem and *in vivo* condition.

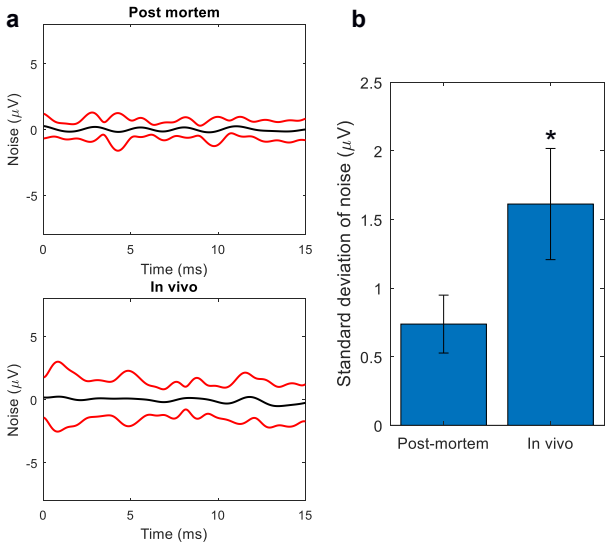

Figure 1. Comparison of noise between *in vivo* and post-mortem recordings obtained in the rat brain. (**a**) Mean ± 1 standard deviation of noise levels in impedance recordings extracted with a bandwidth of ±500 Hz. (**b**) Bar charts displaying mean noise levels (* $p < 0.01$, paired t-test, $n = 154$ traces, $N = 3$ rats).

4 Conclusions

Comparison of *in vivo* and post-mortem baseline impedance recordings obtained in the brain revealed that the main source of noise, in impedance signals extracted using a bandpass filter that provides an adequate temporal resolution for imaging fast neural activity (i.e. ≤5 ms), is physiological. Because noise levels in the sciatic nerve did not differ considerably between the *in vivo* and post-mortem condition, the increased physiological noise in brain recordings can be attributed to spontaneous EEG activity, which is not present in peripheral nerves. The extent of this noise may be reduced by utilising a narrower bandwidth to extract the impedance signal., although this would compromise the temporal resolution of images. Therefore, fast neural EIT currently requires a trade-off between SNR and temporal resolution, which can be tailored for specific applications.

References

[1] K. Aristovich et al., *Neuroimage*. 124(Pt A): 204-213, 2016.
[2] S. Hannan et al., *Neuroimage Clin*. 20:674-684, 2018.
[3] K. Aristovich et al., *J Neural Eng*. 15(5):056025, 2018.

Fast Neural EIT of Peripheral Nerves: Cross-Validation with Invasive Techniques

Enrico Ravagli[1], Svetlana Mastitskaya[1], Nicole Thompson[1], Kirill Aristovich[1] and David Holder[1]

[1] Medical Physics, University College London, Gower Street, London WC1E 6BT, United Kingdom (e-mail: e.ravagli@ucl.ac.uk).

Abstract: Electric Impedance Tomography for imaging of fascicular activity in peripheral nerves was validated using two invasive but higher resolution techniques: Micro Computed Tomography scans of iodine-stained nerves and labelling of fascicles with neural tracers.

1 Introduction

The vagus nerve supplies parasympathetic innervation to nearly all visceral organs and is, therefore, a primary target for neuromodulation. However, the fascicular organisation of the cervical vagus nerve is poorly understood. We propose to use the novel and non-invasive method of fast neural Electrical Impedance Tomography (EIT) [1] to image autonomic functional neural activity and so enable selective stimulation of cervical vagus nerve. Before that, EIT on peripheral nerves needs further validation. In this work we aim for cross-validation of EIT with two other well established but more invasive techniques:

- Neural tracers injected into single fascicles
- Imaging using Micro-Computed Tomography (MicroCT)

Current work is in refining the method in rat sciatic nerve; future studies will be performed in pig vagus nerve.

2 Methods

2.1 EIT

EIT recordings of evoked activity in individual fascicles were performed as in [1], with the improvements of: i) PEDOT electrode coating instead of platinum, to further reduce contact impedance [2], and ii) stimulation of the sural fascicle in addition to tibial and peroneal. EIT images were reconstructed with a Tikhonov-based algorithm over a coarse voxel-based nerve mesh and post-processed using median and mean filtering with radius of 1 and 3 voxels respectively.

2.2 Neural tracers

Under isoflurane anaesthesia, 5 µl of 2.5% Alexa Fluor 488/555 Dextran 10 kDa (ThermoFisher) were injected using glass micropipette into the tibial/peroneal branches of the rat sciatic nerve. The animal recovered for 48h to ensure diffusion of the tracer to the common sciatic nerve.

2.3 MicroCT

Rat sciatic nerves excised after EIT recordings were fixed in formalin and stained with Lugol's solution. Staining and scanning parameters were optimized to achieve the best possible image quality. Image post-processing was performed in MATLAB (Mathworks, USA) to enhance contrast.

3 Results

It was possible to co-localize the tibial (T), peroneal (P) and sural (S) fascicles successfully with EIT (example in Fig. 1), Dextran tracer and micro-CT (Fig. 2) with a spatial accuracy of ≈200µm (n=2).

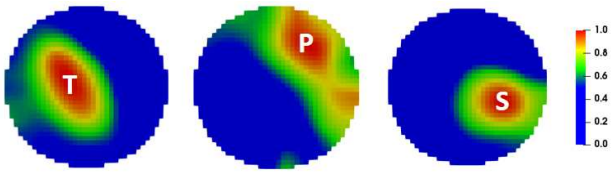

Figure 1. Reconstructed EIT images of evoked activity in tibial (left), peroneal (centre), and sural (right) fascicles. Activity is shown normalized and with full-width at half-maximum (FWHM) color scale.

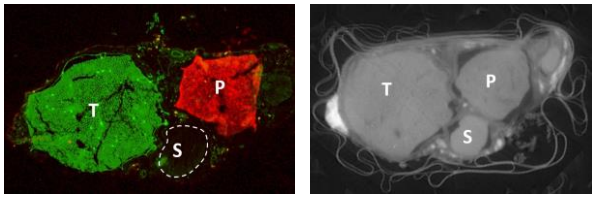

Figure 2. Left: histology showing successful Dextran tracing of tibial (green) and peroneal (red) fascicles. Right: slice from MicroCT scan.

4 Conclusions

Results show consistent co-localization of fascicles between EIT, neural tracers and MicroCT. Work is in progress to quantitatively co-register the images and to enlarge the dataset in rat sciatic nerve. Future work is to extend the methods to pig vagus nerve. EIT is a non-penetrating imaging technique and, once validated in animals, may be used in humans.

5 Acknowledgements

Research supported by the UK Medical Research Council (MRC grant No:MR/R01213X/1 and NIH SPARC 1OT2OD026545-01).

References

[1] K. Aristovich et al., *J Neural Eng*. 15(5):056025, 2018
[2] C.A.R. Chapman et al., *J Neural Eng*. 16(1):016001, 201

Optimisation of stimulation frequency for imaging small unmyelinated fibres with EIT

Ilya Tarotin[1], Kirill Aristovich[1] and David Holder[1]

[1]Medical Physics and Biomedical Engineering, University College London, UK, ilya.tarotin.14@ucl.ac.uk

Abstract: Imaging small unmyelinated fibres with electrical impedance tomography (EIT) is challenging due to small SNR and dispersion. A cumulative imaging technique which theoretically overcomes dispersion was optimised in simulations. The optimal stimulation frequency was found to be 10 Hz with the duty cycle ≈ 6%.

1 Introduction

EIT was shown to be capable to image fascicular activity of large myelinated fibres in peripheral nerve [1]. However, imaging small unmyelinated fibres is challenging due to small magnitudes of the measured dZ and large effect of dispersion. To accomplish imaging, the cumulative paradigm of imaging several consecutive action potentials (APs) is proposed, in which effect of dispersion will be minimised. In order to evaluate the feasibility of the paradigm and maximise the SNR, the optimal conditions for impedance acquisition such as the stimulation frequency, the amplitude and duty cycle of the measured spikes as well as the total time of stimulation before fibre saturates were determined. The increase in the spiking duty cycle cannot be reached by a simple increase in a stimulation rate: the reason is balancing mechanisms of nerve fibres such as neural accommodation and accumulation of potassium ions outside the membrane [3].

2 Methods

Mammalian C fibre model coupled with external space was used as the basis model for simulations [2]. This model was exposed to repetitive stimulation with internally applied suprathreshold 20 nA stimuli with monopolar and monophasic 0.1 ms pulses. The stimulation frequencies of 5, 10, 20 and 50 Hz were applied until the firing stopped due to balancing mechanisms discussed above; the full durations of the simulations were 5s. As the amplitudes of spikes during the repetitive stimulation differed, and the aim was to obtain the maximum number of peaks of the highest amplitude, the total cumulative amplitude of spikes produced at each frequency was found. By inspection of the resulting graphs and finding the times during which the membrane returns to rest, the total amplitudes were extrapolated to 100 s in order to find the maximum cumulative amplitude of spikes that can be measured over long periods of time. Finally, the duty cycle at the optimal frequency was determined for the unmyelinated crab nerve based on its CAP duration ≈ 10 ms [4].

3 Results

The frequency which could be used for continuous repetitive stimulation at up to 5 s was 5 Hz, although the amplitudes of consecutive APs were decreasing so that stimulation will have to be stopped at ~ 7 s until the membrane returns to the resting state (Figure 1, left). At higher frequencies, stimulation could be maintained for: ~3 s at 10 Hz, 0.75 s at 20 Hz and 0.25 s at 50 Hz. Stimulation could be started again after the membrane potential and ionic concentrations returned to the resting value that was observed after ~2 s at all frequencies. Thus, the total amplitude of APs was computed for the measured 5 s and was extrapolated to 100 s on the basis of activation-rest periods: 7 (activation) + 2 (rest) = 9 s at 5 Hz, 5 s at 10 Hz, 2.75 s at 20 Hz and 2.25s at 50 Hz. The resulting total cumulative amplitude was found to be maximal at 10 Hz (Figure 1, right) with the duty cycle for the 10 ms CAP crab nerve equalling (3 s·10 Hz·10^{-2} s)/5 s = 6 %.

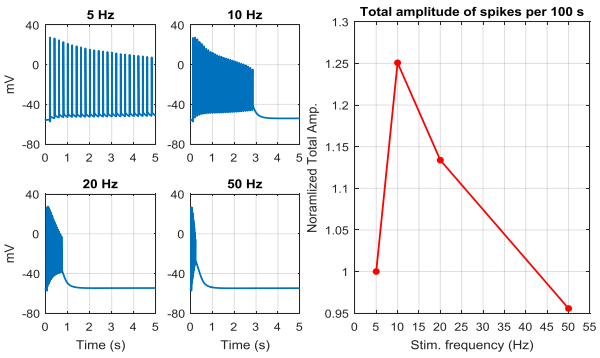

Figure 1: Left: APs (spikes) during repetitive stimulation at various frequencies; right: cumulative amplitude of spikes extrapolated up to 100 s and normalized in respect to 5 Hz.

4 Conclusions and future work

This paper describes the initial stage of the stimulation paradigm optimisation for performing EIT in small unmyelinated fibres. The optimal stimulation frequency was determined to be 10 Hz; the duty cycle for the crab nerve was 6%. For a complete optimisation study, the next step will be to find the frequency of stimulation providing the largest SNR, i.e. the one which also minimises the noise after the signal is band-pass filtered [1-2]. Also, the effect of temporal dispersion needs to be simulated [5] so that different signal processing specifications can be applied to maximize the extracted dZ in realistic nerves.

5 Acknowledgements

The work was supported by NIH SPARC grant no: 1OT2OD026545-01.

References

[1] K Aristovich et *al J. Neural Eng.*, 15 (5): 056025, 2018.
[2] I Tarotin et al. *IEEE Trans. Biomed. Eng.*, 66 (2): 471–484, 2019.
[3] D Scriven. *Biophys. J.* 35 (3): 715-730,1981.
[4] O Gilad et al. *J. Neurosci. Methods*. 180 (1): 87-96, 2009.
[5] I. Tarotin et al. *Physiol meas.* 40: 034001, 2019.

To assess subcutaneous fat thickness using a learning-based method

Ariungerel Jargal[1] and Hyeuknam Kwon[2]

[1]Dept. of Computational Science and Engineering, Yonsei University, Seoul, South Korea. ariunaa@yonsei.ac.kr
[2]College of Science of & Technology, Yonsei University, Wonju, South Korea. hyeuknamkwon@yonsei.ac.kr

Abstract: We evaluate a learning-based method [1] of absolute electrical impedance tomography (EIT) to estimate a thickness of subcutaneous fat [2]. The feasibility of the approach is validated through simulations.

1 Introduction

The absolute EIT techniques from physics-based modelling can not avoid boundary geometry artifacts, because the interpretation of data includes boundary geometry. To overcome this limitation, we adopt deep learning (DL) technique [1] which is developed based on the relation between data and image not physics law. We use the variational autoencoder (VAE), one of the most popular approaches to unsupervised learning, because it can extract features (subcutaneous fat thickness) from complicated distributions (bunch of data). Here, we evaluate the feasibility of the approach through numerical simulations with 600 training images and 48 test images. The results reported confirm the feasibility of the technique to detect and estimate the thickness of subcutaneous fat.

2 Method

The inverse problem in EIT is to find the map $f : \mathbf{V} \mapsto \sigma$ from measured data (electric impedance) $\mathbf{V}$ to electric conductivity distribution σ in human body. We aim to make a reconstruction map f *not using physics-based model* so that there will be no geometry error *but using data-based model* so that it will be only determined by measured data and conductivity distribution. We adopt VAE, one of DL technique, to make f from only training data $\{(\mathbf{V}^i, \sigma^i) : i = 1, 2, \ldots, N\}$ where N is the number of data.

The advantage of using VAE is that we can find *low dimensional representation* $\mathbf{z}$, called latent, of image in measured impedance. The map f is defined based on $\mathbf{z}$:

$$f = \Psi \circ \Xi$$

where Ξ is nonlinear regression map from measured impedance $\mathbf{V}$ to the latent $\mathbf{z}$ and Ψ is generator from latent $\mathbf{z}$ to conductivity distribution σ. The nonlinear regression Ξ is defined by

$$\Xi = \underset{\Xi}{\operatorname{argmin}} \frac{1}{N} \sum_{i=1}^{N} \|\Xi(\mathbf{V}^i) - \mathbf{z}^i\|^2$$

The generator Ψ is defined with inference Φ as

$$(\Phi, \Psi) = \underset{\Phi,\Psi}{\operatorname{argmin}} \frac{1}{N} \sum_{i=1}^{n} [\|\Psi \circ \Phi(\sigma^i) - \sigma^i\|^2 + \mathbb{KL}(\mathcal{N}(\mu^i, (\nu^i)^2) || \mathcal{N}(0, I))]$$

where $\mathbb{KL}$ divergence is difference between two distributions and it is equal to $(\mathrm{tr}[(\nu^i)^2] + \|\mu^i\|_2^2 - \log|\nu^i|)$. The architecture of proposed method is illustrated in fig. 1. The detail of computation is following:

- $\Phi(\sigma) := (\mu, \nu) = W^{\Phi}_{(\mu,\nu)}(\eta(W^{\Phi}_2(\eta(W^{\Phi}_1\sigma))))$
- $z = \mu + e^{\epsilon \odot \nu}$ where $\epsilon \in \mathcal{N}(0, I)$
- $\Psi(z) := \widehat{\sigma} = s(W^{\Psi}_3(\eta(W^{\Psi}_2(\eta(W^{\Psi}_1 z)))))$
- $\Xi(V) := \widehat{z} = W^{\Xi}_2(\eta(W^{\Xi}_1 V))$
- $\eta(x) = \max(0, x)$ and $s(x) = 1/(1 + e^{-x})$
- W is linear transformation.

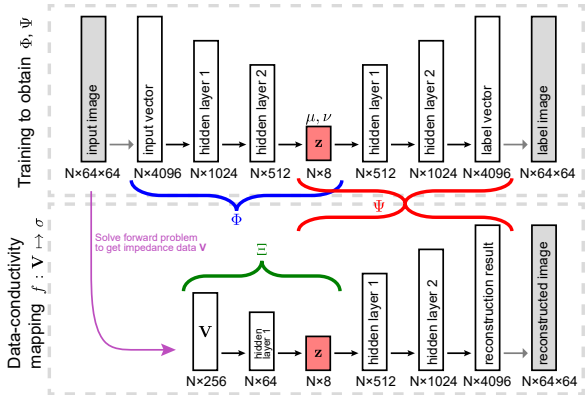

Figure 1: The scheme of learning–based method for absolute EIT. It is composed by two big structures; (1) VAE to find Φ and Ψ, (2) Mapping f to reconstruct σ from $\mathbf{V}$.

3 Result

We uses several types of body but here we present 2 kinds of different body with different subcutaneous and muscle layer thickness. The size of images σ^i and EIT data $\mathbf{V}^i$ are 64×64 and 256×1, respectively. The proposed method successively reconstruct absolute image as shown in fig. 2.

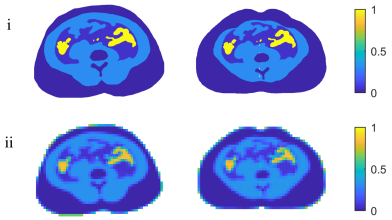

Figure 2: (i) True images. (ii) Reconstructed images.

4 Conclusion

The learning-based method (using VAE) which uses only data–conductivity relation was developed for absolute EIT. We were able to assess subcutaneous fat thickness from the reconstructed image.

5 Acknowledgements

A.J was supported by the National Research Foundation of Korea (NRF) grant 2017R1E1A1A03070653.

References

[1] JK Seo, KC Kim, A Jargal, K Lee, B Harrach, arXiv:1810.10112v2.
[2] H Ammari, H Kwon, S Lee, JK Seo, *SIAM J. Imaging Sci.* v. 10, pp. 900-919, 2017.

Propagation of Measurement Noise into Images

Alistair Boyle, Symon Stowe, Sreeraman Rajan, Andy Adler

Systems and Computer Engineering, Carleton University, Canada, boyle@sce.carleton.ca

Abstract: We examine the relationship between measurement noise and reconstructed images. For linearised EIT reconstruction, the location and distribution of artefacts can be identified exactly for known noise distributions, or approximately for arbitrary distributions. These intricate artefact models help explain how experienced users can often identify "bad" measurements in real-world data.

1 Introduction

Noise exists in all real-world data: undesired fluctuations in measured signal. There are a wide variety of noise sources, many of which are not well modelled by Gaussian distributions. For example certain models of quantization, clipping, burst, thermal, and shot noise are non-Gaussian. EIT measurement noise affects reconstructed conductivity images leading to artefacts. Structured noise can result in persistent artefacts which are difficult to identify from single images and are not removed by temporal filtering.

2 Methods

A single-step Gauss Newton EIT reconstruction matrix $\mathbf{Q}$ for measurements $\mathbf{b}$ contaminated by additive (non-parametric) noise η gives an image $\mathbf{x}$ where

$$\mathbf{x} = (\mathbf{J}^\mathsf{T}\mathbf{W}\mathbf{J} + \lambda^2\mathbf{R})^{-1}\mathbf{J}^\mathsf{T}\mathbf{W}(\mathbf{b}+\eta) = \mathbf{Q}(\mathbf{b}+\eta) \quad (1)$$
$$= \mathbf{x}^{(\mathbf{b})} + \mathbf{x}^{(\eta)} \quad \text{with } \mathbf{x}^{(\mathbf{b})} = \mathbf{Q}\mathbf{b}\,; \quad \mathbf{x}^{(\eta)} = \mathbf{Q}\eta$$

for Jacobian $\mathbf{J}$, inverse measurement covariance $\mathbf{W}$, and regularization $\mathbf{R}$ adjusted by hyperparameter λ. The uncontaminated measurements $\mathbf{b}$ give the image $\mathbf{x}^{(\mathbf{b})}$, while noise generates a distribution of additive changes to the image $\mathbf{x}^{(\eta)}$.

To calculate the distribution of noise afflicted images, a typical technique is the Bootstrap Method [1], where the mean of all images $\hat{\mathbf{x}}^{(\eta)}$, after random sampling of measurement noise η with replacement, gives a generalized distribution for sampled noise η_j where $\hat{\mathbf{x}}^{(\eta)} = \frac{1}{m}\sum_j^m \mathbf{Q}_{/j}\ \eta_j$ over many noise samples $m \gg 100$ will tend to a Gaussian distribution courtesy of the central limit theorem. With many measurements, Leave-One-Out (LOO) will give similar results to the bootstrap.

We see immediately that we need only calculate $\mathbf{x}^{(\mathbf{b})}$ once and in fact, it only shifts our distribution's centre. We can see the individual components of our measurement noise translated into an image distribution as a linear combination of measurements. Furthermore, the bootstrap resampling of measurements is not adding additional information, but is instead converting a point estimate into an approximately continuous distribution. If instead we examine each measurement's noise distribution individually and transform that distribution into the image domain through the reconstruction matrix $\mathbf{Q}$, we have an exact probability distribution for the reconstructed image $\mathbf{x}^{(\eta)} = \mathbf{Q}\eta = \mathbf{Q}\sum_k \mathbf{e}_k D_k = \sum_k \mathbf{x}_k^{(\eta)}$, for $\mathbf{e}_k = [0\ldots1\ldots0]^\mathsf{T}$ and 1 at the k row. The sum of the images gives a probabilistic "mixture model" which fully describes the variation in the reconstruction due to measurement noise.

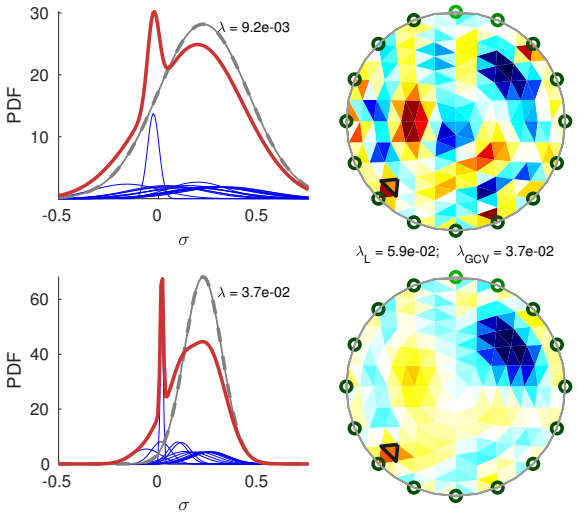

Figure 1: The PDF (blue) for a voxel (black triangle) changes depending on which measurements are dropped, in this case based on leaving out an electrode. Taking the sum of the PDFs (red) shows a distinct peak near the true conductivity. Removing single measurements (LOO) or bootstrap gives distributions driven by the central limit theorem (grey dashed, scaled to red line). Tikhonov regularized, GN-1 step images were reconstructed from noisy data $\eta = \mathcal{N}(0, c/10)$ and electrode#10 $\eta = \mathcal{N}(0, c)$ with $c = \text{std}(\mathbf{b})$. The linear mixture of distributions $\mathbf{Q}$ changes depending on regularization λ (upper versus lower images/plots). Reconstruction at λ for particular samples of noise *(right)* give a conductivity which is most often the max of the grey-dashed plot to the left, but the correct solution is at the red peak; *(above)* reduced regularization $\lambda_{GCV}/4$ produces distributions with greater variance, than *(below)* for λ_{GCV}; λ by L-curve λ_L and GCV λ_{GCV} are similar.

3 Observations and Conclusions

The effects of each measurement noise are separable and are captured by a scalar distribution. The scalar distributions form a linear mixture [2] through the reconstruction $\mathbf{Q}$ (Figure 1). The distribution of noise artefacts is solely a function of the reconstruction matrix $\mathbf{Q}$ and the noise distribution η. The combination of all k noise distributions D_k gives a specific image artefact distribution per voxel.

Greater regularization λ reduces noise variance in the overall mixture model, but does not necessarily "suppress" particular measurements. Noisy images are a mixture of scaled and offset distributions. Regions that are particularly sensitive to a single group of measurements allow isolation of that measurement's noise distribution and allow direct diagnosis of "bad" measurements.

This work demonstrates an efficient and direct method for computing the effect of noise on images and is an enabling tool for identifying noise distributions in artefact affected images using time-series data which may not be amenable to temporal filtering.

References

[1] Efron B. *The Annals of Statistics* **7**(1):1–26, 1979

[2] Richardson S, Green P. *J R Stat Soc Series B Stat Methodol* **59**(4):731–792, 1997

EIT for tissue engineering applications: a case for osteogenic differentiation

Marilisa Cortesi[1], Andrea Samorè[1], Joseph Lovecchio[1], Serena Morigi[1], Emanuele Giordano[1]

[1]University of Bologna, Italy

marilisa.cortesi2@unibo.it, andrea.samore@unibo.it, joseph.lovecchio@unibo.it

Abstract: The development of synthetic bone surrogates is currently hampered by the lack of non-destructive methods for their characterization. We here study the feasibility of using time-difference EIT as an alternative to dynamically monitor the mineralization of these constructs and allow their non-invasive characterization.

1 Introduction

Tissue Engineering (TE) holds great potential for the treatment of osteoporosis and cancer. The development of effective synthetic bone surrogates (scaffolds), is however hampered by the limitations of the assays like Alizarin red, that require the destruction of the sample. This technique, quantifying calcium depositions, is commonly used to evaluate the effectiveness of osteogenic differentiation but requires the sectioning of the scaffold, thus preventing its subsequent implantation or further analysis.

As calcium depositions are expected to affect electical conductivity, we here propose to use EIT to monitor non-invasively the maturation of TEed constructs. Indeed the cumulative effect of small mineral deposits on the scaffold's electrical properties is expected to be quantifiable. To prove this point and demonstrate the feasibility of time-difference EIT for the characterization of TEed bone surrogates, we here compared the reconstructed conductivity maps from a standard osteogenic differentiation experiment with measured Alizarin red concentrations.

2 Methods

We simulated 3 phantoms representing collagen scaffolds containing stem cells undergoing osteogenic differentiation. Cylindric scaffolds (radius 4 mm, height 5 mm) were placed in a tank with the same shape (radius and height 6 mm) and 3 rings of electrodes, each containing 16 elements, placed at height 1, 3 and 5 mm. The conductivity of the tank was set to that of standard cell culture media (1.75 S/m), while that of scaffold was varied according to its calcium content (Eq 1).

$$\sigma = P_{AR} \cdot \sigma_b + (1 - P_{AR}) \cdot \sigma_c \qquad (1)$$

The percentage of calcium depositions (P_{AR}) within the scaffold at different time points was obtained from the Alizarin red concentration reported in [1] and combined with the electrical conductivity of collagen ($\sigma_c = 0.35$ S/m at 2.5 kHz [2]) and cortical bone (σ_b =0.02 S/m at 2.5 kHz [3]) to obtain the phantoms at days 7, 14 and 21.

We then simulated a time-difference EIT experiment (opposite patterns for both injection and measurements) aimed at quantifying the conductivity variation with respect to time 0, when the scaffold was considered to be made entirely of collagen. The reconstruction highlighted an important decrease in average conductivity that accurately reflects the increase in Alyzarin red concentration (Fig 1). The non-linearity of this relationship, that was identified with a 2^{nd} degree equation, shows how calcium deposition is not continuous throughout osteogenic differentiation but is mainly focused between day 7 and 14.

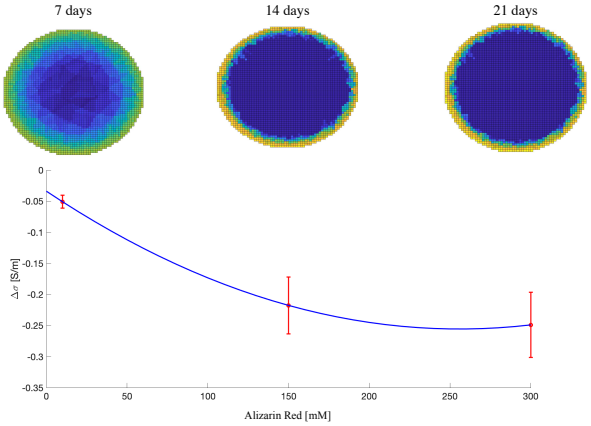

Figure 1: Scaffold reconstruction and comparison with Alizarin Red concentrations.

This analysis was conducted in Matlab (v. R2019a), using Eidors (v 3.9.1) to simulate the EIT stimulation and reconstruct the conductivity map and Netgen (v. 6.2) to create the FEM model.

3 Conclusions

This simulated study shows that EIT can be used to quantify calcium depositions within collagen scaffolds, an index of osteogenic differentiation. The non-invasivity of this method sets is apart from most of the approaches currently available and paves the way for the real-time/in-line monitoring of in-vitro TEed constructs.

References

[1] Petersen *et al.*, 2015. https://doi.org/10.1007/s10529-015-1898-x
[2] Stacl *et al.*, 2017. https://doi.org/10.14311/AP.2017.57.0229
[3] https://itis.swiss/virtual-population/tissue-properties/database/dielectric-properties/

EIT in hybrid imaging setup for tissue engineering applications

Mari Lehti-Polojärvi[1], Olli Koskela[1,2], Aku Seppänen[3], Marek Rist[4,5], Raul Land[5], Paul Annus[5], Mart Min[5], Edite Figueiras[6] and Jari Hyttinen[1]

[1]Faculty of Medicine and Health Technology, Tampere University, Tampere, Finland, mari.lehti-polojarvi@tuni.fi
[2]HAMK Smart Research Unit, Häme University of Applied Sciences, Hämeenlinna, Finland
[3]Department of Applied Physics, University of Eastern Finland, Kuopio, Finland
[4]Competence Center ELIKO, Estonia
[5]Thomas Johann Seebeck Department of Electronics, Tallinn University of Technology, Tallinn, Estonia
[6]Champalimaud Research, Champalimaud Foundation, 1400-038 Lisbon, Portugal

Abstract: This study demonstrates results of a novel hybrid imaging tool where multifrequency electrical impedance tomography is integrated with high resolution three-dimensional (3D) optical imaging.

1 Introduction

There is a need for 3D monitoring methods in the field of tissue engineering and stem cell research [1]. Our approach is to integrate two non-harmful imaging methods into a single setup: multifrequency electrical impedance tomography (MFEIT) [2, 3] and optical projection tomography (OPT) [4].

2 Methods

In this proof of concept work, we measured rectangular piece of carrot (1.8 x 1.6 mm in XY-plane) in saline solution (Fig. 1). The experiment was made in a custom-built chamber (6 x 9 mm in XY-plane) with MFEIT electrodes on two opposing walls and glass walls as the other two walls to enable simultaneous electrical and optical imaging of a rotating sample.

In MFEIT, two sets of four electrodes was used for data acquisition every 10° in full 360° rotation. At each rotational position, 420 tetrapolar measurements were obtained using a novel MFEIT device [3]. Saline solution was measured for reference data. Two dimensional difference images were reconstructed using rotational algorithm [5] with Laplacian prior and hyperparameter 0.2.

Bright-field transmission OPT data was acquired every 0.9° rotation. 3D volume was reconstructed with filtered backprojection algorithm [4].

3 Results

MFEIT images in Fig. 1 (c) were reconstructed with 15 frequencies. Compared to blank saline solution, the carrot is highly resistive at low frequencies and becomes less resistive as applied frequency increases, which is consistent with e.g. [6]. OPT reconstruction in Fig. 1 (b) visualizes the known 3D geometry of the carrot with high structural resolution.

4 Conclusions

We have built a novel hybrid imaging setup and demonstrated its functionality. In future, our technique will provide a tool for monitoring the growth and viability of 3D cell cultures *in vitro*.

5 Acknowledgements

Jane and Aatos Erkko Foundation, Jenny and Antti Wihuri Foundation, Business Finland Human Spare Parts and Academy of Finland CoEBoC projects have provided financial support for this work. Development of MFEIT device was supported by grant IUT1911 of Estonian Research Council, IT Center of Excellence EXCITE and H2020 programme under the grant agreement 668995.

References

[1] A Appel *et al. Biomaterials*, 34:6615-6630, 2013
[2] M Lehti-Polojärvi, O Koskela *et al. Meas Sci Technol*, 29:025401, 2018
[3] M Min *et al. IJBEM*, 209:76-79, 2018
[4] E Figueiras *et al. Biomedical Optics Express*, 5:3443-3449, 2014
[5] O Koskela *et al. IFMBE Proceedings*, 68/2:901-904, 2018
[6] S Ahn *et al. J. Phys.: Conf. Ser.* 224 012152, 2010

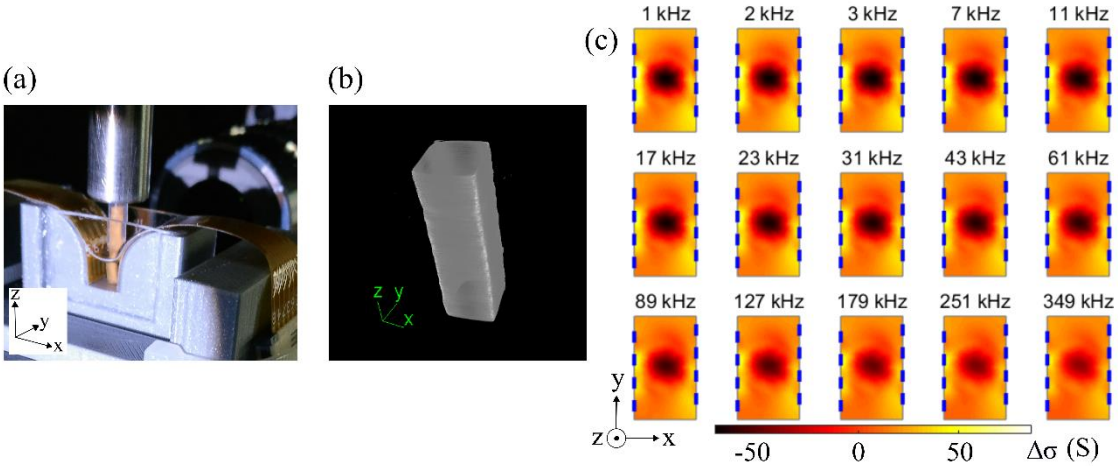

Figure 1: Demonstrating the functionality of MFEIT integration with OPT. (a) Imaging chamber with rotated carrot in saline solution: OPT illumination and detection in y-direction, EIT electrodes on opposing chamber walls. (b) OPT image reconstruction of a rectangular carrot. (c) MFEIT reconstructions of the carrot with 15 frequencies.

Application of Electrical Impedance Tomography to Gesture Recognition

Jiafeng Yao[1], Huaijin Chen[1], Zhupeng Jiang[1], Hongtao Wu[1]

[1]College of Mechanical and Electrical Engineering, Nanjing University of Aeronautics and Astronautics, China
jiaf.yao@nuaa.edu.cn

Abstract: Electrical impedance tomography with Machine Learning Algorithm are applied to realize gesture recognition. The generalized vector pattern matching algorithm (GVSPM) is used to reconstruct the image of the change of conductivity distribution inside the arms. Experimental results show that electrical impedance tomography has the feasibility of gesture recognition.

1 Introduction

EIT has been applied to biomedical and clinical monitoring [1, 2], because it has the advantages of non-intrusion, no harm, simple structure and low cost. In this study, a gesture recognition system based on EIT technology is proposed, which can be used in UAV control and other fields. Compared with other kinds of gesture recognition technology, EIT gesture recognition technology has the advantages of simple equipment and not easy to be disturbed by environment. The principle is that because of different gestures, the internal muscle distribution of the human forearm produces a certain deformation, resulting in regular changes in the distribution of electrical conductivity within the arm. Using EIT technology, the change is collected by custom hand ring electrodes and then classified by Machine Learning Algorithm.

2 Experiments

The developed portable EIT system [3] is used for gesture recognition experiment. The experimental set-up includes Red Pitaya STEMlab, voltage-controlled current source, analog multiplexer modules, electrodes array sensor and PC (Fig 1).

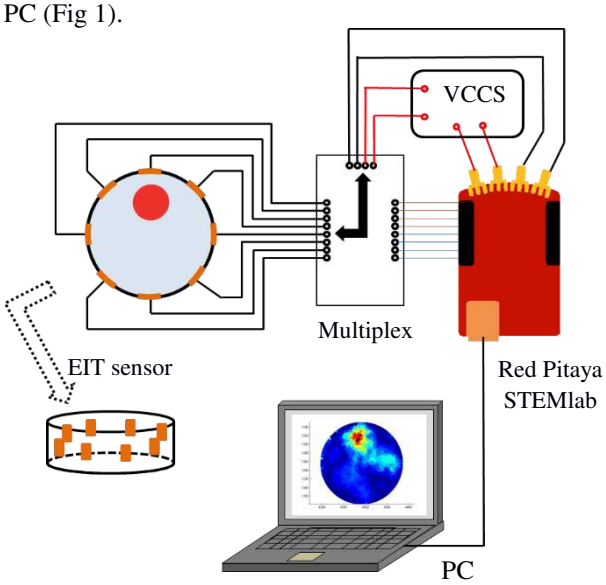

Fig. 1. Experimental set-up.

3 Results and discussion

Without changing the position of the hand ring sensor, three gestures of three subjects were measured 10 times. By using the Machine Learning Algorithm built in MATLAB for gesture recognition, the average accuracy rates is up to 98%. The gesture recognition diagram is shown in Fig 2. Using data of gesture 1 as a control, the data of gesture 2 and gesture 3 were used to reconstruct the image of the change of conductivity distribution inside the subjects arms by GVSPM algorithm, as shown in Fig 3.

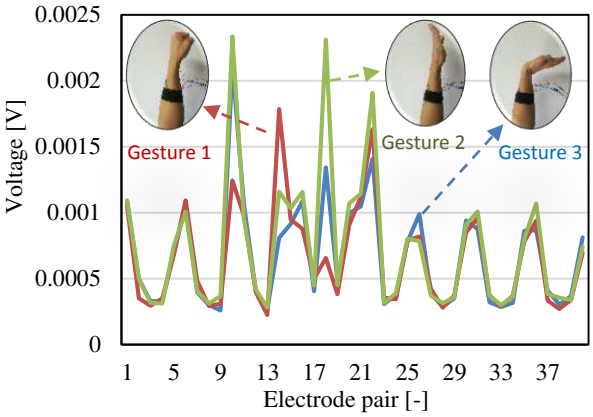

Fig. 2. Gestures reconition with different electrode pair.

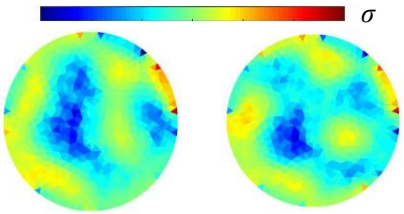

(a) (b)

Fig. 3. Image reconstruction, (a) is gesture 1 compared with gesture 2, (b) is gesture 1 and gesture 3.

4 Conclusions

The EIT technique was used for gesture recognition. The GVSPM algorithm was used to reconstruct the image of the change of conductivity distribution inside the arms. By using the Machine Learning Algorithm built in MATLAB for gesture recognition, the average accuracy is up to 98%.

References

[1] X. Yin, H. Wu, J. Jia et al. *IEEE Sensors Journal*, 18: 54002-5412, 2016.
[2] J. Yao, T. Kodera et al., *Biomicrofluidics,* 9: 044129, 2015.
[3] J. Yao, M. Takei, *IEEE Sensors Journal*, 17: 8196-8205, 2018.

DSP-Based Adaptive Current Source for EIT Applications

G. J. Saulnier, Ahmed Abdelwahab, Farial Nur Maysha

Electrical and Computer Engineering Department, University at Albany - State University of New York, Albany, NY, USA

gsaulnier@albany.edu

Abstract: A new method for achieving a high-precision current source for EIT is proposed, in which the adjustments needed to produce a high output impedance are performed on the signal that is applied to the source. Initial experiments show promising results as the current source maintains a high output impedance over a broad frequency band.

1 Introduction

Current sources used in EIT require high output impedance to deliver the desired current to the load independent of the load voltage. Many circuits that are used to implement current sources can provide high output impedance at low frequencies. However, as the frequency of operation increases, the capacitive portion of the output impedance of the current source presents a lower impedance value and the performance of the current source degrades. To increase the output impedance, circuits such as the negative impedance converter (NIC) [1] and the generalized impedance converter (GIC) [2] have been placed in parallel with a current source to cancel the capacitive part of the output impedance.

In the proposed system, the signal that is applied to the current source is adjusted to increase the output current by the amount that will flow into the output impedance of the current source and any stray impedance to ground, making the desired current flow into the load. Since the compensation is performed in the digital domain, the analog hardware is low-complexity and adjustment-free.

2 Proposed System

A diagram of the system is shown in Fig.1. A sinusoid of a desired amplitude and phase is generated using a digital processor, output through a DAC, and fed to a voltage-to-current (V-I) converter. The output of the V-I converter drives the load and the voltage created on the load is processed by an ADC and fed into the digital processor. In the test system, the V-I converter is implemented using Howland current source [4] (AD8033 op amp and 0.1% resistors) and the digital processor is an Artix 7 FPGA.. A 16-bit DAC (LTC1668,24 MSPS) and 18-bit ADC (AD4002, 1.2 MSPS) are used.

The sinusoid applied to the V-I converter is adjusted to make the V-I output current equal the desired load current (I_L) plus the current flowing in the combination of the V-I converter output impedance and the stray impedance to ground (I_0). The V-I converter output impedance and stray impedance, shown as C_0 and R_0 in Fig.1, is measured using the droop method [3] and stored during a calibration process. During operation, the measured voltage and the stored impedance are used to determine the magnitude and phase of the required current adjustment and this information, along with the value of the desired load current, is fed to the sinusoidal generator. The current adjustments are made continuously, tracking voltage variations.

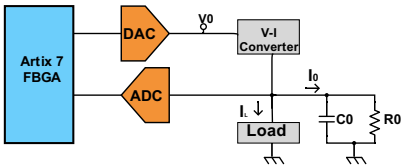

Figure 1: Proposed current source block diagram.

3 Results and Conclusions

Fig.2 shows the measured load resistance and capacitance (modelled as a parallel RC) when delivering current to a 988Ω axial lead resistor with excitation frequencies between 11 kHz to 1 MHz. The measured load is found using the known applied current and the measured voltage. In the “adapt OFF" case, the Howland current source is operating without correction, producing a measured capacitance of approximately 18pF in parallel with the resistor. In the “adapt ON" case, the system uses the previously measured output and stray impedance to correct the applied current, resulting in a decrease in the measured capacitance to approximately 2pF. Since an axial lead resistor has 1 to 2pF of parallel capacitance, the measured capacitance is not expected to become zero. In both the adaptive and non-adaptive cases, the result is nearly independent of frequency, showing only a small decrease in the measured resistance with higher frequency. In both cases, measurements are made by integrating over 0.85ms of a 1.2ms burst of sinusoid. In the adaptive case, the system is given 27μs to adapt before the measurement is taken.

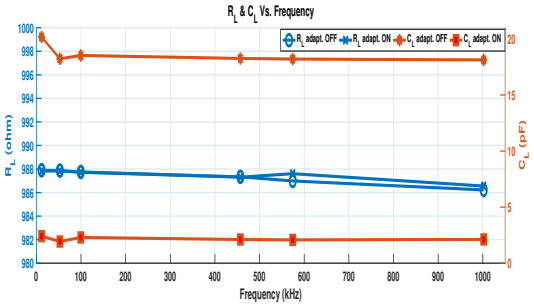

Figure 2: System response across 1 MHz band.

By showing a decrease in measured load capacitance, these results provide an initial validation that the new approach can increase the effective current source output impedance over a wide range of frequencies.

References

[1] DS Holder *Electrical Impedance Tomography* IOP Publishing: Bristol, 2005

[2] S Ross, Alexander and J Saulnier, G and Newell, Jonathan and Isaacson, D *Physiol Meas*, 24:509–525, 2003

[3] R. D. Cook, G. J. Saulnier, D. G. Gisser, J. G. Goble, J. C. Newell, and D. Isaacson, *IEEE Trans. Biomed. Eng.*, , 1994

[4] S. Aguiar Santos, T. Schlebusch and S. Leonhardt *Conf 35th EMBC*, p.6445, Osaka, Japan, 2013

Do current sources perform to "spec," as simulated? Hardware for evaluating simulator accuracy

Alistair Boyle

Systems and Computer Engineering, Carleton University, Canada, boyle@sce.carleton.ca

Abstract: Ultimately, we aim to test the performance of current sources in SPICE simulation and on biological loads by building representative hardware. We present a preliminary hardware design in this paper.

1 Introduction

In this work, we describe our hardware under development (Figure 1), the drive portion of an EIT system, which implements a variety of current source topologies. We aim to use this hardware to take lab measurements and characterize deviations from expected (SPICE simulated) results on resistor or resistor-capacitor (R/RC) phantoms, biological models, and human volunteers. In the following, we describe the preliminary hardware design.

2 Back end: digital control and synthesis

The back end of the hardware design consists of a microcontroller (STM32F205, ARM Cortex-M3, STMicroelectronics) supporting USB 2.0 and microSD storage. Power is supplied via USB port and a lithium ion battery. An FPGA (XC6SLX9, Spartan6, Xilinx) provides direct digital synthesis (DDS) connected to a 16-bit digital to analog convertor (DAC) (AD5542A, Analog Devices). An integrated DDS/DAC (AD9837, Analog Devices) is also supported. Sync and trigger connectors (SMA) wired to the FPGA support external test and measurement infrastructure.

3 Front end: current sources, switching, isolation

The preliminary design supports current source topologies often selected for EIT designs. These topologies include Howland [1], enhanced Howland [2–5], modified enhanced Howland [6], bipolarity source-sink [1], current conveyor II (CCII) / current feedback opamp [4, 7], and cascode current sources [1]. Except for the last two sources, these current sources are all closely related designs. A repeated common layout is supported for the majority of the current sources so that a variety of designs can be explored with minimal board rework.

To model instrument loads, a transformer-based isolation strategy is implemented at the current source. Beyond the isolation, a switch network models capacitive loads for (effectively) an 8 to 256 electrode array. At the board output, off-board connectors (SMA) enable wiring harness and electrode connections to alternative phantoms and human volunteers.

4 Simulated Performance

Performance of an enhanced Howland current source was simulated in Figure 2 (a) transient simulation, and (b) frequency response for an LM741-based design (Texas Instruments) when resistors exhibit a 10% mismatch.

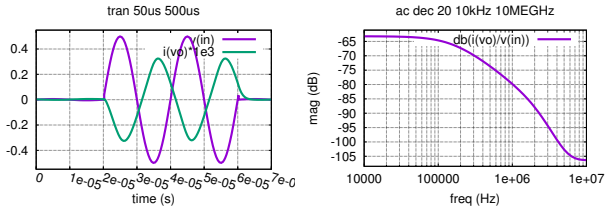

Figure 2: Howland current source (left) transient (50 kHz input), and (right) current gain versus frequency simulated in `ngspice-30` using an LM741 SPICE model (Texas Instruments)

5 Conclusions

This work illustrates preliminary work on hardware to be used in validating SPICE simulations of a variety of current source topologies. It is hypothesized that simulations will *not* correlate for biological media due to Cole-Cole type dispersions.

We welcome input on your personal experiences designing EIT hardware and any comments or suggestions you have on our own hardware design.

References

[1] Horowitz P, Hill W. *The Art of Electronics*. Cambridge University Press, 3 ed., 2015. ISBN 0521809266

[2] Cook R, Saulnier G, et al. *IEEE Trans Biomed Eng* **41**(8):713–722, 1994

[3] Ross A, Saulnier G, et al. *Physiol Meas* **24**(2):509–516, 2003

[4] Holder D (ed.) *Electrical impedance tomography: Methods, history and applications*. IOP Publishing Ltd, 2005. ISBN 0750309520

[5] Rafiei-Naeini M, McCann H. *Physiol Meas* **29**(6):S173–S184, 2008

[6] Maundy B, Elwakil A, et al. *International Journal of Circuit Theory and Applications* **0**(0):1–10, 2019

[7] Bragós R, Rosell J, et al. *Physiol Meas* **15**(Supplement 2A):A91–A99, 1994

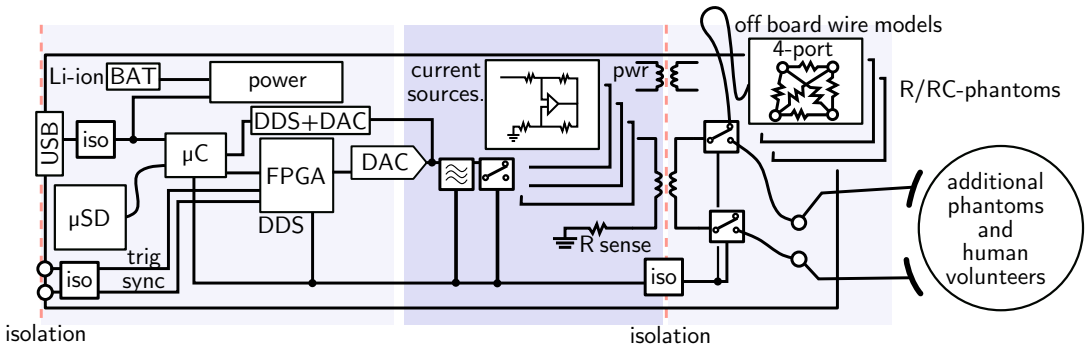

Figure 1: Block diagram showing the structure of the EIT current source test fixture

EIT Tissue Growth Monitor for 3D Imaging of Tissue Viability

Kendall R. Farnham[1], Ethan K. Murphy[1], and Ryan J. Halter[1,2]

[1]Thayer School of Engineering, Dartmouth College, Hanover, NH, USA kendall.r.farnham.th@dartmouth.edu

[2]Geisel School of Medicine, Dartmouth College, Hanover, NH, USA

Abstract: This work describes a novel EIT-based tissue growth monitoring system to fit within the tissue engineering manufacturing pipeline. A 64-channel EIT system has been built and integrated with a custom electrode array. Cellular imaging experiments are in progress, and initial results demonstrate continuous 3D imaging within a standard tissue growth vessel.

1 Introduction

To realize the full benefits of engineered tissues, a robust manufacturing pipeline with high throughput and consistency is needed. The next step and challenge is process automation and monitoring, with the specific need for real-time testing and validation during tissue manufacturing. The US's National Cell Manufacturing Consortium has identified "Process Monitoring and Control" as a critical feature to be solved. Electrical impedance tomography (EIT) is a low cost, non-invasive imaging technique with ability to monitor cell-growth and viability in real-time, making it a promising candidate for large-scale tissue manufacturing. We present an innovative 64-channel EIT system fit to a standard growth vessel to demonstrate longitudinal imaging and viability monitoring capabilities within the existing manufacturing pipeline.

2 Methods

2.1 Hardware Design

A 4x64-channel multiplexing front end was designed to enable tetrapolar impedance measurements through any combination of current-driving and pickup electrode pairs. A custom flexible printed circuit board-based electrode array was designed to fit inside a 35 mm diameter standard 6-well cell-culture dish, with 32 round, 2 mm diameter electrodes on the bottom plane and 32 rectangular, 2x4 mm^2 electrodes arranged in 2 vertical rows around the inside of the dish. The multiplexing front end was controlled by a digital I/O board and interfaced the 64-channel electrode array to an HP impedance analyzer to record impedance from 100 Hz to 1 MHz.

2.2 Software Design

Data acquisition (DAQ) control software was written in MATLAB and Python. A finite element method (FEM) mesh representing the volume within the growth vessel was created, and 3D images of the conductivity distribution within the mesh were reconstructed using Dartmouth's image reconstruction software [1].

2.3 Performance Evaluation and Validation

The DAQ was validated via bench-top electrical tests prior to integrating with the electrode array. Impedance measurements of tetrapolar electrode patterns were simulated with the FEM mesh and validated with saline measurements (conductivities 0.07 S/m to 1.5 S/m) over the 100 Hz to 1 MHz bandwidth. Phantom imaging of yeast growth in media (0.06 S/m saline with sucrose) was performed to demonstrate 3D imaging. Dry active yeast was adhered to the base of the array with double-sided tape prior to adding media. Measurements were taken ~15 minutes apart, with time 0 serving as baseline for difference imaging. The experimental setup and preliminary results shown in Figure 1 highlight the ability to detect planar and vertical sample growth as an initial step toward 3D tissue viability monitoring. During this first round of testing we were able to detect the approximate 3D location of the yeast within the culture well, and by optimizing the tetrapolar electrode patterns and reconstruction parameters we expect to improve resolution within the growth vessel. We have successfully plated cells on our electrode array and are in the process of performing cell-growth imaging to validate the monitor.

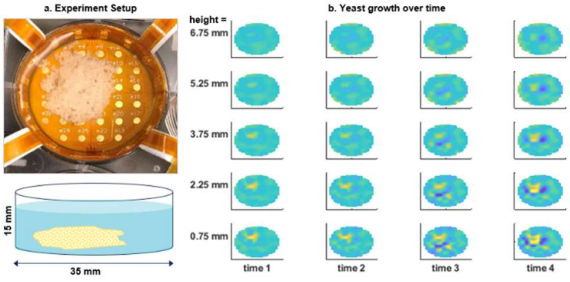

Figure 1. Phantom growth imaging of yeast in 0.06 S/m saline/sucrose media. **a.** Yeast growing on the custom electrode array. **b.** Difference images of the sample conductivity every 15 minutes. The yellow region represents the conductivity of the yeast, with plots showing cross-sections of the culture well up to 6.75 mm high. Planar and vertical conductivity changes occur as the yeast grows, in line with visual observations.

3 Conclusions

EIT-based cell culture imaging is an emerging field [2], however using EIT to monitor tissue viability in 3D has yet to be studied. Coupling 3D DAQ and image reconstruction, we anticipate that our EIT tissue growth monitor can be coupled to standard tissue growth vessels to provide a low-cost, 3D imaging solution to monitor manufacturing of engineered tissues.

4 Acknowledgements

Cells used in this project were graciously provided by Rendell Strawbridge (Dartmouth). Funding support comes from Thayer School of Engineering at Dartmouth College.

References

[1] Murphy, EK, *et al.* (2016). A Novel Regularization Technique for Microendoscopic Electrical Impedance Tomography. *IEEE Transactions on Medical Imaging*, *35*(7), 1593–1603.

[2] Lee, E J, *et al.* (2014). Design of a microscopic electrical impedance tomography system for 3D continuous non-destructive monitoring of tissue culture. *BioMedical Engineering Online*, *13*(1), 1–15.

Using miniature EIT system for the diagnosis of the cervical intraepithelial precancer

Y A Chijova[1], O V Trokhanova[1], A V Korjenevsky[2] and T S Tuykin[2]

[1] Yaroslavl State Medical University, Trokhanova@yandex.ru

[2] Kotel'nikov Institute of Radioengineering and Electronics of the RAS

Abstract: The results of a clinical study on the diagnosis of precursors of cervical cancer using the electrical impedance tomography are presented.

1 Introduction

Cervical carcinogenesis is a multi-stage long-term process. Despite the use of modern methods of diagnosing (cytological examination, HPV test, colposcopy, biopsy and curettage), the mortality in this pathology is high. This is associated with the identification of only late stages of the disease. But the search continues for methods that allow to visualize and assess objectively the state of the cervix at the stage of precancer. We try to develop criteria for the detection and differential diagnosis of mild and severe squamous intraepithelial lesions in women of reproductive age using the method of electrical impedance tomography. The miniature EIT system for such applications was developed.

2 Methods

A comprehensive examination of the cervix was performed in 142 women aged from 18 to 50 (63 women formed the control group without cervix pathology, 46 women with squamous intraepithelial lesions of low degree (LSIL) formed the second group and 33 women with squamous intraepithelial lesions of high degree (NSIL) formed the third group). In the groups, subgroups were selected taking into account the phase of the menstrual cycle (MC) and age (up to 30, over 30). The following diagnostic methods were used for the formation of clinical groups: clinical and anamnestic, gynaecological examination, oncocytology, colposcopy, cervical biopsy. Electrical impedance tomography of the cervix was carried out at 50 kHz using 48-channel measuring system with diameter 32 mm. The static 3D image reconstruction was carried out using generalised backprojection algorithm. The cross-sectional EIT images at depth 2, 5 and 8 mm were used. Standard statistical analysis including logistic regression method was performed.

3 Results

The obtained parameters of the cervix conductivity are presented in Table 1. There are significant differences ($p < 0.01$, $p < 0.05$) in the electrical conductivity of LSIL and HSIL, suggesting their diagnostic significance for specific nosological forms. In order to increase the diagnostic power, the integral index was calculated using the logistic regression method. The diagnostic significance of the regression model (integral indicator) in patients under the age of 30 is: for LSIL in the 1st phase of MC AUC = 0.848, Se = 100%, Sp = 75.76%; for LSIL in 2nd phase AUC = 0.680, Se = 64%, Sp = 87.88%; for HSIL in 1st phase of MC AUC = 0.682, Se = 100%, Sp = 45.45%; for HSIL in the 2nd phase of the MC AUC = 0.935, Se = 100%, Sp = 87.88%. The diagnostic significance of the regression model (integral indicator) in patients in age over 30: for LSIL in the 1st phase of MC AUC = 0.740, Se = 60%, Sp = 90%; for LSIL in the 2nd phase of MC AUC = 0.797, Se = 100%, Sp = 56.67%; for HSIL in 1st phase of MC AUC = 0.740, Se = 100%, Sp = 56.67%; for HSIL in the 2nd phase of MC AUC = 0.787, Se = 100%, Sp = 70%.

Thus, the greatest diagnostic value was noted in the model created for the detection of HSIL in the 2nd phase of MC, which is important, because this pathological condition requires active tactics of the patient's management, even in spite of the young, due to the high rate of progression of the disease.

4 Conclusion

The differences in the electrical conductivity between norm and cervical intraepithelial neoplasia can be used as diagnostic criteria when the method of electrical impedance tomography of the cervix is applied.

Table 1: Comparative characteristics of mean values of electrical conductivity parameters of cervical tissue in norm and cervical pathology, the '*' mark corresponds to the statistically significant difference with the control group ($p < 0.05$).

Group	Depth, zone / MC phase/Edge		1 level (2 mm)	2 level (5 mm)	3 level (8 mm)	Transformation zone (2 mm)
Control	1st phase	Before 30. n = 33	0.917±0.05	0.869±0.05	0.852±0.07	1.084±0.08
		Over 30. n = 30	0.945±0.03	0.896±0.02	0.857±0.02	1.082±0.06
	2nd phase	Before 30. n = 33	0.949±0.06	0.903±0.04	0.885±0.04	1.024±0.05
		Over 30. n = 30	0.985±0.06	0.916±0.03	0.901±0.03	1.055±0.08
LSIL	1st phase	Before 30. n = 28	0.906±0.05	0.885±0.04	0.866±0.06	1.002±0.04*
		Over 30. n = 18	0.956±0.02	0.925±0.02	0.918±0.02*	1.065±0.04
	2nd phase	Before 30. n = 28	0.939±0.03	0.930±0.04	0.924±0.05	1.074±0.06
		Over 30. n = 18	0.980±0.01	0.967±0.03*	0.967±0.01*	1.141±0.03*
HSIL	1st phase	Before 30. n = 15	0.955±0.02	0.946±0.01*	0.949±0.02*	1.070±0.01
		Over 30. n = 18	1.006±0.06*	1.001±0.06*	0.986±0.06*	1.114±0.08
	2nd phase	Before 30. n = 15	0.988±0.09	0.980±0.11*	0.974±0.12*	1.127±0.07*
		Over 30. n = 18	1.087±0.07*	1.078±0.07*	1.089±0.07*	1.141±0.01*

Dead Cell Concentration Imaging in Microchannel by EIT

Daisuke Kawashima[1], Kento Nishibayashi[1], Hiromichi Obara[2] and Masahiro Takei[1]

[1] Graduate School of Science & Engineering, Chiba University, Chiba, Japan, dkawa@chiba-u.jp

[2]Graduate School of System Design, Tokyo, Japan

Abstract: An image reconstruction of dead cell concentration by electrical impedance tomography (EIT) is demonstrated considering the difference in frequency response of imaginary impedance between living and dead cells. Based on the frequency response of the cells, a characteristic frequency f_d in which impedance is sensitive to dead cell concentration is found. In experiment, the performance of image reconstruction of dead cell concentration by EIT in microchannel is evaluated.

1 Introduction

Dead cell concentration is a key factor in tissue engineering and cell analysis. Although a microscope is conventionally utilized for dead cell measurement, the problems are in time consuming and necessity of a fluorescent dye. As a non-invasive measurement, electrical impedance spectroscopy (EIS) method is useful for measuring electrical property of cell such as conductivity and permittivity which reflects on cell condition [1]. On the other hand, electrical impedance tomography (EIT) method is widely used for reconstructing two dimensional conductivity from the multiple one dimensional electrical responses [2]. Nevertheless those two methods have a complemental relationship, they haven't collaborated with each other, deeply.

Recently, Kawashima et al. numerically simulated an image reconstruction of dead cell concentration using the frequency characteristics of cell membrane [3]. Thus, this study experimentally demonstrates the image reconstruction of dead cell concentration using a microchannel with multiple electrodes. The results are quantitatively evaluated.

2 Methods

2.1 Image reconstruction method

Instead of conventional image reconstruction by EIT, the following equation is applied:

$$\mathbf{\Phi_{EIT}}=\mathbf{J}^{\mathrm{T}}\mathbf{\Psi}, \tag{1}$$

where $\mathbf{\Phi_{EIT}}$ is the reconstructed distribution of dead cell concentration ϕ_{EIT}, $\mathbf{J}$ is Jacobi matrix, and $\mathbf{\Psi}$ is a matrix of ψ defined as

$$\Psi(f)=\frac{Z''(\phi_{EIT},f)}{Z''(\phi_{EIT}=1.0,f)}. \tag{2}$$

Z'' is imaginary impedance and f is frequency [Hz]. In previous study, ψ is sensitive to ϕ [3].

2.2 Experimental setup and method

An experimental setup is composed of a microchannel with 16 electrodes on the square-shaped wall, a multiplexer and an impedance analyser (IM3570, HIOKI, Japan) connecting to a PC for controlling measurement devices. For injecting a test sample a syringe pump is used to keep the constant flow rate and to make the field homogeneous concentration ϕ_{ref}.

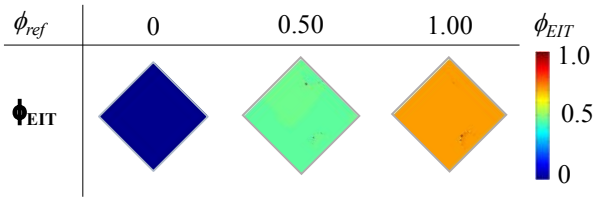

Figure 1: Reconstructed image using Eq. (1).

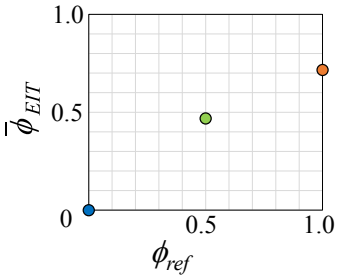

Figure 2: Cross sectional average concentration vs. controlled one.

2.3 Experimental condition

For impedance measurement, constant current was stimulated into two electrodes among 16 electrodes in the microchannel and voltage was measured at the same electrode position. Totally, 120 patterns of current stimulation were applied for applying the image reconstruction.

3 Results and discussion

Fig. 1 shows the reconstructed image $\mathbf{\Phi_{EIT}}$ at 3 different controlled dead cell concentration ϕ_{ref}. All images shows homogeneous distribution. Fig. 2 shows cross sectional average concentration $\bar{\phi}_{EIT}$ plotted with ϕ_{ref}. Quantitatively, $\bar{\phi}_{EIT}$ match with ϕ_{ref} until $\phi_{ref}=0.5$. $\bar{\phi}_{EIT}$ doesn't linearly change with ϕ_{ref} in $\phi_{ref}>0.5$ because Jacobian is calculated based on the relationship between conductivity and impedance.

4 Conclusions

This paper demonstrated the image reconstruction of dead cell concentration in microchannel by EIT considering frequency response of imaginary impedance. The image successfully shows dead cell concentration.

References

[1] K. Asami, *Colloids Surfaces B Biointerfaces*, 119: 1–5, 2014.
[2] X. Liu et al., *IEEE Trans Biomed Circ Sys*, 12:623-631, 2018
[3] D. Kawashima et al., *9th Conf WCIPT9*, Session7-04, Bath, UK, Sep 2

Noninvasive Continuous Monitoring of Stroke Volume during Fluid Challenge Test of Swine Subjects

Geuk Young Jang[1], Ryoung-Eun Ko[2], Tong In Oh[3], Gee Young Suh[2] and Eung Je Woo[3]

[1]Department of Biomedical Engineering, Graduate School, Kyung Hee University, Yongin, Korea
[2]Department of Critical Care Medicine, Samsung Medical Center, Sungkyunkwan University School of Medicine, Seoul, Korea
[3]Department of Biomedical Engineering, College of Medicine, Kyung Hee University, Seoul, Korea, tioh@khu.ac.kr

Abstract: Hemodynamic monitoring is routinely conducted to hemodynamically unstable patients in ICU. Fluid responsiveness is assessed using the fluid challenge technique for proper fluid management. We investigated the feasibility of the electrical impedance tomography (EIT) technique to estimate stroke volume (SV) changes during fluid challenge tests of hypovolemic swine models. During each fluid challenge test, the SV values were simultaneously measured by using the EIT method and the invasive method of pulse contour analysis (PCA) calibrated by the transpulmonary thermodilution (TPTD). The results showed excellent matches between those two methods.

1 Introduction

Proper fluid management of hemodynamically unstable patients in ICU is desirable for enhanced recovery [1]. Based on the Frank Starling law, the fluid challenge test is conducted to confirm the fluid responsiveness of the patient and also to determine the amount of fluid to be injected [2]. The gold standard has been the pulmonary artery catheterization (PAC) using the Swan Ganz catheter to implement the conventional thermodilution method. Lately, this has been largely replaced by the TPTD method using a central venous catheter and an arterial catheter. It is still invasive and provides SV measurements in every 20 seconds. We propose using a fast EIT device with 100 frames per second temporal resolution equipped with a novel signal separation algorithm to produce cardiac blood flow images simultaneously with lung ventilation images. A SV signal can be extracted from the time series of the obtained cardiac blood flow images. This paper presents the results of fluid challenge experiments using swine subjects.

2 Methods

All animal experiments using four healthy swine (weights of 29 to 31 kg) were conducted in accordance with the regulations of the Institutional Animal Care and Use Committee (20150804001). The animal was intravenously anesthetized and mechanically ventilated (Hamilton-G5, Hamilton Medical, Switzerland) by tracheal intubation. The normal ventilation was set as a volume control mode with 8 ml/kg of tidal volume (TV) and 5 cmH_20 of positive end-expiratory pressure (PEEP) in the supine position. Respiration rate was 20 breaths per minute.

The SV signal in the heart region was continuously monitored using a portable 16-channel EIT device (AirTom-R, BiLab, Korea) with 100 frames per second temporal resolution [3]. The SV values were also measured by using the invasive PCA method with EV1000 (Edwards Lifesciences, U.S.A) at 20-second intervals After removing 30% of the estimated total blood volume, we conducted 10 times of 100 ml crystalloid fluid challenges. Each fluid injection was 1-minute long and the time gab between consecutive injections was 2 minutes.

3 Results

Fig. 1 and 2 show the measured SV values from the first and second animals during the fluid challenge experiments, respectively. At the early stage, SV increased significantly in response to the increased preload by injected fluid. The first and second animals showed that target volumes were achieved after the 8th and 5th injection, respectively. We could observe the volume overload phase in Fig.2.

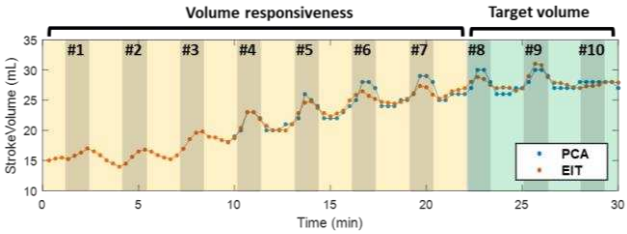

Figure 1: Measured SV values using EIT (red) and EV1000 (blue) from the first animal during the fluid challenge test.

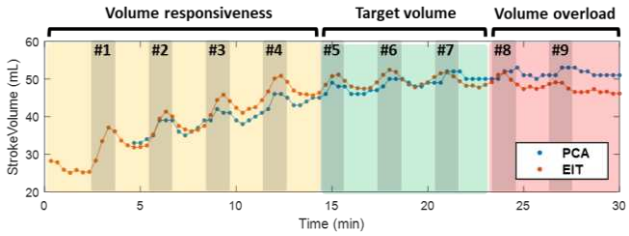

Figure 2: Measured SV values using EIT (red) and EV1000 (blue) from the second animal during the fluid challenge test.

4 Conclusions

The EIT technique could successfully measure SV values from swine subjects during fluid challenge tests. The measured values were highly comparable to those from the conventional invasive method. Future clinical studies are needed to further validate the EIT method for noninvasive continuous SV monitoring in ICU.

5 Acknowledgements

This work was supported by a grant of the Ministry of Health and Welfare (HI14C0743) in Republic of Korea.

References

[1] M. Cecconi et al. *Int. Care Med.* 41:1529-37, 2015
[2] S.W. Patterson and E. H. Starling J. *Physiol.* 48:357-9, 1914
[3] H. Wi, H. Sohal, L. M. Alistair, E. J. Woo and T. I. Oh *IEEE Trans Biomed Circuits Syst.* 8:119-128, 2014

Monitoring regional lung volumes during weighted restraint

Symon Stowe, Mark Campbell, Jeff Dawson, Andy Adler
Carleton University, Ottawa, Canada symonstowe@sce.carleton.ca

Abstract: Law enforcement and medical staff may need to physically restrain subjects, and there are many unknowns about the physiological effects of such restraint. We describe an EIT-based experimental methodology to analyze breathing parameters and regional lung volumes in healthy subjects during weighted restraint.

1 Introduction

Agitated and violent subjects are often physically restrained by law enforcement and medical staff for the safety of the subject, personnel or others. Subjects are often restrained in a horizontal position (typically prone) with a large weight applied to the upper torso. Although restraint can cause significant physical trauma [1], it is often necessary [2].

One key concern is the risk of asphyxia in the restrained subject, which is related to several factors: applied weight to the torso, agitation, physical exertion and obesity [3]. Since it is difficult to measure breathing physiology during restraint, it is unclear how reduced respiratory function and possible asphyxia are caused.

Especially in the context of law enforcement, restraint is subject to widespread public and media concern. Due to the risk posed, it is important to develop experimental models of restraint from which the mechanisms of injury can be investigated, and thus inform the development of restraint techniques and training to minimize the risk to subjects.

We propose that EIT is an ideal non-invasive technology to monitor lung (and eventually cardiac) function during experimental models of restraint. We describe an experimental procedure in which changes in lung function can be measured as a function of the applied weight, body position, and prior exercise (to simulate agitation or conflict).

2 Methods

With ethics approval, EIT measurements were made in three healthy male volunteers. Each subject assumed 3 postures for 5 minutes each: standing, lying in a prone position and lying prone with 50% bodyweight placed on the back. The weight was applied by placing sand bags evenly across the back from between the shoulder blades to the bottom of the rib cage. Arm positions whole prone were randomized between-subject, alternating between arms at the sides and arms extended above the head.

Electrodes were placed on the thorax in an evenly-spaced 2×16 pattern with 5-10 cm vertical separation, following [4]. Data were acquired with the Swisstom Pioneer set, and reconstructed using the GREIT 3D algorithm [5].

3 Results

Preliminary results show distinct and measurable changes in ventilation as measured with EIT across experimental models of restraint. During weighted restraint a reduction in tidal lung volume of up to 50% is observed across the first two minutes of the applied weight. Figure 1 shows the global impedance signal over the 2 minutes with selected tidal ventilation images displayed below. The regional ventilation images clearly show the reduction in ventilation regions as well as a clear shift in the centre of ventilation.

4 Conclusion

A weighted restraint protocol is able to induce repeatable and measurable changes in tidal lung volume and induce a shift in ventilated region. Impedance related to tidal lung volume decreases by up to 50% in restrained subjects. Using this protocol, we plan to add more subjects to further explore the effect of posture, weight and prior exercise.

References

[1] M Rakhmatullina, A Taub, T Jacob *Psychiatr Q*, 84:499–512, 2013
[2] W Fisher *Am J Psychiatry*, 11:1584–1591, 1994
[3] S Stratton, C Rogers, K Green *Ann Emerg Med*, 25:710–712, 1995
[4] B Grychtol et al, *In Press: Physiol Meas*, 2019
[5] B Grychtol, B Müller, A Adler, *Physiol Meas*, 37:785–800, 2016

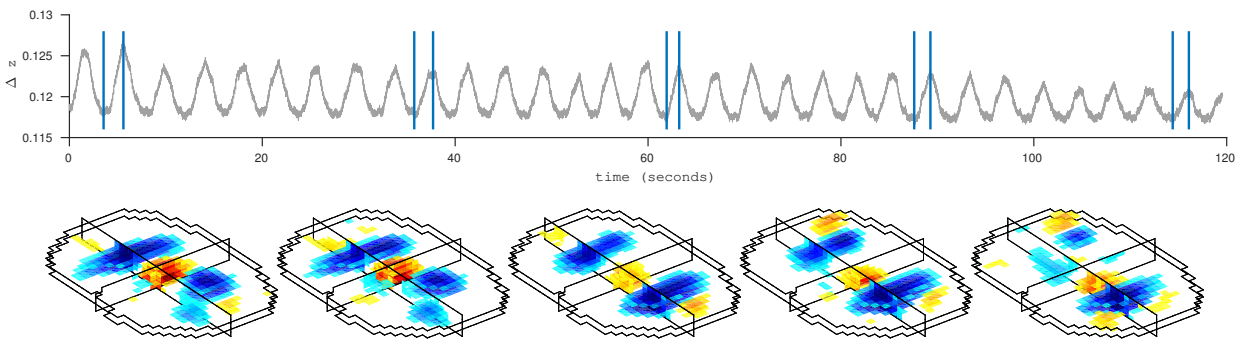

Figure 1: The sum of the impedance signal across all measurements over 2 minutes of weighted restraint is displayed with 5 reconstructed breaths shown with imaged breaths highlighted. The breaths displayed below in 3D clearly show the reduction in ventilation regions as well as a visible shift in the centre of mass.

Multiple measurement vector based image reconstruction for multi-frequency impedance imaging using capacitive sensor

Zhijin Sun[1], Haokun Wang[1], Maomao Zhang[2] and Yunjie Yang[1]

[1]Agile Tomography Group, University of Edinburgh, UK, y.yang@ed.ac.uk

[2]Graduate School at Shenzhen, Tsinghua University, China

Abstract: A multiple measurement vector (MMV) model based image reconstruction algorithm is proposed to reconstruct simultaneously conductivity and permittivity distribution based on multi-frequency and complex-valued electrical capacitance tomography (ECT) data. Alternating direction method of multipliers (ADMM) is applied to solve the multi-frequency image reconstruction problem.

1 Introduction

Traditional ECT model and corresponding image reconstruction algorithms can only reconstruct permittivity distribution at a single frequency [1]. Some recent work has demonstrated the concept of complex-valued multi-frequency ECT in simulation, which can, in theory, reconstruct distributions of permittivity and conductivity simultaneously by using non-invasive capacitive sensors [2]. This paper further explores the practical feasibility to perform simultaneous reconstruction of permittivity and conductivity based on experimental data. A MMV model based image reconstruction algorithm is proposed to improve reconstruction quality by utilising spatial and frequency correlations of multi-frequency images.

2 Methods

A complex-valued ECT forward model is firstly established in Eq. (1) to describe the relation of the complex-valued capacitance measurement and the distribution of permittivity and conductivity.

$$\begin{bmatrix}\Delta C_r\\ \Delta C_i\end{bmatrix}=\begin{bmatrix}J_{r,\varepsilon} & J_{r,\sigma}\\ J_{i,\varepsilon} & J_{i,\sigma}\end{bmatrix}\begin{bmatrix}\Delta\varepsilon_r\\ \Delta\varepsilon_i\end{bmatrix} \quad (1)$$

In the above equation, ΔC_r and ΔC_i represent the real and imaginary part of the complex capacitance measurement respectively. $\Delta\varepsilon_r$ and $\Delta\varepsilon_i$ are the real and imaginary part of the complex admittance respectively. J denotes the Jacobian matrix. For simplicity, Eq. (1) can also be expressed by

$$C = JG \quad (2)$$

where $G=\begin{bmatrix}\Delta\varepsilon_r\\ \Delta\varepsilon_i\end{bmatrix}\in\mathbb{R}^{n\times 1}$, $J=\begin{bmatrix}J_{r,\varepsilon} & J_{r,\sigma}\\ J_{i,\varepsilon} & J_{i,\sigma}\end{bmatrix}\in\mathbb{R}^{m\times n}$, and $C=\begin{bmatrix}\Delta C_r\\ \Delta C_i\end{bmatrix}\in\mathbb{R}^{m\times 1}$.

Then MMV based image reconstruction is proposed to encode the structural features and frequency correlations of the images under different frequencies. The resulting optimisation problem is described by

$$\begin{cases}\min\limits_{Q} \|Q\|_{\omega,2,1} := \sum_{i=1}^{n}\omega_i\|G^i\|_2\\ s.t.\ \ JQ=K\end{cases} \quad (3)$$

where $Q=[G_1,G_2,\dots,G_q]\in\mathbb{R}^{n\times q}$ is a collection solutions under q frequencies. $K=[C_1,C_2,\dots,C_q]\in\mathbb{R}^{m\times q}$ is the collection of q multi-frequency measurements. ω is weighting factors.

The ADMM method [3] is applied to solve the image reconstruction problem described by Eq. (3).

3 Results

A single object (non-conductive) imaging experiments were conducted. A typical 8-electrode ECT sensor was used and the background substance is saline of varying conductivity, e.g. 0.2 S·m^{-1} and 0.5 S·m^{-1}. Impedance analyser were used to obtain complex-valued capacitance measurements, which were performed within a frequency range of 2.1MHz to 2.4MHz. The simultaneous image reconstruction results are shown in Figure 1.

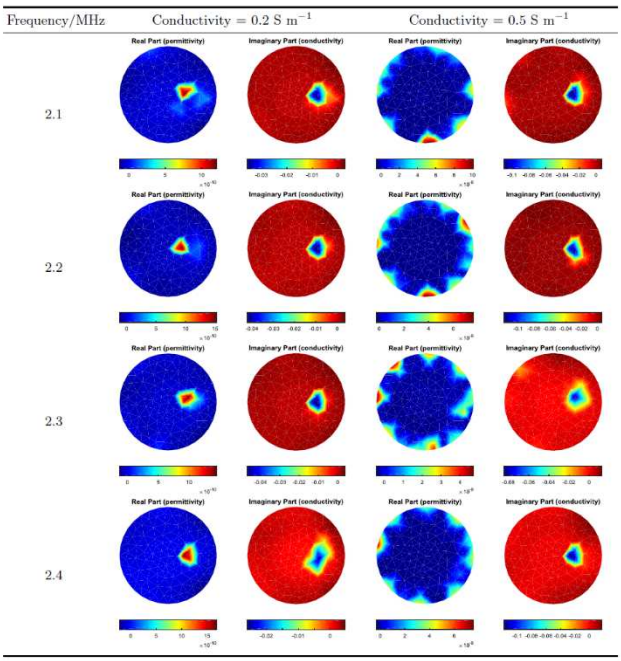

Figure 1: Permittivity and conductivity reconstruction results.

4 Conclusions

The results show that multi-frequency permittivity and conductivity can be reconstructed simultaneously and in high quality based on complex-valued measurement data using ECT sensor and the proposed MMV method. The method is promising for non-invasive biomedical imaging.

References

[1] W Yang, L Peng *Meas Sci Technol*, 14(1), p.R1, 2002
[2] M Zhang, M Soleimani *Meas Sci Technol*, 27(2):025405, 2016
[3] Y Yang, J Jia *IEEE Trans Instrum Meas*, 66(9):2295-305, 2017

Differential measurements in Electric Field Tomography

Pavel Kobrisev, Alexander Korjenevsky, Sergey Sapetsky, Timur Tuykin[1]

[1] Kotelnikov Institute of Radioengineering and Electronics of Russian Academy of Sciences, Russia, drkobrisev1@gmail.com

Abstract: The feasibility of differential measurements is demonstrated with the help of numerical simulation. The reconstruction of images was held using the method of convolution and back projection along the lines of maximum sensitivity. Both amplitude and phase measurements were utilized for reconstruction.

1 Introduction

Electric Field Tomography (EFT) is a kind of Quasistatic Tomography Methods which provides contactless way to visualize a spatial distribution of electrical properties of objects probed by electromagnetic field. Unlike Electrical Impedance Tomography (EIT) it has no problems with precise positioning of electrodes. Moreover, EIT doesn't allow obtaining scull tomography image. Magnetic Induction Tomography succeeds in this issue although it suffers from undesired electrical signals. Electrical Capacitance Tomography is not applicable for medias with relatively high conductivity (more than 0.1 S/m) and so hardly applicable for biomedicine. Taking into account all this facts EFT seems the only method that is free from mentioned disadvantages. The results of interaction of the object with electromagnetic field are changes in phase and amplitude of the primary field caused by Maxwell-Wagner relaxation phenomena [1]. Both of the changes can be utilized for reconstruction. Despite all of the benefits of EFT there are also some problems showed up in common-mode measurements [2]. A sufficient inaccuracy is caused by capacity to ground variation of the electrodes and the object. Differential measurements are intended to fix this problem. The numerical simulation of multielectrode system will demonstrate feasibility of such measurements.

2 Methods

In EFT the method of Finite-Difference Time-Domain (FDTD) is more preferable than Finite Element Method as it takes into account a wave propagation of electromagnetic field. Beside that FDTD is tolerant to modeling of conductive and non-conductive medias' boundaries. The method is based on Maxwell's equations in differential form:

$$\nabla \times \boldsymbol{E} = -\frac{\partial \boldsymbol{B}}{\partial t}, \qquad (1)$$

$$\nabla \times \boldsymbol{H} = \frac{\partial \boldsymbol{D}}{\partial t} + \boldsymbol{J},$$

the rest of two equations are satisfied automatically as a result of proper boundary and initial conditions. In FDTD method the derivatives in (1) are approximated by finite differences of second order using technique developed by Yee [3].

The measurement system is a hexagonal metal camera with 8 metal electrodes inside it. Dipole excitation is used in the system. It means that one couple of adjacent electrodes is fed by the excitation signal and the valid signal is detected on the rest of free couples of adjacent electrodes. The measurement system including the object with nonuniform distribution of conductivity is shown on the figure 1. The object has greater conductive area, about 0.1 S/m, (yellow) and less conductive area, about 0.001 S/m (red). The blue color corresponds to metal.

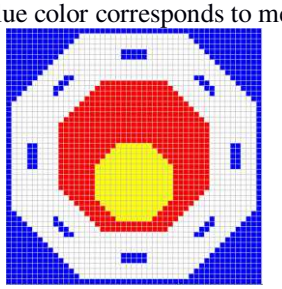

Figure 1: Measurement system including the object with nonuniform distribution of conductivity.

The excitation signal represents a Gaussian impulse. It makes possible to obtain results in a wide frequency range at once using Fourier transform during the signal processing. The relevant values of phase shift and change in amplitude are at 21 MHz which corresponds to relaxation frequency of chosen media. Differential measurements allow using the method of convolution and back projection along the lines of maximum sensitivity [4].

3 Conclusions

To perform reconstruction reference data is necessary. We utilized two variants: "dynamic" visualization, when a model with red area is used (excluding yellow area), and "static" visualization, when an empty camera is used. The reconstruction image of nonuniform object is demonstrated on the figure 2. It shows the feasibility of differential measurements in EFT. The next step of investigation is an attempt to make a physical experiment with installation according to the model.

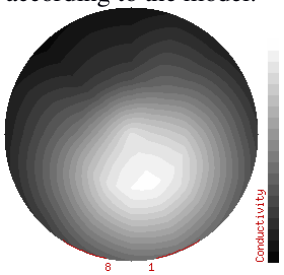

Figure 2: Reconstruction image of nonuniform object.

References

[1] A.V. Korjenevsky *Physiol Meas*, 26:101-110, 2005.
[2] A.V. Korjenevsky, T. S. Tuykin, *Physiol Meas*, 31:127-134, 2010
[3] K.S Yee *IEEE Transactions on Antennas and Propagation*, 14: 302-307, 1966
[4] S Webb *The Physics of medical imaging*, CRC Press, 1988

Tissue classification during surgical drilling using impedance spectroscopy

Yves Jegge[1], Andy Adler[2,3], Mareike Apelt[1], Gürkan Yilmaz[2], Damien Ferario[2], Kathleen Seidel[4], Juan Ansó[1]

[1]ARTORG, Bern, Switzerland, [2]CSEM, Neuchâtel, Switzerland, [3]Carleton University, Ottawa, Canada [4]Department of Neurosurgery, Inselspital, Bern, Switzerland

Abstract: Many types of surgery involve drilling through bone, and it is important to avoid inadvertently cutting sensitive tissues such as nerves. This study investigates whether it is possible to distinguish tissue types from their impedance characteristics over 100 Hz – 1 MHz using electrodes mounted on a probe.

1 Introduction

Drilling through cortical tissue is a key step in many surgeries and many technologies, such as surgical robots [1], focus on improving the accuracy and repeatability of this task. We are motivated by the constraints of Robotic Cochlear Implantation where it is important to avoid damage to the facial nerve. Since nerves have different impedance characteristics to other tissues (and specifically to cortical and cancellous bone), we explore whether electrodes mounted on a probe (or eventually a drill) can be used to measure and distinguish tissue types.

2 Methods and Results

Experiments were performed on three anesthetized and ventilated sheep. Titanium reference screws were implanted into the mastoid for registration. Using a surgical robot system designed for cochlear implantation [2] drill trajectories (eight per animal) were implemented. For each trajectory, up to five measurement points were planned starting at 1.2 mm before the facial nerve. At each point, the drill was removed, the trajectory irrigated (NaCl 0.9%) and an impedance spectroscopy probe inserted to measure Z at 100 Hz – 1 MHz between the probe tip and a body-surface electrode. After the experiment, the mastoid was removed and μCT images acquired to assess drill-to-facial nerve distances.

Example results are shown in Fig 1, corresponding to the μCT image in Fig 2. There is a decrease in $|Z|$ and change of $\angle Z$ as the probe moves from the cancellous bone into the nerve (p4).

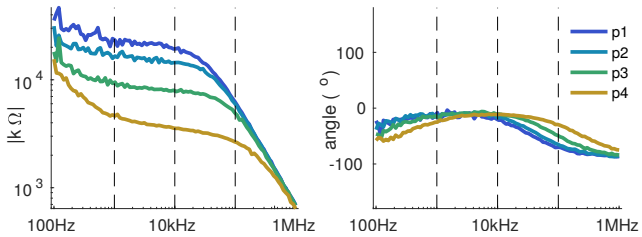

Figure 1: Impedance magnitude (left) and phase (right) for a representative trajectory. Points indicate the approach of the probe to the nerve, entering it at p4.

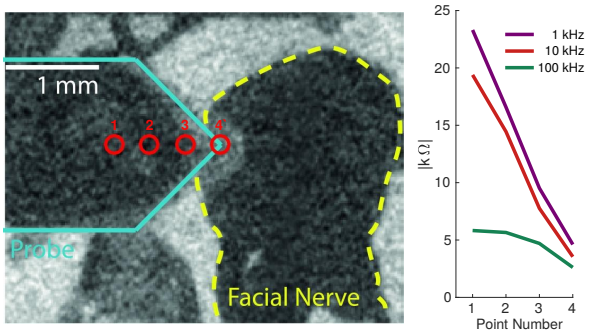

Figure 2: Post-operative μCT slice (left) of the drill trajectory where red dots indicate the probe tip at points p1 ... p4. $|Z|$ (right) at three frequencies as a function of point number.

3 Discussion

Preliminary results show a promising ability to distinguish tissue types using impedance measurements. The most sensitive range appears to be 1 – 10 kHz with useful contributions at other frequencies. Using the in-vivo data and a ground-truth classification of tissue types from the μCT data, we will assess the accuracy with which it is possible to distinguish tissues with impedance data.

Analysis is continuing to optimizing the probe for increased sensitivity. Using a finite element model (Fig 3) we are exploring probe designs and conducting in-vitro tests.

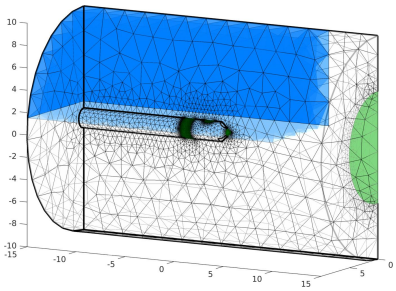

Figure 3: FEM of a probe in a uniform cylindrical tissue near to a lateral transition between tissue types. A large external electrode is shown at right. Different electrode designs are shown on the probe.

References

[1] J Anso et al, *IEEE T Biomed Eng*, 66:237–245, 2019.
[2] Weber et al *Sci Robot*, 2:eaal4916, 2017.

A Simulation Study on the Effect of Ribs on EIT Thorax Imaging

Ke Zhang[1], Maokun Li[1], Fan Yang[1], Shenheng Xu[1], Aria Abubakar[2]

[1]Department of Electronic Engineering, Tsinghua University, Beijing, China maokunli@tsinghua.edu.cn
[2]Schlumberger, Houston, TX, USA

Abstract: In this paper, we study the effect of ribs on EIT forward simulation and reconstruction in the context of thorax imaging. Realistic 3D thorax models are built and used in the simulation. The results show that the ribs have significant effects on both the forward simulation and the reconstruction results.

1 Introduction

EIT reconstruction is a nonlinear inverse problem. As a result, the solution is easily get stuck into local minima when using gradient-based minimization methods if the initial model is not chosen properly. On the other hand, the conductivity distribution in the human thorax is highly non-homogeneous. In particular, the ribs are complex structures with a relatively low conductivity compared with other tissues in the thorax [1]. As a result, the ribs may cause problems to the imaging of the lungs. In this paper, we study the effects of ribs on EIT forward simulation and reconstruction based on realistic numerical phantoms.

2 Methods

2.1 Construction of 3D thorax models

Three-dimensional thorax models are reconstructed from CT scan images. The models are shown in Figure 1. They are discretized into tetrahedral meshes using HyperMesh®. The non-rib model contains 63091 nodes and 353508 tetrahedral elements. The rib model contains 84509 nodes and 485140 tetrahedral elements.

(a) (b)

Figure 1: Three-dimensional thorax models used in the simulation. Both models are equipped with 16 electrodes. (a) Non-rib model with the lungs and the heart. (b) Rib model with the lungs, the heart, and the ribs.

2.2 Forward simulation

In the forward simulation, the complete electrode model (CEM) [2] is used. The electric potential in the investigation domain is solved by using the finite element method (FEM). The adjacent protocol [3] is used. A frame of data contains 104 data points for the 16-electrode configuration.

2.3 Image reconstruction

The image reconstruction of EIT is formulated into a minimization problem with multiplicative regularization. A cost function is constructed as:

$$C(\sigma) = ||\mathbf{s}(\sigma) - \mathbf{d}||^2 \times \mathcal{R}(\sigma), \qquad (1)$$

where σ is the conductivity, $\mathbf{s}(\sigma)$ is the forward solver, $\mathbf{d}$ is the measured data, and $\mathcal{R}(\sigma)$ is the regularization. Gauss-Newton method is used to minimize the cost function (1).

3 Results

3.1 Simulated data

Simulated data are generated using the models introduced in Section 2.1. For the non-rib model, the conductivity settings are as follows: lungs: 0.065 S/m, heart: 0.337 S/m, background: 0.186 S/m. For the rib model, the conductivity settings are the same as those of the non-rib model except that the conductivity of the ribs is set to be 0.053 S/m.

We calculate the relative data difference between the simulated data using the two models for each data point. The minimum relative data difference is 0.026%, the maximum relative data difference is 21.04%, and the average relative data difference is 9.14%. It can be concluded that the ribs have a significant effect on the simulated data.

3.2 Reconstruction results

The simulated data using the rib model are used for reconstruction. Two kinds of initial models are used: 1) Homogeneous initial model; 2) Initial model with the prior information of the ribs (no prior information of the lungs and the heart). The reconstruction results are shown in Figure 2. There are several observations. Firstly, the result using the rib initial model is more accurate than that using the homogeneous initial model. Secondly, the ribs can not be differentiated from the lungs using both the two kinds of initial models. This may cause errors to the estimation of the lung conductivity.

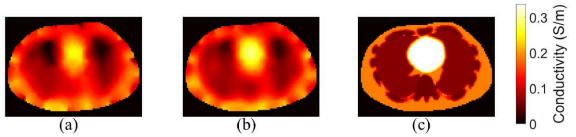

(a) (b) (c)

Figure 2: Reconstruction results using the synthetic data from the rib model. (a) Result using a homogeneous initial model. (b) Result using an initial model with the prior information of the ribs. (c) True profile.

4 Conclusions

The ribs have significant effects on both the forward simulation and the image reconstruction of EIT. They may cause errors to the estimation of the lung conductivity.

References

[1] C Gabriel, S Gabriel, E Corthout *Phys Med Biol*, 41:2231, 1996
[2] K Cheng, D Isaacson, J Newell, D Gisser *IEEE Trans Biomed Eng*, 36:918–924, 1989
[3] A Adler, R Guardo *IEEE Trans Med Imag*, 15:170–179, 1996

Investigation of the effect of varying water content on conductivity distribution in lower leg fat tissue using Electrical Impedance Tomography

M R Baidillah, M W Sifuna, R Ogawa, R Yanagisawa, D Kawasima, and M Takei

Graduate School of Science & Engineering, Chiba University, Chiba, Japan, mr.baidillah@c-techlabs.com

Abstract: This paper investigates the effect of varying water content on the electrical conductivity distribution in the subcutaneous fat tissues of the lower leg based on the reconstructed images by electrical impedance tomography (EIT). The subjects underwent localized EIT measurements on their lower leg with one row of 16 dry-electrodes attached on flexible clothes in a 90 minutes standing posture. The EIT outputs are analyzed with an SVD-based image in the space-time domain. The correlation of determination (R^2) of EIT outputs and varying water content were calculated and compared with results from a bioelectrical impedance analysis (BIA). The results showed a high correlation between the EIT and BIA results.

1 Introduction

Lymphedema is a disease caused by inadequate lymph drainage and is characterized by swelling and accumulation of excess fat and protein rich-fluid in arm or leg. At the early stages, a fat assessment along with the combination of physical therapy and daily bandage are considered to prevent a fat deposition and an accumulation of protein-rich fluid in order to prevent lymphedema progress to chronical phases.

A new method which is more accurate in determination of the location of accumulation of water and protein-rich fluid in the fat tissue as compared to existing methods for fat assessment such as bioelectrical impedance analysis (BIA) is needed. In this regard, this study proposes the use of electrical impedance tomography (EIT) as a fat assessment method in order to monitor fat deposition and accumulation of protein-rich fluid in Lymphedema patient. In order to demonstrate the feasibility of EIT proposal, varying water contents is used as an artificial physiological changes in this study. As a comparison to present methods, a bioelectrical impedance analysis (BIA) was also applied.

2 Methods

EIT sensor used in this study is a one row of 16 dry-electrodes attached on a flexible clothe. The sensor is attached on the right lower leg. The frequency range of impedance measurement is f = 500 Hz – 2 kHz with maximum current I = 1mA. The detail explanation EIT method can be seen in [1]. Healthy subjects with BMI = 23.2~ 26 were used in a 90 minutes standing posture. EIT and BIA measurements were done every after 30 minutes. After the 90th minute, massage was applied on the legs to enhance drainage of water in the subcutaneous fat tissues. These experiments were conducted repeatedly for 7 days. The reconstructed images at time series **G** are analysed based on a singular value decomposition (SVD) in order to decompose the linearly independent component between the varying water content and EIT reconstructed images.

3 Results

Fig. 1 shows time series of conductivity distribution **G** based on a static imaging at f = 1 kHz. Fig. 2 shows the comparison between segmental resistance R_L of BIA and varying water content cycles V_L of EIT represented as a right singular value. The correlation of determination (R^2) results between BIA and EIT is R^2 = 0.81 [-].

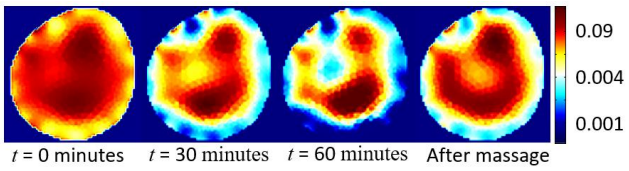

Figure 1. Sagital view of right lower leg based on the normalised conductivity distribution at time series.

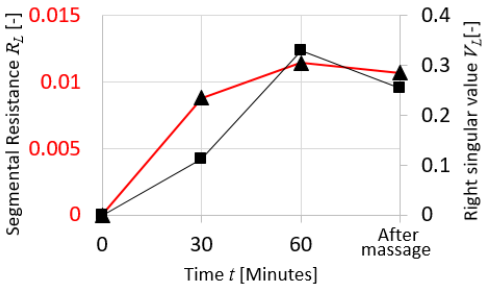

Figure 2. The comparison between segmental resistance R_L of BIA and varying water content cycles V_L of EIT.

4 Conclusions

This paper demonstrates the feasibility of applying EIT for detection of varying water content of the subcutaneous fat tissues in the lower leg. The EIT results have high agreement with BIA results. Moreover, the SVD-based images has a potential method to decompose a fat deposition on our further studies.

5 Acknowledgements

This work was supported in part by International Research Fellow of Japan Society for the Promotion of Science (Graduate School of Science and Engineering, Chiba University) and JSPS KAKENHI Grant Number JP18F18060.

References

[1] MR Baidillah, A Iman, Y Sun, M Takei, *IEEE Sensors J*, 17(24): 8251-826

Individualised Priors in Neonatal Chest EIT via Absolute Imaging

Nima Seifnaraghi[1], Serena de Gelidi[1], Sven Nordebo[2], Davood Khodadad[2], Merja Kallio[3], Inéz Frerichs[4], Maria Suo-Palosaari[3], Erich Sorantin[5], Andreas Demosthenous[6], Richard Bayford[1]

[1]Department of Natural Sciences, Middlesex University, London, UK n.seifnaraghi@mdx.ac.uk [2]Dept. of Physics and Electrical Engineering, Linnaeus University, Sweden [3] Dept. of Paediatrics, Oulu University Hospital and University of Oulu, Finland [4] Dept. of Anaesthesiology and Intensive Care Medicine, University Medical Centre Schleswig-Holstein, Germany [5]Dept. of Radiology, Medical University of Graz, Austria [6]Dept. of Electronic & Electrical Engineering, UCL, UK

Abstract: We present a method for the creation of patient specific prior models for neonate lung EIT. It is based on a probabilistic approach to select the model which best fits the real anatomy of the patient.

1 Introduction

The improvement of EIT image reconstruction and its effect on clinical extracted parameters using more realistic prior models has already been shown [1]. Moreover the outer boundary shape of the thorax can be discovered exploiting sensors embedded in the electrode belt [2]. However there is a need to understand the distribution of internal organs to improve the forward model.

The approach is based on using a prior to select a model from existing 3D model library. The selection procedure is done as a first stage calibration step before applying a real-time reconstruction based on GREIT algorithm (different image reconstruction).

2 Method

First step consists of performing an iterative Gauss-Newton absolute image reconstruction using a 2D general homogeneous model to generate a reference image. Subsequently the library models are cut at the corresponding electrode plane. The cross-sectional map

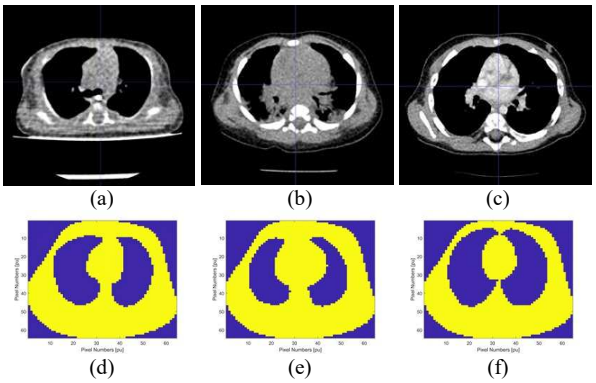

(a) (b) (c) (d) (e) (f)

Figure 1: Cross-sections of three library models (a)-(c) CT scans at the plane of electrodes, (d)-(f) corresponding pixelised images sharing the same outer boundary.

of each model is scaled and then enclosed by the common known outer boundary for all models (Fig. 1). A Bayesian probability is then computed for each model to describe how likely each model fits the reconstructed reference image. The model with the highest probability is then chosen and implemented in real-time reconstructions.

3 Results

The Bayesian probabilities are computed as a function of time. The model used as validation tool is a neonate patient both CTscanned and monitored via EIT suffering from a specific disorder causing an abnormal distribution of inner thoracic tissues (see Fig. 2).

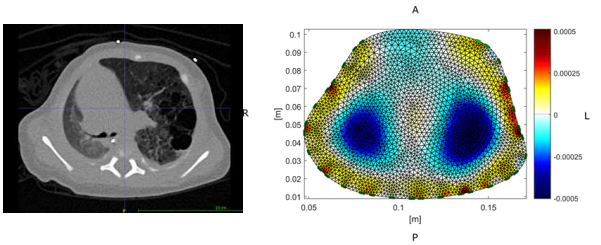

(a) (b)

Figure 2: Cross-section of patient's thorax (a) CT scan (b) absolute imaging result using homogeneous prior.

It's evident that the probability of the first model (the true model) is superior to all other models in the considered time interval (see Fig. 3).

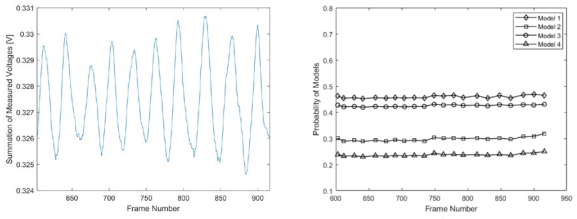

(a) (b)

Figure 3: (a) Recorded EIT signal, (b) assigned probabilities.

Acknowledgements

This work is supported by the CRADL project which has received funding from the European Union's Horizon 2020, under grant agreement No 668259.

References

[1] J.-F. P. J. Abascal *et al.*, *Neuroimage*, 2008.

[2] S. de Gelidi *et al.*, *Physiol. Meas.*, vol. 39, no. 7, 2018.

Novel Approach to Identifying Lung Regions in EIT Images

Lisa Krukewitt[1], Andreas D. Waldmann[1], Gerardo Tusman[2], Emiliano Gogniat[3], Fabian Müller-Graf[1], Stephan H. Böhm[1], Daniel A. Reuter[1]

[1]Department of Anesthesiology and Intensive Care Medicine, University Medical Center Rostock, Rostock, Germany
lisa.krukewitt@uni-rostock.de
[2]Department of Anesthesiology, Hospital Privado de Comunidad, Mar del Plata, Argentina
[3]Department of Intensive Care Medicine, Hospital Italiano de Buenos Aires, Buenos Aires, Argentina

Abstract: We propose a definition of the total lung region as all pixels showing ventilation at one of several levels of positive end expiratory pressure (PEEP) and discuss the differences between this area and regions of interest (ROI) defined at just one PEEP or from CT images. We found that the latter two exclude areas where ventilation may occur.

1 Introduction

The impact of different lung contours on various electrical impedance tomography (EIT) parameters has been discussed extensively [1, 2]. Functional ROIs were defined e.g. based on a fixed threshold or in recent publications anatomical ROIs based on CT scans [3–5] were used. Functional ROIs do not allow to measure non-ventilated areas while anatomical ROIs stemming from CT data do not match the functional lung perfectly. Therefore, we suggest a novel method to calculate a ROI using a wide range of PEEP levels.

2 Methods

After approval of the local authority (CICUAL – register number 08/14) we established an acute respiratory distress (ARDS) model in eight pigs (29 ± 10) kg by repeated lavage with saline and by ventilating the pigs with large tidal volumes for two hours. Thereafter, PEEP levels between 0 and 30 cmH2O were randomly assigned in steps of 5.

At each PEEP level, 2 min of EIT data were recorded. Then, so called tidal images were calculated by subtracting the ventilation distribution at start of inspiration from the one at end of inspiration. The functional lung area at each PEEP level was then defined as all pixels in the tidal image with an amplitude higher than 10 % of the maximum. The overall ventilated area was finally established by all areas showing ventilation at least during one PEEP step (see figure 1, upper left corner).

The image was then divided into a gravity-dependent and non-dependent half and the percentage of non-ventilated area in both halves was calculated at each PEEP level. Furthermore, we plotted the anatomical lung regions of an averaged 3D pig model described by Waldmann et al. [6] and compared them with the functional region.

3 Results and Conclusions

The ventilated area was (45 ± 2) % of the thorax. Based on our approach, non-ventilated areas in the non-dependent and dependent lung could be estimated by subtracting the functional lung region at each PEEP from the total ventilated area. At high PEEP levels, the gravity non-dependent lung area did not participate in tidal breathing, while at lower PEEP levels the dependent lung areas showed reduced ventilation (see table 1).

The anatomical lung regions were within the ventilated area. In all four directions – ventral, dorsal, right, left – the anatomical lung contours described the border of this area.

However, in the anatomical heart region we also found ventilation, and thus the anatomical lung regions might underestimate overdistended lung regions in the non-dependent lungs. Establishing regional lung areas based on regional ventilation distribution at different PEEP levels provided a promising approach to defining the lung's overall functional dimensions.

Table 1: Mean differences Δ between calculated total ventilated area and ventilated area in percent at each individual PEEP level.

PEEP	Δ dep. lung	Δ non-dep. lung	Δ total lung
30	4.2 ± 2.6	12.2 ± 8.5	8.2 ± 0.5
25	4.1 ± 2.5	17.2 ± 9.6	10.2 ± 0.5
20	5.7 ± 4.2	18.4 ± 9.9	11.4 ± 0.4
15	14.2 ± 9.3	16.9 ± 7.2	15.0 ± 0.8
10	30.6 ± 13.4	9.3 ± 6.1	20.2 ± 0.9
5	47.3 ± 16.4	8.7 ± 6.9	27.9 ± 0.9
0	52.3 ± 15.7	3.8 ± 2.9	28.4 ± 0.8

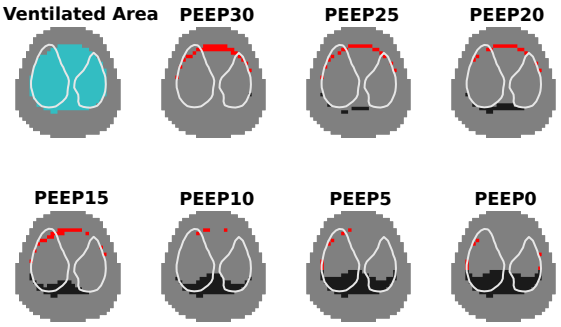

Figure 1: Blue: Total ventilated area defined as all pixels that show tidal change at one of the PEEP levels. Black/red: The difference between the total ventilated area and the ventilated area in the dependent/non-dependent lung for one animal .

References

[1] T Becher, B. Vogt, M Kott, D Schädler, N Weiler, I Frerichs *PLoS One*, 11:1–16, 2016

[2] S Liu, L Tan, K Möller, I Frerichs, T Yu, L Liu, Y Huang, F Guo, J Xu, Y Yang, H Qiu, Z Zhao *Critical Care*, 20:119–128, 2016

[3] D Tingay, P Pereira-Fantini, R Oakley, K McCall, E Perkins, Martijn Miedema, M Sourial, J Thomson, A Waldmann, R Dellaca, P Davis; P Dargaville *Am J Respir Crit Care Med.*, [Epub ahead of print] PubMed PMID: 30730759, 2019

[4] S Spadaro, T Mauri, S Böhm, G Scaramuzzo, C Turrini, A Waldmann, R Ragazzi, A Pesenti, C Volta. *Critical Care*, 22:26, 2018

[5] A Ukere, A März, K Wodack, C Trepte, A Haese, A Waldmann, S Böhm, D Reuter *Br J Anaesth.*, 117:228–235, 2016

[6] A Waldmann, C Meira, U Auer, S Böhme, C Braun, S Bohm, M Mosing *Abstracts of the 16th International Conference on Electrical Bio-Impedance and 17th International Conference on Electrical Impedance Tomography*, 163, 2016

Cuckoo search optimization method for fetus boundary estimation using electrical impedance tomography

Sravan Kumar Konki[1], Anil Kumar Khambampati[2], Sunam Kumar Sharma[3] and Kyung Youn Kim[4]

[1,3,4]Department of Electronic Engineering Jeju National University, Jeju, South Korea, kyungyk@jejunu.ac.kr

[2]BK21+ Clean Energy Convergence and Integration Center for Human Resources Training and Education Jeju National University, South Korea

Abstract: Newton Raphson method for estimating boundary using EIT yet not accurate estimation due to the complex Jacobian calculations, and depends on initial guess. Cuckoo search method is proposed to estimate fetus boundary and provide better estimation in reconstructed images.

1 Introduction

Fetus monitoring during pregnancy period is important to prevent fetal death. EIT has a potential to monitor fetus shape inside the pregnant women. Fetal image reconstruction problem of EIT is considered as fetal boundary estimation. EIT inverse problem is highly ill-posed and nonlinear. However, the traditional inverse solver such as modified Newton Raphson method does not reconstruct accurate boundary of complex shaped region. In this paper, we introduced Cuckoo search method for fetal boundary reconstruction. From the reconstruction results it can be said that the proposed algorithm improves the boundary estimation with good accuracy in the reconstructed fetal images.

2 Methods

2.1 Representation of fetus boundary

In EIT inverse problem, the resistivity distribution of fetus shaped objects in abdominal domain is estimated using measured boundary potentials and applied electrical currents. In this study, estimation of the phase boundary problem is treated as the inverse problem. Fetus is parameterized using Fourier series approach [1,3]. The Boundary of the abdomen C_l and fetus is assumed as

$$C_l(s) = \begin{pmatrix} x_l(s) \\ y_l(s) \end{pmatrix} = \sum_{n=1}^{N_\theta} \begin{pmatrix} \gamma_n^{x_l} \theta_n^x(s) \\ \gamma_n^{y_l} \theta_n^y(s) \end{pmatrix} \quad (1)$$

Where $\gamma_n^{x,y}$ are Fourier coefficients, s is the no.of objects in the abdomen and N_θ is order of truncated Fourier series.

2.2 Cuckoo Search optimization method

A cuckoo search optimization algorithm is a meta-heuristic algorithm based on the brood parasitic behavior of female cuckoo birds [2]. Here, the cuckoo search optimization algorithm is to estimate the Fourier coefficients which minimizes the EIT Objective function in equation (3). The new solution γ_{k+1} is produced based on the current solution γ_k with Lévy flights

$$\gamma_{k+1} = \gamma_k + \alpha * S * (\gamma_k - \gamma_k^{best}) * r \quad (2)$$

The objective function of EIT is defined as

$$\Phi(\gamma_k) = \frac{1}{2}(V(\gamma_k) - \bar{u})^T (V(\gamma_k) - \bar{u}) \quad (3)$$

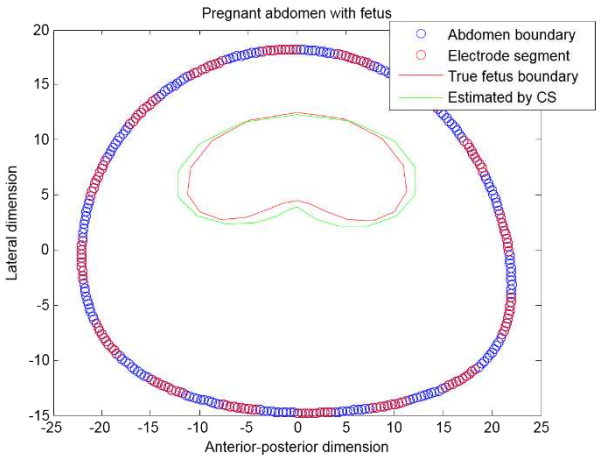

Figure 1: Simulation results for fetus boundary estimation with Cuckoo Search method.

3 Results

An abdomen boundary is assumed based on CT scan image for simulation studies. Fetus and abdomen background conductivity are taken as 0.0065 S/cm and 0.0017 S/cm respectively. To represent shape of fetus and abdomen domain, 4 Fourier coefficients are used. 2% of noise is added to boundary potential to make simulations as realistic experiments.

4 Conclusions

The reconstruction results show that Cuckoo search method has better fetus boundary estimation as compared to modified Newton Raphson method.

5 Acknowledgements

This work was supported by Mid-career Researcher Program through the National Research Foundation of Korea (NRF) grant funded by the Korea government (MSIP) (No. NRF-2017R1A2B4002224).

References

[1] X S Yang and S Deb, *Journal of Mathematical Model*, Jan 1;1 (4) :330-43, 2010.

[2] M C Kim, K Y Kim and S Kim, *Journal of Industrial and Engineering Chemistry*. 10(5):710-6, 2004.

[3] B S Kim, U Z Ijaz, J H Kim, M C Kim, S Kim and K Y Kim, *Measurement Science and Technology*. Nov 23;18 (1): 62, 2006.

3D lung imaging using the 64-channel R3M EIT system

Paul Wright*[1], Wrichik Basu[1], Michael G. Crabb[2], Peter M. Green[1],
Ashley Seepujak[1], and William R. B. Lionheart[2]
paul.wright@manchester.ac.uk
[1]School of Electrical and Electronic Engineering, [2]School of Mathematics, University of Manchester, Manchester, UK

Abstract: Present lung EIT systems typically employ measurements made from electrodes describing a single transverse section through the chest. The images reconstructed from these measurements are essentially 2D since conductivity changes in the craniocaudal direction cannot be resolved spatially using this data. True 3D lung EIT, comprising of a grid of electrodes distributed both axially and radially over the thorax can offer clinicians vital information about changes in lung tissue properties in the upper, middle and lower thirds of the lungs. Preliminary 3D lung EIT results from an ongoing volunteer study using the 64-channel R3M EIT system are presented and compared against 2D lung EIT results.

1 Introduction

Commercial lung EIT systems typically position surface electrodes around the thorax in a planar arrangement. The resulting transimpedance measurements are therefore most sensitive to conductivity changes in the thoracic cross-section coplanar to the electrodes with sensitivity to out-of-plane changes diminishing with distance from the plane of electrodes. Moreover, under this configuration, changes above and below the plane cannot be differentiated due to the complete lack of axial (craniocaudal) resolution. This is a significant shortcoming of the status quo since lung pathologies can disproportionately affect either the upper or lower lobes of lungs which in turn may prompt different remedial strategies [1][2]. Thus far, 3D lung EIT has received sparse attention despite 3D EIT being well established for cranial, breast and industrial imaging applications. Moreover, the few previous attempts at 3D lung EIT have been typically limited to the independent acquisition of EIT measurements from multiple (2-3) sets of electrodes with both excitation and measurements conducted within plane only [3].

Here, we present a set of preliminary experimental results from a 3D lung EIT scheme that interrogates the thoracic volume enclosed by a 16x4 grid of surface electrodes. This is achieved through a combination of in-plane and cross-plane current injection patterns along with simultaneous measurements across electrodes in all planes using the highly flexible 64-channel R3M EIT system [4].

2 Methods

Standard ECG electrodes (3M™ 2228) were affixed on to the subject's torso, arranged into 4 rings of 16 uniformly spaced electrodes each and connected to the R3M unit using shielded ECG leads (150 cm, CAM 14 compatible). Various current injection patterns were applied, including adjacent, non-adjacent ('skip-N') and cross-planar. For each excitation pattern, differential voltage measurements were carried out simultaneously across adjacent electrode pairs. The experiment consisted of the subject breathing normally for multiple cycles, followed by a sequence of breath-hold manoeuvres.

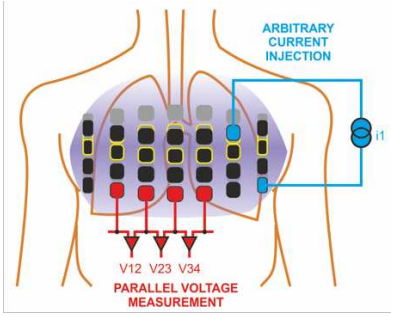

Figure 1: 3D electrode arrangements for lung EIT

3 Results

The dynamic conductivity changes in the interrogated thoracic volume were first reconstructed using the full set of 3D measurements. These were then compared with reconstructions based on measurements from individual planes. In order to determine the impact of inaccurate electrode position information, a subset of the test data was reconstructed using deliberately offset electrode positions.

4 Conclusions

3D lung EIT promises to produce clinically relevant information that is not obtainable using conventional 2D schemes. Our study confirms the feasibility of 3D lung EIT and the benefits of a truly 3D approach. Further steps need to be taken to maximise the convenience of implementing a 3D electrode arrangement in a clinical environment, improve robustness to modelling errors of electrode positions and identify optimal measurement protocols for 3D lung EIT.

References

[1] S. F. Nemec, A. A. Bankier, and R. L. Eisenberg, American Journal of Roentgenology, vol. 200:3, pp. W222-W237, 2013
[2] S. F. Nemec, A. A. Bankier, and R. L. Eisenberg, American Journal of Roentgenology, vol. 200:4, pp. 712-728, 2013
[3] M. Miedema, A. Waldmann, K. E. McCall, S. H. Böhm, A. H. v. Kaam, and D. G. Tingay, American Journal of Respiratory and Critical Care Medicine, vol. 195, pp. 536-538, 2017.
[4] P Wright, P. M. Green, W. Basu, M. G. Crabb, W. R. B. Lionheart, *Conf 19th EIT*, p.61, Edinburgh, UK, Jun 2018

zedhat: an EIT tool library

Alistair Boyle

Systems and Computer Engineering, Carleton University, Canada, boyle@sce.carleton.ca

Abstract: We describe the preliminary release of zedhat, an open source C library and command line interface for EIT image reconstruction. The goals and rationale for the development of this code are described.

1 Introduction

The new software zedhat ($\hat{\mathbf{z}}$) is a dynamically and statically linkable C library of EIT algorithms which provides a stable and tested infrastructure for building further EIT-based tools or for incorporating EIT into higher-level software which combines functionality from a variety of disciplines or modalities. The key idea is that EIT is not the end point but a building block that can and should be integrated with other techniques and tools. The software described here aims to follow that idea to a concrete implementation as a scalable and flexible library.

Zedhat initially aims to provide minimal, core EIT functionality sufficient to calculate an iterative solution. With a solid base and stable interface, the software will be expanded to incorporate greater functionality as it evolves. The software is open-source (BSD licensed) and available at zedhat.org and github.com/boyle/zedhat.

2 Purpose

The vision is to provide a building block (Figure 1) with minimal dependencies which can be used to develop solutions that incorporate EIT techniques.

One such realization is a SPICE circuit simulator where re-implementing SPICE in a monolithic SPICE+EIDORS solution would be an undertaking of large complexity. Instead, our approach is to build this EIT core and link to an open source simulator (ngspice) to build an integrated solution with minimal redundancy.

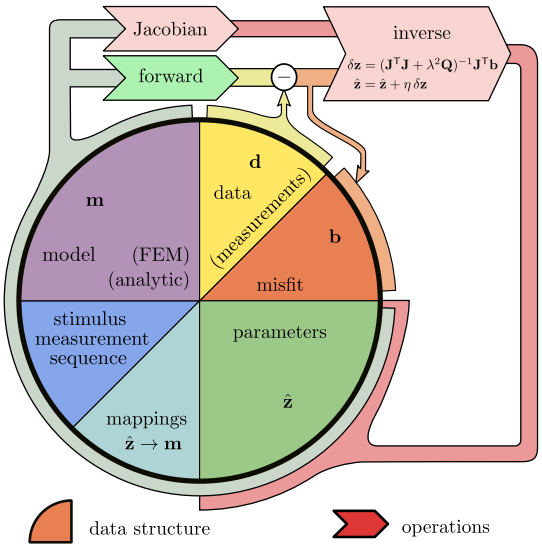

Figure 1: Gauss-Newton (GN) solver; operations define the library interface; core data structures are generic; the forward solutions cancel for time-difference 1-step GN ($\mathbf{b} = \Delta\mathbf{d}$)

3 Preliminary Release

This preliminary release offers a minimal set of numerical tools and interfaces. The release supports mesh loading for Netgen initially, with FEM assembly and CEM boundary conditions. Forward model conductivities may be fixed values, time varying, or frequency dependent Cole-Cole models. Initial support for storage and loading of measurement data $\mathbf{d}$ uses a simple text format. The library supplies an efficient implementation for calculating the forward solution, the Jacobian $\mathbf{J}$, and a time difference conductivity reconstruction $\hat{\mathbf{z}}$ from difference measurements $\mathbf{b} = \Delta\mathbf{d}$ using an $\ell 2$-norm Tikhonov regularized ($\mathbf{Q} = \mathbf{L}^\mathsf{T}\mathbf{L} = \mathbf{I}$) Gauss-Newton single-step method

$$\hat{\mathbf{z}} = \arg\min_{\mathbf{z}} ||\mathbf{J}\mathbf{b} - \mathbf{z}||_2^2 + ||\lambda\mathbf{L}\mathbf{z}||_2^2$$
$$\hat{\mathbf{z}} = (\mathbf{J}^\mathsf{T}\mathbf{J} + \lambda^2\mathbf{Q})^{-1}\mathbf{J}^\mathsf{T}\mathbf{b}$$

for hyperparameter λ. A command line program offers a minimal working example for use of the library.

In the near future, we plan to support Python and Matlab language bindings. This enables a path to validating implementations against EIDORS/Matlab solutions, while isolating the library itself from the challenges of supporting these environments directly. Python, due to its continuing popularity and open source status, is currently the language of choice for many scientific domains. A binding to Python enables low-overhead integration with other tools, the ability to script functionality, and programming language features that many users have come to expect. The code is initially available on Linux platforms and does not provide a graphical user interface (GUI). Without GUI dependencies, we anticipate support for Windows and OSX in the short-term. We aim to achieve and maintain 100% line coverage for testing our code in a continuous integration framework enabling rapid evolution of the codebase and frequent releases without the accumulation of technical debt which can cripple rapid innovation.

We explicitly avoid, at this point, dealing with the complexities of mesh design, device specific file formats, and output visualization. EIDORS [1, 2] offers an exceptional array of application specific mesh generation tools and instrument file format support. EIDORS also enables rapid and efficient visualization of 2D and 3D simulation models and reconstructions. This library, particularly with a Matlab language binding, should eventually be complementary to EIDORS' comprehensive collection of inverse problems "ingredients" and exceptional selection of data handling and model generation tools.

References

[1] Adler A, Lionheart WRB **27**(5):S25–S42, 2006
[2] Adler A, Boyle A, Braun F, et al. In *EIT2017*. Dartmouth, USA, 2017

EIDORS Version 3.10

Andy Adler

Carleton University, Ottawa, Canada

Abstract: This paper announces the release of version 3.10 of the EIDORS software suite. We review its new features, and discusses its growth and use.

1 Introduction

We proudly announce the release of EIDORS version 3.10, for the 20th Int. Conf. on Biomedical Applications of EIT, in July 2019. The software is available at eidors.org and licensed under the GNU GPLv2 or GPLv3. Archived versions are now available on Zenodo [1–4].

EIDORS provides free software algorithms for forward modelling and inverse solutions of Electrical Impedance and (to some extent) Diffusion-based Optical Tomography, in medical, industrial and geophysical settings. EIDORS also aims to share data and promote collaboration amongst its users.

2 New Features

Release 3.10 of EIDORS builds upon a strong foundation in reconstruction algorithms, adding and improving a number of aspects.

- Modelling and management of internal electrodes.
- New electrode specifications on electrode faces (in addition to nodes)
- Improved FEM utility methods (mesh merging, removal, faster boundary calculations)
- Improved support for GNU Octave
- Improved support for GREIT reconstructions in 3D [5]
- Support for caching to disk
- Improved graphics and visualization functions
- Improved support for geophysical FEM models
- Updated utilities for device file formats (new datafile_utility) and integration with SenTec ibeX software.
- Expanded shape library with new species shapes
- (As always) bug fixes

3 Growth

EIDORS-related citations continue to grow. Current citation results are shown in table 1. The EIDORS code-base is growing (fig. 1) with significant effort being applied to improving test coverage, refining performance and implementing new features. In 2012, a `dev` (development) staging area was created for contributions in progress.

Table 1: EIDORS Citations (June 2019, scholar.google.com).

Paper	Date	Citations
[6] A MATLAB package for the EIDORS project ...	2001	255
[7] Image reconstruction algorithms for ...	2002	150
[8] A Matlab toolkit for three-dimensional ...	2002	417
[9] EIDORS: Towards a community-based ...	2005	17
[10] Uses and abuses of EIDORS: An extensible ...	2006	519
[11] Simple FEMs aren't as good as we thought ...	2008	20
[12] EIDORS version 3.8	2015	4
[13] EIDORS version 3.9	2017	6

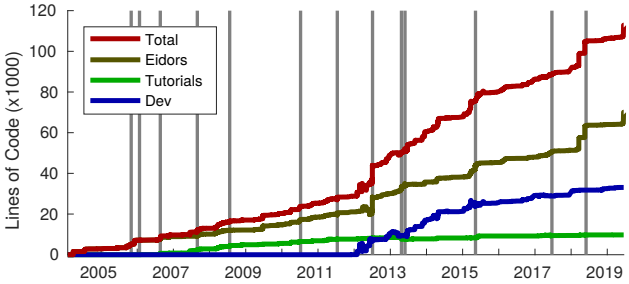

Figure 1: Lines of Code (LoC) in Matlab files in the EIDORS codebase vs. time; Total (red), EIDORS (i.e. release branch, brown), Tutorials (green), development code (blue). Releases are indicated by gray bars (The 3.10 release is at the right).

4 Discussion

The structure of EIDORS has been relatively stable due, in part, to some early design choices: a modular framework and data structure, cross-platform support, integration of meshing, tutorials, and the contributed data repository. These aspects, along with an open source code-base, have enabled EIDORS to maintain research relevance. Version 3.10 (hopefully) continues the tradition.

References

[1] Adler A, "EIDORS version 3.10", DOI:10.5281/zenodo.3247168, 2019.
[2] Adler A *et al*, "EIDORS version 3.9.1", DOI:10.5281/zenodo.1257670, 2018.
[3] Adler A *et al*, "EIDORS v3.9", DOI:10.5281/zenodo.583266, 2017.
[4] Adler A *et al*, "EIDORS v3.8", DOI:10.5281/zenodo.17559, 2015.
[5] Grychtol B *et al* https://iopscience.iop.org/article/10.1088/1361-6579/ab291d *Physiol Meas*, 2019.
[6] Vauhkonen M, Lionheart WRB *et al*, *Physiol Meas*, 22:107–111, 2001.
[7] Polydorides N, *Ph.D. thesis*, U Manchester, UK, 2002.
[8] Polydorides N, Lionheart WRB, *Meas Sci Tech*, 13:1871–1883, 2002.
[9] Adler A, Lionheart WRB, *Proc EIT2005*, London, UK, 2005.
[10] Adler A, Lionheart WRB, *Physiol Meas* 27:S25–S42, 2006.
[11] Adler A, Borsic A *et al*, *Proc EIT2008*, Hannover, NH, USA, 2008.
[12] Adler A *et al*, *Proc EIT2015*, p.19, Neuchâtel, Switzerland, 2015.
[13] Adler A *et al*, *Proc EIT2017*, p.63, Dartmouth, NH, USA, 2017.

Distribution of Pulmonary Pulse Arrival in the Healthy Human Lung

Fabian Braun[1], Martin Proença[1], Mathieu Lemay[1], Andy Adler[1,2]

[1]CSEM, Neuchâtel, Switzerland, [2]Carleton University, Ottawa, Canada

Abstract: The pulmonary artery pressure (PAP) can be noninvasively assessent using the EIT-derived pulmonary pulse arrival time (PAT). However, the spatial distribution of PAT is poorly understood. We analyzed the spatial distribution of PAT in healthy human lungs using cardiac-gated 3D EIT data. Results show PAT varies laterally (and is more than 20 ms lower in the middle) but has little cradio-caudal variation.

1 Introduction

Cardiac-gated EIT can be used to image the pulsatile component; this has been used in several applications, including monitoring of pulmonary arterial pressure [1]. However, the characteristics of the spatial distribution and timing of this signal are poorly understood.

In this study we seek to understand the spatial distribution of the pulmonary pulsatility signal in more detail, in particular the pulse arrival time (PAT) in healthy human lungs.

2 Methods

In our analysis we used previously-measured cardiac-gated EIT data [2], in which healthy volunteers had 32 EIT electrodes placed on the chest in two vertical bands and 3D EIT and synchronized ECG data were acquired, as described in [3].

From these data we analyzed one-minute averages of 3D cardio-synchronous EIT images recorded in supine position during recovery after bicycle exercise. These images were reconstructed using GREIT [4] on five different planes (L1 to L5), with L2 and L4 corresponding to the level of the upper and lower electrode bands [3].

For each of the nine available subjects we calculated the pulmonary PAT for each voxel as detailed in [1]. In a next step we analyzed the inter-subject spatial distribution of pulmonary PAT in two ways: (a) from right to left, i.e. in five vertical segments (see Figure 2) on L2, the EIT plane with strongest pulmonary activity; and (b) along the craniocaudal axis, i.e. EIT planes L1 to L5.

3 Results and Discussion

Figure 1a shows the horizontal distribution of PAT between the five different vertical segments. We can observe a lower PAT in the middle which increases towards the side. On the left the PAT is lower than on the right, probably due to the fact that the left lung lobes are closer to the pulmonary valve, resulting in a lower PAT.

In contrast, over the three uppermost EIT planes (L1 to L3) the PAT does not seem to change remarkably as shown in Figure 1b. The unexpected earlier PATs on L4 are hypothesized to be not due to a reduction of the real PAT but more due to interference with heart-related EIT signals leading to a diminution of the EIT-based PATs.

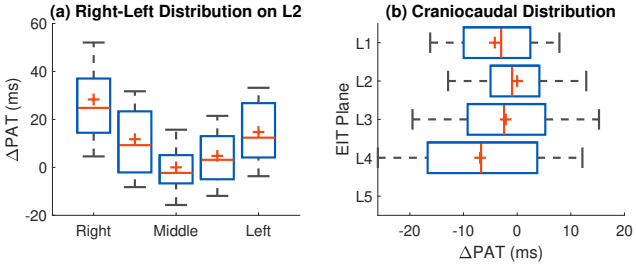

Figure 1: Distribution of the differences in EIT-derived pulmonary PAT from all nine subjects on (a) the five different vertical segments (see Figure 2) on the EIT plane L2 and (b) the five different EIT planes. Note that differences in PAT were calculated for each subject individually by subtracting the mean of (a) the middle segment and (b) the EIT plane L2. The whiskers represent ± one standard-deviation, + the mean, and − the median.

In summary, we could show via ECG-gated 3D EIT that in healthy volunteers the EIT-derived pulmonary PAT is (a) varying from left to right, being lowest in the middle, larger on the left and largest to the right; but (b) barely changing in craniocaudal direction. These findings are in line with PAT values derived from a 3D circulatory lung model [5].

References

[1] M Proença *et al* Physiol Meas, 37:713–726, 2016.
[2] F Braun, *et al*, Zenodo, 2018, DOI:10.5281/zenodo.1145751.
[3] F Braun, *et al*, PLoS One, 13:e0191870, 2018.
[4] B Grychtol *et al*, Physiol Meas 37:785–800, 2016.
[5] M Proença *et al* Med Biol Eng Comput, 55:949–963, 2017.

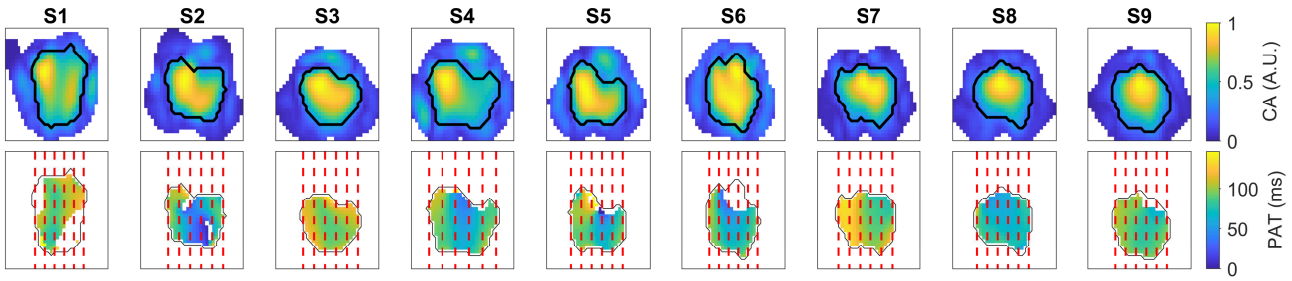

Figure 2: For each of the nine subjects (S1 to S9) we show: (Top) cardio-synchronous activity (CA) image as the pixel-wise temporal standard deviation of the EIT plane L2 with the lung ROI delineated in black. (Bottom) Spatial distribution of the pulmonary PAT in the lung ROI and on the same EIT plane with the five vertical segments separated by dashed red lines.

Software to automate functional analysis of reconstructed EIT data

Symon Stowe[1], Martina Mosing[2], Andy Adler[1]

[1]Systems and Computer Engineering, Carleton University, Canada aadler@sce.carleton.ca
[2]College of Veterinary Medicine, Murdoch University, Perth, WA, Australia

Abstract: In order to make Electrical Impedance Tomography (EIT) analysis more accessible to clinical researchers, we have developed a tool to analyse and display functional EIT measures of reconstructed EIT data of the thorax. Features have been implemented to analyze flow, volume of breaths and basic cardiac frequency analysis.

1 Introduction

Electrical Impedance Tomography (EIT) can have high barriers to entry due to the complexity of analysis on reconstructed data. Existing clinical software performs reconstruction and basic analysis, typically providing an overview of the data and some basic analysis such as: ventilation images, regions of interest, perfusion calculation and data selection.

Several EIT analysis tools have been developed such as AUSPEX (University of Amsterdam) and IBEX [1]. Here, we seek to create an open-source and automated tool that offers the flexibility of a pluggable interface for new functional algorithms. We set out to design a tool that enables the user to select from several different analysis techniques on their reconstructed data, and run an identical analysis across a large number of files simultaneously, decreasing the complexity of EIT analysis.

Focus has been placed on flow-volume analysis for its potential for detecting and analyzing a wide variety of respiratory diseases [2].

2 Implementation and Discussion

Reconstructed EIT data is imported and options are set by user input in a config file. Several open source algorithms are available for selection which can then be run on all files contained within a directory. The results across all files are then displayed in an HTML table so they can be quickly compared across all files. The analysis works on both raw EIT data and reconstructed images. An overview of the analysis procedure including sample results shown for horse ventilation is shown in Fig 1.

The tool presented for the customisable analysis of reconstructed data allows a user to select an appropriate technique for images acquired and reconstructed using data from commercial or academic EIT systems.

References

[1] P Róka et al *Conf 16th EIT*, p.59, Neuchâtel Switzerland, Jun 2015
[2] A Troyer, S Borenstein, R Cordier *Thorax*, 35:603–610, 1980

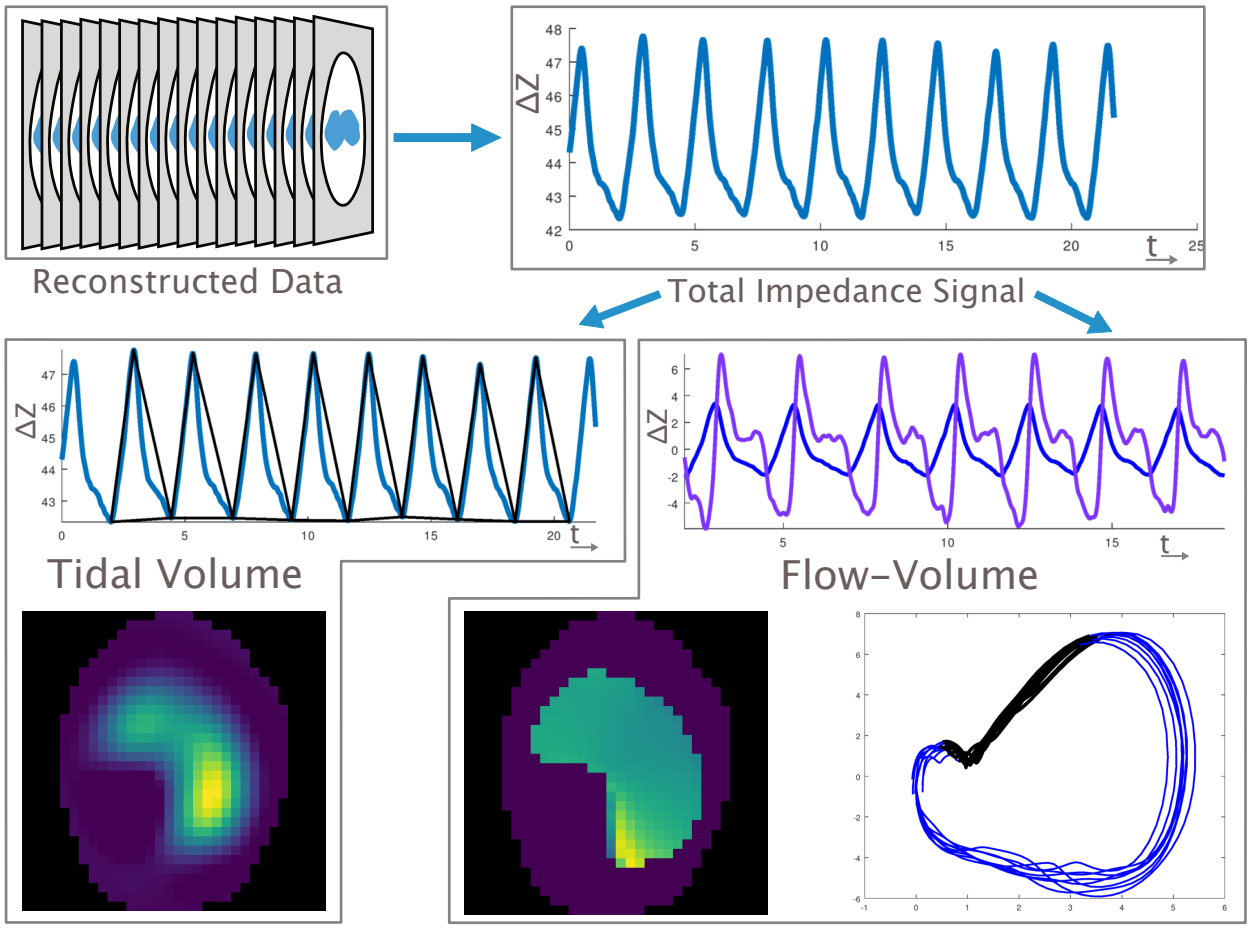

Figure 1: Reconstructed EIT images of horse ventilation are processed as the total impedance signal to detect breaths and plot the flow. Detected breaths are ensemble averaged to generate a tidal volume image. The flow signal is used to generate a flow image and create a flow-volume curve across all detected breaths.

Author Index

Thank you to the sponsors of EIT2019

scio spec
scientific instruments

sentec

kama